

# High Pressure Pelton Turbine Design

Mladen Brajovic 4597117

Technische Universiteit Delft



nospine

# High Pressure Pelton Turbine Design

by

**Mladen Brajovic 4597117**

For obtaining the degree of Master of Science  
in Engineering Wind Energy at Technical University of Denmark and in Aerospace Engineering at Delft  
University of Technology,  
to be defended publicly on September 18th, 2018 at 12:30 AM.

Student number: 4597117  
Project duration: November 1, 2017 – August 20, 2018  
Thesis committee: Dr.ir. N. Diepeveen, DOT  
Dr.ir. M. Zaayer, TU Delft  
Dr.ir. M.O.L. Hansen, DTU  
Prof. S. Watson, TU Delft, chair of the thesis committee

*This thesis is confidential and cannot be made public until December 31, 2023.*

An electronic version of this thesis is available at <http://repository.tudelft.nl/>.



# Acknowledgements

When I started the European Wind Energy Master programme I did not know what to expect as I had never experienced something like this before. Over the past two years I lived and studied in two wonderful countries, Denmark and the Netherlands. During my studies I met the most amazing people from all around the world: people of different nations, different languages, different religions and different cultures but also people with no hate or prejudice of any kind. Finishing this programme along with this thesis would not be nearly as valuable without them. I want to express special gratitude to my great friend Arsalan Khan who helped me and taught me a lot during these two years. I owe him so much and hopefully I can do the same for him in the future.

Furthermore I want to thank to all of my supervisors. My company supervisor Niels Diepeveen, who gave me an opportunity to work on this extremely interesting topic and learn so many new things: his enthusiasm and support for all my suggestions gave me a large boost during my thesis work. My TU Delft supervisor Michiel Zaayer, who was always supportive and open for questions, even when I come to his office unannounced. Also he always had detailed analysis and feedback on my report. My DTU supervisor Martin Hansen, for understanding the difficulties I was facing during the thesis and helping with thesis deadline extension. Finally, I would like to thank to my external advisor Bjørn Winther Solemslie from NTNU, who took the time to answer all of my question during our Skype meetings. His expertise in the field of hydraulic turbines was a major help to me, as well as literature he recommended and provided.

Also I would like to thank all the people from DOT who were very patient with all of my questions and gave me great advice during this project. Their expertise, enthusiasm and team work was very inspiring to me. Making a whole test set up and conducting the tests in a very short time period would not be possible without their help.

And last but not least, I would like to thank to my family for their love and support, not just during these last two years but through my whole life. I would not be here without them.

Mladen Brajovic  
Delft, August 2018



# Abstract

Cost of energy is one of the main reasons why wind power generation hasn't been able to compete with fossil fuels. However, in the past decade wind energy field has made quite a big leap in making this way of energy generation cheaper and more competitive. As a result, the price of onshore wind energy has already reached the price of fossil fuel power generation. The progress has been made with offshore wind turbine technology as well, however ever increasing energy demand has forced industry to push the limits even further. Attempts are being made to build wind farms further offshore where wind resource is much higher and where more space is available. This on the other side requires new technological development and finding new ways to decrease the cost of energy.

This thesis is a part of a larger project (*DOT - Delft Offshore Turbine*) which represents one such attempt to make the offshore wind energy much more competitive by combining wind turbine and hydraulic turbine technology. DOT company works on the development of the fluid power transmission in offshore wind turbines, using seawater as medium. The idea is that every wind turbine drives a hydraulic pump. Each turbine thus creates a flow of water under high pressure which is converted to electricity using a Pelton turbine generator. The main objective of this thesis is to identify and try to overcome challenges in design of Pelton turbines for high water pressures, variable flow rates and seawater conditions. In order to accomplish this objective, theoretical, experimental and numerical approach was used.

Theoretical approach was used to develop a tool for initial Pelton turbine design. Small program was developed in Python programming language which enabled faster and easier turbine dimensioning for any operating conditions based on standard Pelton turbine design procedure.

Next, test rig was designed and built as part of the experimental investigation. Test was divided in two phases. Phase I was meant to show the influence of the flow rate, pressure and pressure fluctuations on the development and quality of the water jet. Pressure is measured at the inlet of the injector and flow visualization of the jet was conducted with the high speed camera. Experimental set-up for Phase II was concluded while performing experimentation has been left out for a future research project.

As last step, CFD simulation of the designed model was conducted using Ansys CFX commercial solver and results were presented and discussed.

Although, all three approaches are conducted independently each of them contributed to answering the research questions and giving a better insight in problem definition. Furthermore it helped identifying the differences between the standard Pelton turbine design and the DOT concept. The research brings us one step closer to making DOT concept a viable sustainable energy solution for the future.



# Contents

<b>List of Figures</b>	<b>x</b>
<b>List of Tables</b>	<b>xiii</b>
<b>Nomenclature</b>	<b>xv</b>
<b>1 Introduction</b>	<b>2</b>
1.1 Offshore wind energy	2
1.2 Delft Offshore Turbine	2
1.2.1 Overview of the DOT concept	2
1.2.2 Hydraulic drive train system	3
1.2.3 Positive displacement pump	4
1.2.4 Hydraulic motor	6
1.2.5 Hydraulic turbine	6
1.3 Problem analysis	6
1.4 Objectives/Research questions and methodology	6
1.5 Outline	8
<b>2 Literature review</b>	<b>9</b>
2.1 Hydraulic drivetrain model for DOT concept	9
2.2 Working principle of the Pelton turbines	11
2.3 Theoretical approach for Pelton turbine design	11
2.3.1 Losses in the Pelton turbine	17
2.3.2 High speed jet flow	17
2.3.3 Stresses in the bucket of a Pelton turbine	17
2.3.4 Influence of seawater conditions on a Pelton turbines	18
2.4 Experimental investigation of the flows inside the Pelton turbines	18
2.4.1 Experimental investigations on a fixed bucket configuration	19
2.4.2 Experimental investigations on a rotating bucket configuration	20
2.4.3 Experimental investigations of a high speed jet flow	22
2.5 Numerical investigation of the flow inside the Pelton turbines	25
2.5.1 Governing equations of fluid dynamics	25
2.5.2 Turbulent flow and turbulence modelling	26
2.5.3 Computational Fluid Dynamics	27
2.5.4 Previous research on application of CFD for flow modelling in Pelton turbines	27
<b>3 Preliminary design of a Pelton turbine</b>	<b>34</b>
3.1 Creating a tool for Pelton turbine design with Python	34
3.2 Design test case	34
<b>4 Experimental analysis of the Pelton turbine jet flow</b>	<b>39</b>
4.1 Test set-up	39
4.1.1 Test equipment specifications	39
4.1.2 Phase I: Investigation about influence of different parameters on quality of the high speed jet	41
4.1.3 Phase II: Investigation about influence of different parameters on pressure distribution inside a Pelton turbine bucket	44
4.2 Result analysis of the Phase I: High speed jet flow visualization	48
4.2.1 Pressure at the inlet of the injector	50
4.2.2 Flow visualization	51

---

<b>5</b>	<b>CFD analysis of the flows inside a Pelton turbine</b>	<b>56</b>
5.1	CFD software and simulation set-up . . . . .	56
5.2	ANSYS Workbench project schematic and workflow . . . . .	57
5.3	Model and test operating points . . . . .	58
5.4	Meshing . . . . .	59
5.5	Solver set-up . . . . .	60
5.5.1	Analysis type . . . . .	60
5.5.2	Domain definition . . . . .	62
5.5.3	Boundary definition . . . . .	62
5.5.4	Solver and output control . . . . .	63
5.6	Analysis of the simulation results . . . . .	63
<b>6</b>	<b>Conclusions and recommendations</b>	<b>71</b>
6.1	Conclusions . . . . .	71
6.2	Recommendations . . . . .	72
	<b>Bibliography</b>	<b>74</b>
<b>A</b>	<b>Preliminary design</b>	<b>76</b>
<b>B</b>	<b>Technical drawings</b>	<b>78</b>



# List of Figures

1.1	Conceptual design of DOT project (Taken from [1]) . . . . .	3
1.2	Schematic representation of the hydraulic transmission systems for DOT concept (Taken from [2]). . . . .	3
1.3	DOT concept with intermediate solution (Taken from [2]) . . . . .	4
1.4	Types of PD pumps: Radial and axial piston (plunger) pump (top row), lobe and gear pump (bottom row) (Taken from [3]) . . . . .	5
1.5	Flow ripple of radial displacement pump for 100 RPM and 1500 RPM (Taken from [2]) . . . . .	6
1.6	Project flowchart. Note: Full lines show the steps that will be conducted in this thesis project. Dotted lines represent steps, planned for future works, necessary to close the design process. . . . .	7
2.1	Hydraulic scheme for DOT intermediate solution (Taken from [2]) . . . . .	9
2.2	Pelton turbine injector . . . . .	10
2.3	Pelton turbine with two injectors and the jet-bucket flow interaction (Taken from [4]). . . . .	12
2.4	Geometric specifications of the Pelton wheel. . . . .	13
2.5	Characteristic bucket position angle (Taken from [4]). . . . .	14
2.6	Forces exerted on the moving bucket (Taken from [4]). . . . .	15
2.7	Exit flow conditions (Taken from [4]) . . . . .	16
2.8	Exit flow conditions at bucket root and cut-out area and flow overshoot (Taken from [4]). . . . .	16
2.9	Locations of pressure intakes for pressure distribution measurements (Taken from [5]) . . . . .	19
2.10	Locations of five pressure zones[6] . . . . .	20
2.11	Pressure zones in the bucket and their individual contribution to the power exchange with respect to the bucket angular position [7]. . . . .	21
2.12	Contribution of the bucket backside to the total torque with respect to runner angular position[7]. . . . .	21
2.13	Location of endoscope for relative flow measurements [8]. . . . .	22
2.14	Locations of external endoscopes [8]. . . . .	22
2.15	Example of onboard endoscope bucket flow visualization [8]. . . . .	22
2.16	Example of external endoscope bucket flow visualization [8]. . . . .	22
2.17	Simplified optical model[8] . . . . .	22
2.18	Injector with external servomotor (Taken from [4]) . . . . .	23
2.19	Dual measurement method set-up[9] . . . . .	23
2.20	Velocity distribution in the pipe (Taken from [10]) . . . . .	23
2.21	Velocity distribution in the jet (Taken from [10]) . . . . .	24
2.22	Test set-up for pulsating nozzle technology (Taken from [11]) . . . . .	24
2.23	Flow visualization of the jet[11] . . . . .	25
2.24	Pressure transducer signal[11] . . . . .	25
2.25	Volume fraction for a 2D bucket [12] . . . . .	29
2.26	Comparison between experimental and numerical results for 0 degrees inclination angle (Taken from [13]) . . . . .	30
2.27	Test rig for plane wall measurements (Taken from [13]) . . . . .	30
2.28	Flow distribution inside the bucket with three different jet diameters (Taken from [5]) . . . . .	31
2.29	Pressure (left) and volume fraction (right) distribution inside the bucket surface for different impingement angles (Taken from [5]) . . . . .	31
2.30	Torque and thrust force, respectively, versus different jet diameters (Taken from [5]) . . . . .	32
2.31	Comparison of pressure coefficients between numerical and experimental results for two pressure zones (Taken from [7]) . . . . .	32
3.1	Program for dimensioning of the Pelton turbine based on main design parameters . . . . .	35

3.2	Pelton turbine size parameters for pressure difference $\Delta p = 200$ bar . . . . .	37
3.3	Pelton turbine size parameters for pressure difference $\Delta p = 400$ bar . . . . .	37
3.4	Pelton turbine size parameters for pressure difference $\Delta p = 200$ bar and fixed rotational speed $n = 1500$ rpm . . . . .	38
3.5	Specific speed as a function of the number of injectors. Rotational speed is kept constant at $n = 1500$ rpm . . . . .	38
4.1	3D model of the test rig designed for the experiment. Two polycarbonate transparent plates are placed from one side and on top of the steel cage to enable optical visibility. Thick steel plates are placed on other sides. The detailed technical drawings for the test rig are given in the Appendix B. . . . .	40
4.2	Complete set-up for the experiment, assembled and placed in DOT testing hall. Test rig is placed at the top of the water container. . . . .	41
4.3	Schematic representation of the full test set-up designed by engineers in DOT. Note: Only one injector is used for the experiment (Courtesy of DOT). . . . .	42
4.6	ATM 250 pressure sensor. . . . .	42
4.7	Photron FASTCAM SA1.1 High Speed camera. . . . .	42
4.4	Performance curves of the axial PD pump. Left: Flow rate for range of rotational speeds of the pump. Right: Required power input for different flow's and different pressures. . . . .	43
4.5	Effective nozzle area as a function of spear position for different nozzle diameters. Taken from [14]. Note: For the test, 25 mm nozzle will be used. . . . .	43
4.8	Astra LED light-panels used as light source for the flow visualization of the high speed jet. . . . .	44
4.9	Graphical explanation of the Pelton turbine bucket cycle: top: Start of the jet-bucket interaction; middle: End of the full impingement; bottom: End of the bucket cycle. . . . .	46
4.10	Stationary jet-bucket configuration designed for the experiment. Note: All dimensions and positioning are based on existing Pelton turbine manufactured for DOT. . . . .	47
4.11	Results of FEA (Finite Element Analysis) for Von-Mises stresses in the bucket with normal force of $F = 20$ kN applied on the bucket surface. . . . .	48
4.12	Results of FEA (Finite Element Analysis) for total deformation of the bucket with normal force of $F = 20$ kN applied on the bucket surface. . . . .	49
4.13	Pressure time series signal and its power spectrum at pump motor speed of 600 rpm and set pressure of 20 bar. . . . .	50
4.14	Pressure time series signal and its power spectrum at pump motor speed of 1000 rpm and set pressure of 20 bar. . . . .	50
4.15	Pressure time series signal and its power spectrum at pump motor speed of 1400 rpm and set pressure of 20 bar. . . . .	51
4.16	Distance of separation (dispersion) of the water jet as a function of the flow rate (left) and pressure (right) normalized with the nozzle diameter. . . . .	52
4.18	Jet speed as a function of pressure measured at different flow rates. . . . .	52
4.17	Flow visualization of the high speed jet at the flow rate $Q = 315$ l/min and rotational speed 1400 rpm. Dispersion of the water droplets and separation distance from the injector nozzle. Note: Dashed line represent distance of the separation point from the nozzle exit ( $l_s$ ); Blue arrows indicate the region where jet transparency is blocked by dispersed flow behind the jet. . . . .	53
4.19	Flow visualization of the high speed jet at the flow rate $Q = 315$ l/min and rotational speed 1400 rpm. Procedure for determination of the jet speed. . . . .	54
4.20	Jet diameter (left) and bucket volumetric load (right) as a function of pressure and the flow rate. . . . .	55
5.1	CFX vertex-centered FV discretization scheme (left) and Fluent cell-centered FV discretization scheme (right). . . . .	56
5.2	Example of workbench project schematic. Steady state and transient simulation for 60 bar case. . . . .	58
5.3	Injector-bucket configuration for the numerical analysis. Note that three cylinders are created to represent jet flow domain. . . . .	58
5.4	Boundaries at the domains defined for the simulation. . . . .	60

5.5	Mesh generated using Ansys automatic meshing tool shown at the symmetry plane. . .	61
5.6	Mesh for the jet and bucket flow domain shown at the symmetry plane. . . . .	61
5.7	Flow domains defined for the simulation. . . . .	63
5.8	Example of the development of high speed jet at pressure of 20 bar and constant flow rate of 315 l/min. . . . .	64
5.9	Analysis of pressure forces exerted on the bucket surface. Note: Double black arrow represents direction of rotation. Pressure force is marked with $F_p$ , force acting in the direction of runner rotation is $F_n$ and force normal to direction of rotation is marked with $F_t$ . . . . .	64
5.10	Pressure distribution inside the bucket at final timestep for different positions of the spear valve and constant flow rate of 315 l/min. . . . .	66
5.11	Water layer thickness at deepest point in the bucket at pressure of 20 bar and constant flow rate of 315 l/min. . . . .	67
5.12	Water layer pressure distribution in the bucket at pressure of 20 bar and constant flow rate of 315 l/min. . . . .	68
5.13	Water layer pressure distribution at deepest point in the bucket at constant flow rate of 315 l/min. . . . .	68
5.14	Diameter of the high speed jet and water/air interface for different positions of the spear valve and constant flow rate of 315 l/min. . . . .	70
B.1	Manufactured bucket for phase II testing . . . . .	83

# List of Tables

1.1	Main components of intermediate DOT concept . . . . .	4
3.1	Flow rate for pressures of 200 and 400 bar . . . . .	35
3.2	Calculated parameters for $P=100\text{MW}$ and $\Delta p = 200$ bar . . . . .	35
3.3	Calculated parameters for $P=100$ MW and $\Delta p = 400$ bar . . . . .	36
4.1	Axial PD pump characteristics . . . . .	40
4.2	Main characteristics of the boost pump . . . . .	40
4.3	ATM 250 pressure sensor characteristics. . . . .	42
4.4	Photron FASTCAM camera main performance characteristics. . . . .	42
4.5	Astra LED light-panel main characteristics. . . . .	44
4.6	Summary of the required instruments for the both test phases. Note that for pressure distribution two solutions are mentioned, however only one will be used. . . . .	45
4.7	Material properties . . . . .	48
4.8	Pressure/flow measurement points for the phase I of the test. Note: First number in the pressure range column also defines the pressure step. . . . .	49
5.1	Dimensionless parameters for investigated flows. Characteristic lengths for injector, water jet and bucket are, respectively: internal diameter of the injector pipe, diameter of the jet and bucket width; Characteristic speeds are: water speed inside the injector and jet speed for both jet and bucket domain. . . . .	57
5.2	Operating points simulated with Ansys CFX. Each case correspond to different spear position which is given by the percentage of the spear valve opening. Fully opened position is at 100 %. Note: Correct spear position is acquired from the experiments for the corresponding set pressure. Furthermore, pressure at the inlet of the injector is also acquired from the measurements and it is not constant but varies with time. . . . .	59
5.3	Mesh statistics for investigated cases. . . . .	62
5.4	Time steps for investigated cases. . . . .	62
5.5	Boundary properties and initial boundary condition. Note: ID - Injector Domain; JBD - Jet-Bucket domain. . . . .	63
5.6	Water layer thickness for investigated cases at the bucket deepest point. . . . .	67
5.7	High speed jet parameters and efficiency of the nozzle. Note: Simulated flow rate is calculated using simulated jet speed and simulated jet diameter. . . . .	69
A.1	Calculated parameters for $P=30\text{MW}$ and $\Delta p = 200$ bar . . . . .	76
A.2	Calculated parameters for $P=30\text{MW}$ and $\Delta p = 400$ bar . . . . .	76
A.3	Calculated parameters for $P=50\text{MW}$ and $\Delta p = 200$ bar . . . . .	76
A.4	Calculated parameters for $P=50\text{MW}$ and $\Delta p = 400$ bar . . . . .	77
A.5	Calculated parameters for $P=200\text{MW}$ and $\Delta p = 200$ bar . . . . .	77
A.6	Calculated parameters for $P=200\text{MW}$ and $\Delta p = 400$ bar . . . . .	77
A.7	Calculated parameters for $P=400\text{MW}$ and $\Delta p = 200$ bar . . . . .	77
A.8	Calculated parameters for $P=400\text{MW}$ and $\Delta p = 400$ bar . . . . .	77



# Nomenclature

## Abbreviations

CFD	Computational Fluid Dynamics
DMM	Dual Measurement Method
DOT	Delft Offshore Turbine
FEA	Finite Element Analysis
FEM	Finite Element Method
GUI	Graphical User Interface
ID	Injector Domain
JBD	Jet-Bucket Domain
LDA	Laser Doppler Anemometry
VOF	Volume-Of-Fluid

## Symbols

$\alpha_0$	Characteristic bucket position angle
$\beta_2$	Bucket exit angle
$\Delta p$	Pressure difference
$\Delta t$	Time step
$\Delta x$	Spatial step
$\dot{m}_c$	Mass flow rate
$\gamma$	Bucket cycle angle
$\lambda$	Multi-bucket factor
$\omega$	Rotational speed
$\Phi$	Nozzle efficiency
$\rho$	Density of water
$\sigma$	Surface tension coefficient
$\varphi_B$	Bucket volumetric load
$\vec{F}_t$	Tangential force
$\vec{W}$	Relative velocity
$B$	Bucket width
$C_0$	Jet velocity
$C_2$	Bucket exit velocity

---

$C_o$	Courant number
$D_0$	Runner diameter
$d_0$	Jet diameter
$D_m$	Pitch circle diameter
$F_{cf}$	Centrifugal force
$F_{co}$	Coriolis force
$F_n$	Normal force
$F_p$	Pressure force
$Fr$	Froude number
$g$	Gravitational acceleration
$H$	Net hydraulic head
$k_m$	Peripheral speed coefficient
$l_s$	Distance of separation
$N$	Number of buckets
$n$	Synchronous generator speed
$n_q$	Specific speed
$p$	Number of pole pairs
$p_d$	Dynamic pressure
$P_h$	Hydraulic power
$Q$	Volumetric flow rate
$R$	Rotor radius
$Re$	Reynolds number
$t$	Time
$U_\infty$	Undisturbed wind speed
$U_m$	Peripheral speed
$V$	Volumetric displacement
$We$	Weber number
$z_{jet}$	Number of injectors



# 1

## Introduction

### 1.1. Offshore wind energy

Necessity for renewable energy has increased rapidly over the past decade. Global awareness about climate change gave a large boost towards the development of new technologies for extraction of energy from clean renewable sources. Amongst all clean energy sources hydro, wind and solar power take the biggest share in production of electricity today. Hydraulic turbine efficiency exceeds 90%, which makes hydraulic turbines most efficient machines after generators. On the other hand, the maximum power that can be extracted from the wind has a theoretical limit (Betz limit) of 59.3%. Today state-of-the-art wind turbines can operate with maximum efficiency of around 50 %[\[15\]](#). The reason why wind turbine technology was not used more in the past was not the lower efficiency but mainly the cost of wind energy production. However today onshore wind generation is one of the cheapest forms of new power generation in Europe, while offshore is rapidly decreasing the cost and setting a firm direction towards replacement of fossil fuel power generation and lowering the global carbon emission. According to *Wind Europe Central Scenario* 330 GW of wind energy will be installed until 2030 which is equal to 30% of EU power demand. More than 230 billions of investment and more than 500 thousands new jobs opened in wind energy.[\[16\]](#)

In order to achieve these goals and guarantee the competitiveness of the offshore wind it is necessary to build the wind turbines further from the shore on the extreme sites but in the same time lower the price of wind energy even more in order to be able to compete with fossil fuel power generation. One such attempt is the *North Sea project* which gathers several countries in an attempt to build offshore farm in the North Sea and collect all electricity at the central platform, on a artificial island, and from there deliver and connect with electrical grid of partner countries by subsea cables[\[17\]](#). So the main motivation for this project is to increase the share of electricity extracted from wind by combining hydro and wind energy production technology in order to further reduce the cost of the energy produced from the wind and make it competitive with fossil fuel power generation.

### 1.2. Delft Offshore Turbine

#### 1.2.1. Overview of the DOT concept

The goal of Delft Offshore Turbine (*DOT*) company is to develop a fluid power transmission in offshore wind turbines. The main idea is to centralize the power production for whole wind farm by using a Pelton turbine with a single generator. Each wind turbine drives displacement pump which creates flow with high pressure which is then used to run the Pelton turbine (Figure 1.1). In this way the wind energy is converted to mechanical energy by means of wind turbine rotor, then to pressure energy by means of displacement pump and again to mechanical energy in Pelton turbine and finally to electrical energy. One of the advantages of this approach in offshore wind is possible reduction of maintenance and capital cost by using a single generator instead of one generator for every wind turbine of the wind farm, removing a gearbox and power electronics. This will also decrease weight of the nacelle which might lead to reduction of material and thus total cost of the turbine. Furthermore, by placing pressure

accumulator tank, this system can be viable solution for energy storage problems. In comparison with classical pumped-hydro storage systems it shortens the energy conversion chain, by eliminating the necessity for intermediate electrical conversion step, thus decreasing the losses in conversion process.[1]

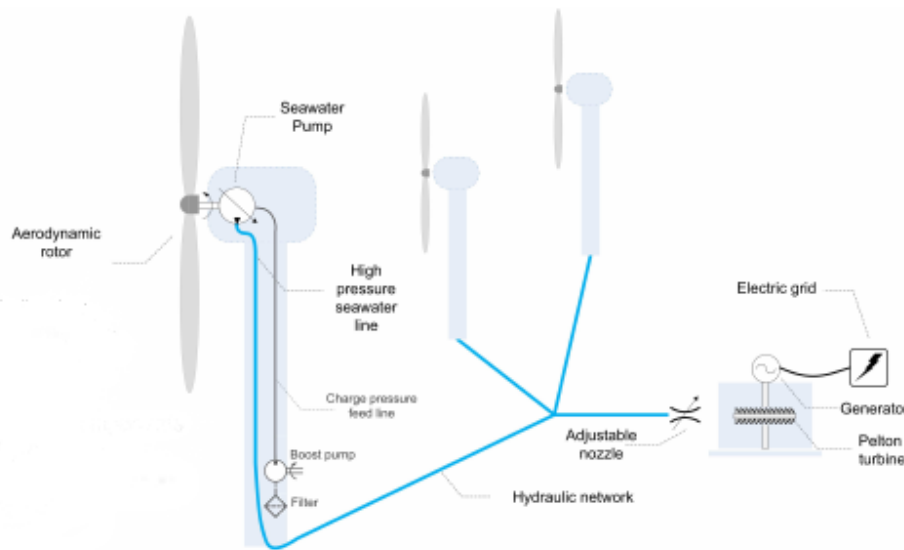


Figure 1.1: Conceptual design of DOT project (Taken from [1])

### 1.2.2. Hydraulic drive train system

With the conventional drive trains generator is coupled with the rotor shaft through the gearbox. The main idea of DOT concept is to replace conventional drive train system with hydraulic drive train where robust and heavy gearbox is taken out of the nacelle and replaced with hydraulic transmission system which then takes the role of the gearbox. At the initial phase, two hydraulic transmission systems are envisioned: closed circuit and open circuit transmission system. Schematic representation for both transmission systems is given in figure 1.2.

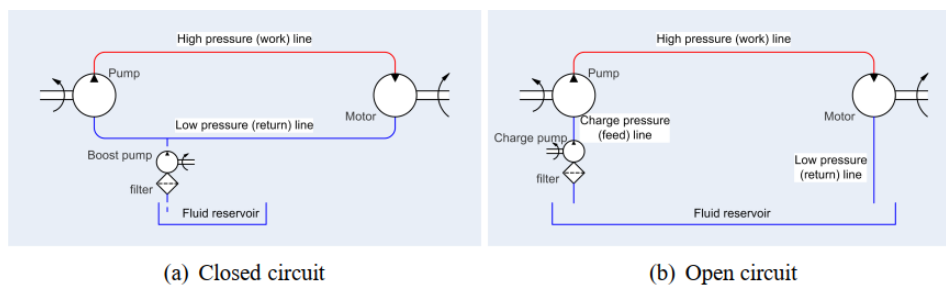


Figure 1.2: Schematic representation of the hydraulic transmission systems for DOT concept (Taken from [2]).

For both systems positive displacement pump is directly coupled with the rotor shaft. With closed circuit system, the pump converts mechanical power of the wind turbine rotor to hydraulic power which is then, again, converted to mechanical power by means of hydraulic motor. The motor then drives another water pump which then creates the high pressure water flow. With open circuit configuration, displacement pump now directly creates high pressure water flow which is then convected towards the hydraulic turbine with no intermediate conversion to mechanical power. The boost pumps are creating additional pressure at the inlet of the main pumps at the nacelle in order to avoid cavitation and enable continuous water supply.

Since low-speed positive displacement water pump is currently being developed in DOT, which means that it is not yet available, the closed circuit intermediate solution is used at this stage. This intermediate

solution implies use of commercially available low-speed oil pump directly connected to wind turbine rotor which, through a closed circuit, drives high speed oil motor which in return drives water pump placed at the tower bottom (Figure 1.3).

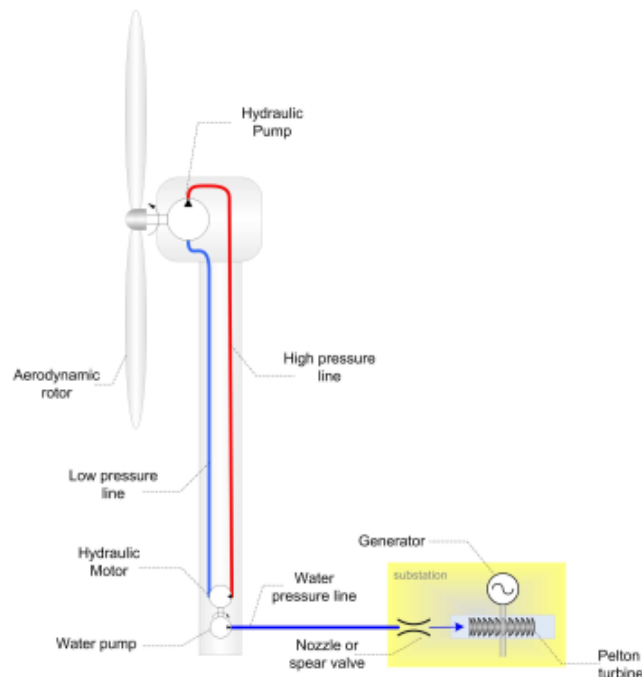


Figure 1.3: DOT concept with intermediate solution (Taken from [2])

The main components of DOT concept with intermediate solution are given in table 1.1.

Table 1.1: Main components of intermediate DOT concept

Component	Type
Wind turbine	Horizontal axis
Hydraulic pump	Radial piston pump
Hydraulic motor	Axial piston motor
Hydraulic turbine	Pelton turbine

### 1.2.3. Positive displacement pump

All the pumps can be divided in two categories:

- centrifugal and
- displacement pumps.

*Centrifugal pumps* are most widely used pumps today. They use rotating impeller to create low pressure at the inlet of the pump, suck the fluid inside the pump and rotation of impeller increases the kinetic and pressure energy of the fluid. These pumps are best suited for high flow and low pressure applications. The flow rate changes with counter pressure.

*Positive displacement pumps* use expanding and contracting cavity at the inlet and the outlet, respectively, to draw the fluid in and push it out, thus creating constant flow, at constant rotation, no matter the pressure difference they need to overcome. That's why they are also known as constant flow machines, although at higher pressures they can have a small leakage that can cause a small reduction of the flow.

The main requirements for DOT concept is creating the high pressure of water which then will be converted to mechanical energy inside the hydraulic turbine. Thus the logical choice for DOT is positive displacement pump.

There are also several types of PD pumps (Some of them are given in figure 1.4):

- Rotary pumps
  - progressive cavity pumps
  - vane pumps
  - gear pumps
  - lobe pumps
  - ...
- Reciprocating pumps
  - plunger pumps
  - diaphragm pumps

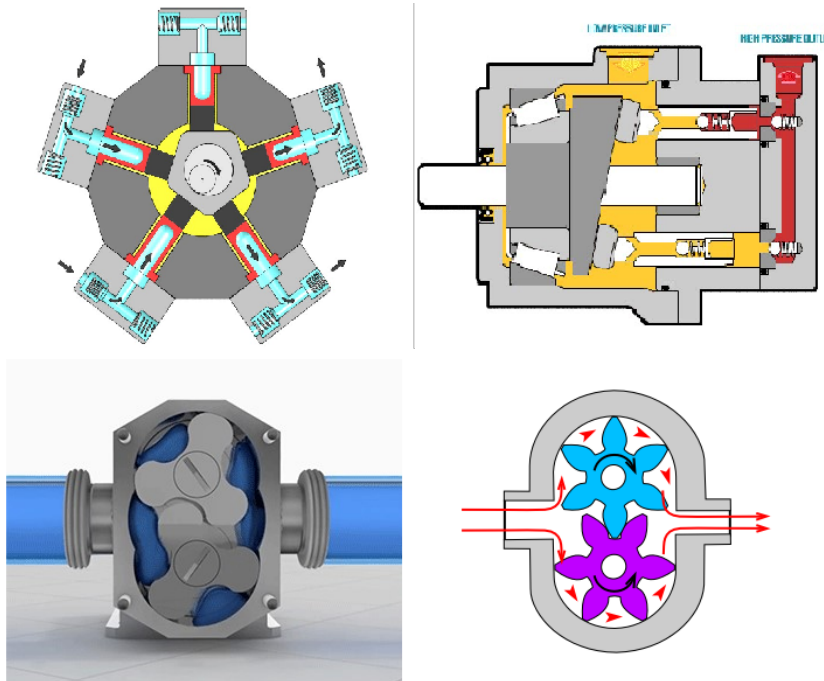


Figure 1.4: Types of PD pumps: Radial and axial piston (plunger) pump (top row), lobe and gear pump (bottom row) (Taken from [3])

The comparison of some of these types which are currently commercially available is conducted, by N. Diepveen, according to several main design objectives: flow rate, maximum pressure, simplicity, cost, efficiency... The radial piston pump was found to be the most suitable choice [2].

The example of this pump is given in figure 1.4 (top left). It has pistons radially distributed around cylindrical block which is placed eccentrically from the piston housing. Due to eccentricity, during the rotation, cylindrical block pushes or pulls the pistons which in return causes fluid expansion or compression. The one issue with PD pumps is that the flow isn't continuous but instead it oscillates around mean value causing so called flow ripples (see figure 1.5). The number of pistons, rotational speed of the pump and relative motion of pistons with respect to each other gives the ripple frequency. The number of pistons determines the magnitude of ripples. The oscillations of the flow will cause oscillation of the pressure, which is something that needs to be taken into account when designing a whole system and especially hydraulic turbine.

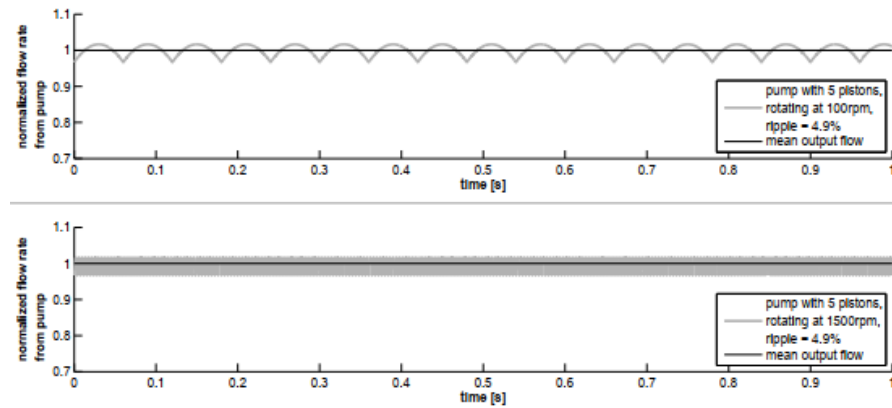


Figure 1.5: Flow ripple of radial displacement pump for 100 RPM and 1500 RPM (Taken from [2])

### 1.2.4. Hydraulic motor

The same comparison for different types of hydraulic motors was done as for the hydraulic pump and axial piston motor was picked as the best option for the intermediate solution.

### 1.2.5. Hydraulic turbine

One of the most important aspects of DOT concept is centralization of wind farm electricity production. Replacing all the wind turbine generators with one or more (depending of wind farm capacity) generators located on central platform and driven by hydraulic turbine. Two main criteria for choice of suitable type of hydraulic turbine were: pressure range and efficiency during the partial loads. The logical choice was Pelton turbine. Pelton turbine is impulse water turbine which extracts the energy from water by converting kinetic energy of high speed water jet to mechanical energy. Since the main objective of this thesis is a design of Pelton turbine, this will be discussed in more details in the following chapters.

## 1.3. Problem analysis

The main content of the thesis is designing the Pelton turbine for DOT concept. The goal is to identify and try to overcome the challenges in working with the seawater, variable pressure and variable wind conditions. The highest pressure for Pelton turbines goes up to 190 bar, so another goal will be to identify the challenges in designing the turbine which can withstand even higher pressures and operate with highest efficiency.

There is little or no research about application of Pelton turbines with sea water conditions. The reason for this is because Pelton turbines are constant pressure devices and they are ordinarily used for pressure heads above 700 m (around 50 bar). These are impulse machines which use kinetic energy of water to rotate the wheel of the turbine. Pressure energy remains almost constant from the inlet to the outlet. Kinetic energy is usually converted potential energy represented as hydraulic head or the height difference between upper and lower water reservoir. Since these turbines needed elevated water reservoir, their seawater application was never really considered.

Hydraulic turbines today are state-of-the-art technology and most efficient machines after electric generators. This project wants to show that using Pelton turbine in combination with hydraulic pumps and wind turbines in offshore conditions is not just feasible but also profitable in terms of reduction of the cost of energy.

## 1.4. Objectives/Research questions and methodology

This master thesis tries to overcome challenges in designing high pressure Pelton turbine for use in offshore conditions and coupling with wind farm. Since this is a new concept and Pelton turbines were never used before in offshore applications or in combination with wind turbines, there will be a few main questions that are necessary to address:

- **Influence of wind conditions on the efficiency of Pelton turbines?** - Pelton turbines work with high pressures and relatively low flow rates. Flow rate is regulated by the spear valve and pressure is determined by the height difference between upper and lower reservoir. In DOT concept, pressure is regulated by the spear valve and flow rate by the rotational speed of the pump and thus wind turbine rotor. This means that the flow rate is dependent on the wind speed. During the partial loads, in order to keep high pressure constant at low flow rates the spear valve needs to be closer to fully closed position. This will have the influence on formation and shape of the jet which in return will influence the total efficiency of the turbine.
- **Variable pressure on a Pelton turbine?** - Pelton turbines are also known as constant pressure turbines, as they operate under constant pressure (or hydraulic head) which only slightly changes in accumulation itself. However since positive displacement pumps can not provide continuous flow but instead create ripples, due to finite number of pistons, there will be fluctuations in pressure which might influence fatigue of the buckets as well as cracking in the root of the bucket. Furthermore, pressure fluctuations can diminish the quality of the jet which can have an impact on the total efficiency of the turbine as well.

Note that influence of seawater and marine life on a Pelton turbine are also questions that need closer consideration. However these questions are outside of the scope of this thesis and they will be addressed only through literature review.

The figure 1.6 is the project flow chart that shows all the steps and methodologies that will be used in order to tackle these questions. The general idea is that all of these steps should be interconnected with each other and form the final tool that will help identify the problem, speed up the design process and find optimal solution. However this is only possible if all the steps, connected with dotted line, are conducted. Due to lack of time and unavailability of the equipment, the Phase II of the experiment had to be canceled. Nevertheless, the test set-up is designed and measurement procedure is explained for both phases to ensure that second phase is ready for a future work.

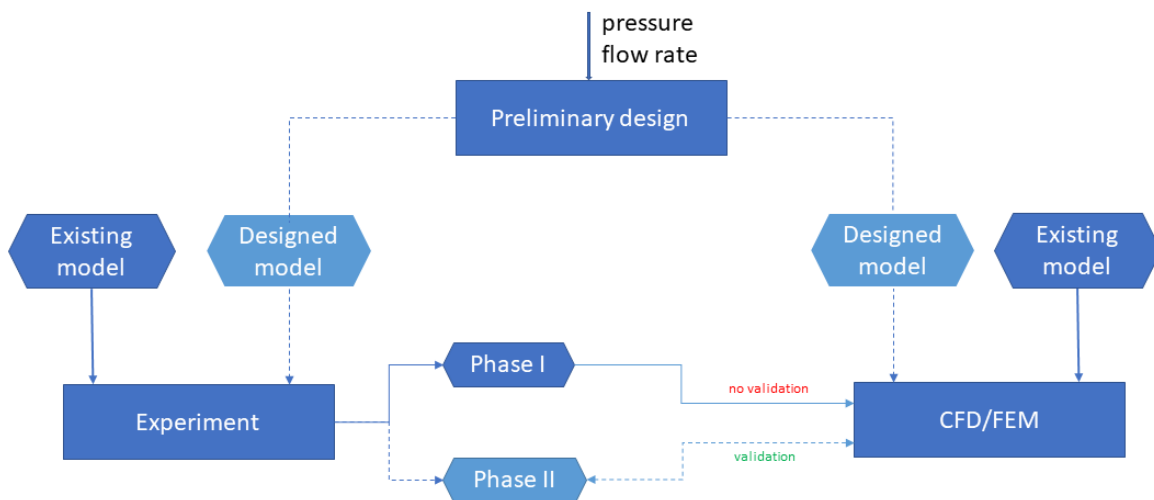


Figure 1.6: Project flowchart. Note: Full lines show the steps that will be conducted in this thesis project. Dotted lines represent steps, planned for future works, necessary to close the design process.

Three different steps or approaches that will be used are:

1. Preliminary theoretical design - In the first stage, preliminary design of the turbine will be done using classical Pelton turbine design based on theoretical understanding of the flow processes that are occurring within the turbine itself. Using, both, parametric formulas, derived from classical fluid mechanics describing the flow inside the turbine, and formulas gained from empirical observations, dimensions of the turbine (diameter of the wheel, bucket width, bucket height etc.) will be determined as well as number of buckets, number of injectors and their respective positions.
2. Experimental approach - Test set-up will be built and flow visualization and different measurements will be conducted in order to gain better insight and identify the differences in operating conditions for DOT concept from standard Pelton turbines. This in turn will help to adjust the design to compensate for these differences and ensure the high efficiency of the turbine. The existence and the effect of the pressure fluctuations on the quality of the jet will be investigated in the first phase of the test. In the next phase the flow inside the bucket, pressure distribution and the stresses at the root of the bucket should be measured. Two experimental configurations are considered for the phase II:
  - Fixed bucket
  - Rotating bucket

The final choice of which test configuration will be used, will be made and explained in the next chapter.

3. Numerical analysis - The final approach will use CFD analysis of the flow inside the injector, high speed jet and flow inside the bucket. Results will be compared with experimental investigation.

## 1.5. Outline

The thesis is outlined as follows. Chapter 2, refers to the literature review. Theory behind the Pelton turbine is explained and research relevant for the thesis and three methodologies, mentioned above, is reported. In Chapter 3 small program with GUI created for preliminary design of the Pelton turbine is described. Standard Pelton turbine design procedure based on theoretical and empirical formulas is applied. Analysis, dissuasion and design recommendations are provided. Chapter 4 describes the design of the test set-up, measurement campaign and the analysis of results. In Chapter 5, results from conducted CFD simulations are presented and discussed. In the final chapter all previous work is summarized and main conclusions are extracted. Recommendations for improvements and for future work are presented.

# 2

## Literature review

### 2.1. Hydraulic drivetrain model for DOT concept

For the modelling of rotor dynamics Newton law of motion can be used. Simplified equation for describing hydraulic drivetrain system is:

$$J_t \dot{\omega} = \tau_{Rotor} - \tau_{Pump} \quad (2.1)$$

Where  $J_t$  is mass moment of inertia of the wind turbine rotor and displacement pump,  $\omega$  is a rotational speed of the rotor and  $\tau_{Rotor}$  and  $\tau_{Pump}$  are torques produced by the wind turbine rotor and the pump.

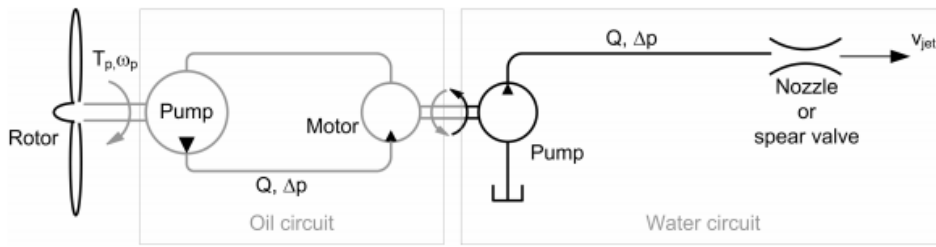


Figure 2.1: Hydraulic scheme for DOT intermediate solution (Taken from [2])

#### Wind turbine rotor

Wind turbine torque, as derived from Blade Element Momentum theory is calculated as:

$$\tau_{Rotor} = C_\tau(\lambda, \theta) \frac{1}{2} \rho_{air} U_\infty^2 \pi R^3 \quad (2.2)$$

Where  $\rho_{air}$  is the air density,  $U_\infty$  is undisturbed upstream wind velocity,  $R$  is the rotor radius and  $C_\tau$  is torque coefficient which is dependent on tip speed ratio  $\lambda$  and blade pitch angle  $\theta$ .

Tip speed ratio represents the ratio between the wind turbine blade tip and undisturbed wind speed:

$$\lambda = \frac{\omega R}{U_\infty} \quad (2.3)$$

Power coefficient represents dimensionless quantity defined as ratio between aerodynamic power produced by wind turbine rotor and available power

$$C_p = \frac{P}{P_{avail}} = \frac{\tau_{Rotor} \omega}{\frac{1}{2} \rho \pi R^2 U_\infty^3} \quad (2.4)$$

In similar manner, the torque coefficient is defined as

$$C_\tau = \frac{\tau_{Rotor}}{\frac{1}{2} \rho \pi R^2 U_\infty^2} \quad (2.5)$$

From the equations 2.4 and 2.5 connection can be established between power and torque coefficient

$$C_\tau = \frac{C_P}{\lambda} \quad (2.6)$$

### Oil and water circuit

As previously explained, PD pump in the oil loop is directly coupled with wind turbine rotor so the flow rate of the pump is determined by the rotational speed of the rotor.

$$Q_{oil} = V_{p,o} \omega \eta_{v,o} \quad (2.7)$$

Where  $V_{p,o}$  is volumetric displacement of the oil pump and  $\eta_{v,o}$  is the volumetric efficiency of the pump. The flow generated by the oil pump drives the hydraulic motor who's rotational speed is determined as

$$\omega_m = \frac{Q_{oil}}{V_{p,m}} \eta_{v,m} \quad (2.8)$$

Where  $V_{p,m}$  is volumetric displacement of the hydraulic motor and  $\eta_{v,m}$  is its volumetric efficiency.

Hydraulic motor then drives the water pump which creates the high pressure flow that is similarly function of volumetric displacement of the water pump  $V_{p,w}$  and rotational speed of the hydraulic motor

$$Q_w = V_{p,w} \omega_m \eta_{v,w} \quad (2.9)$$

Where  $\eta_{v,w}$  is the volumetric efficiency of the water pump.

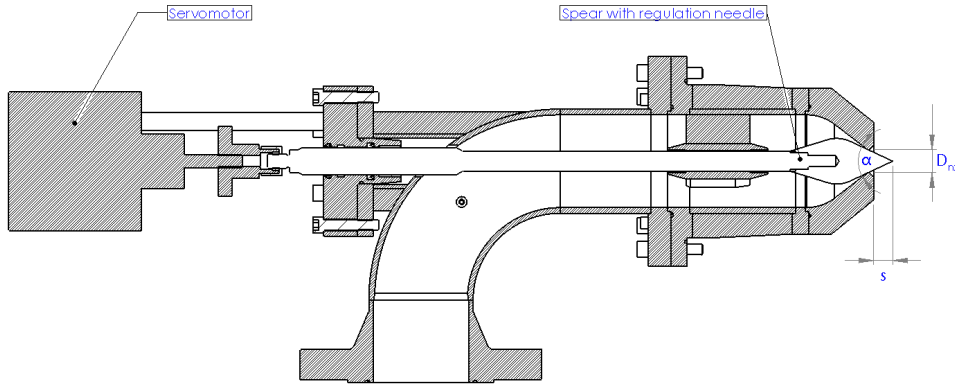


Figure 2.2: Pelton turbine injector

The pressure in the injector can be regulated by linear movement of the spear valve by using servomotor. It increases or decreases effective nozzle area by conically shaped needle. The shape of the needle is extremely important for generation of high quality jet. The main function of the spear valve is to convert water pressure energy to kinetic energy of high speed jet.[4] The effective nozzle area is calculated as:

$$A_{nz} = \frac{D_{nz}^2 \pi}{4} - (s_{max} - s)^2 \tan^2\left(\frac{\alpha}{2}\right) \pi \quad (2.10)$$

Where  $D_{nz}$  is the nozzle diameter,  $s_{max}$  is the maximum open position of the spear valve and  $\alpha$  is the needle tip angle. The discharge water pressure is calculated using the Bernoulli equation and it is defined as

$$p_w = \frac{\rho}{2} \left( \frac{Q_w}{C_D A_{nz}} \right)^2 \quad (2.11)$$

Where  $C_D$  is the discharge coefficient.

Another big advantage and important aspect of hydraulic transmission system is that it can be implemented in a way that no active control of the wind turbine is needed. Only nozzle and relief valve are used to passively control the drive train during operation to ensure that wind turbine operates with optimal parameters. Theoretical derivation and experimental investigation and validation of the passive

control method was conducted by N. Diepeveen during his PhD research[2]. So the discharge pressure created by the injector is the parameter that dictates the torque between the PD pump and hydraulic motor.

$$\tau_m = \frac{V_{p,w}\Delta p_w}{\eta_{m,k}} \quad (2.12)$$

Where  $\eta_{m,w}$  is the mechanical efficiency of the PD water pump. The pressure difference in the oil circuit is then determined as

$$\Delta p_o = \frac{\tau_m}{V_{p,m}\eta_{m,m}} \quad (2.13)$$

Where  $\eta_{m,m}$  is the mechanical efficiency of the hydraulic(oil) motor. In the end, the total counter torque opposing the rotor torque is calculated as

$$\tau_{sys} = \frac{V_{p,o}\Delta p_o}{\eta_{m,o}} \quad (2.14)$$

Where  $\eta_{m,o}$  is the mechanical efficiency of the PD oil pump.

The formulas and derivation above are for steady state drive train modelling. More detailed derivation, including modeling of dynamics of the drivetrain are given in [2] and [14].

## 2.2. Working principle of the Pelton turbines

The main focus of the project is to design and dimension Pelton turbine for offshore application. Hydraulic turbines are the state-of-the-art technology, with standard Pelton turbines reaching efficiency above 90 %. Hydro power plants with this type of turbines are usually built in the areas with high elevation and large reservoirs of water (natural or artificial) on high altitudes(generally more than 700 m above the power plant). The water from these reservoirs is then transferred through pipes towards the turbines. Pelton turbine consist of the runner with buckets, casing and injectors(see figure 2.3). Water with high pressure goes to an injector which then creates high speed jet and shoots it onto the buckets. Through interaction between the jet and rotating buckets there is conversion of energy from kinetic to mechanical and after to electrical in the generator. So generally, there are two aspects of Pelton turbine design: hydromechanics and structural mechanics. The first one ensures the maximum efficiency design while second one guarantee reliability and the lifetime of the turbine.[4]

## 2.3. Theoretical approach for Pelton turbine design

Pelton turbines are impulse machines. Velocity of a high speed jet can be over 200 m/s and the impact forces exerted on the buckets are so large that even strongest materials can't resist erosion for a longer time. Furthermore, buckets are exposed to cyclic loading due to rotation so fatigue of the material is also a problem that needs strong consideration.

There are also other aspects in the design process that require closer attention:

- Injector regulation of the flow rate
- Forces on the servomotor
- Angle between injectors
- Design of the bucket (cutout edge, exit flow condition, number of buckets, backside of the bucket)
- Casing design
- Runaway speed

The high speed jet is formed in the injector nozzle and the flow rate can be adjusted by the injector needle which is controlled by a servomotor. The flow rate is calculated as:

$$Q = \frac{d_0^2\pi}{4}C_0 \quad (2.15)$$

Jet speed  $C_0$  is defined as

$$C_0 = \phi \sqrt{2gH} \quad (2.16)$$

Where  $\phi$  is the efficiency of the nozzle and its generally in range of 0.95 to 0.98, and  $H$  is the net pressure head.

The relative velocity between the jet and the rotating bucket (figure 2.3) is a difference between the mean jet speed and speed of the bucket:

$$W_1 = C_1 - U \quad (2.17)$$

Since relative velocities at the entrance and exit of the bucket are the same, the absolute velocity at the bucket exit is calculated as

$$C_2^2 = U^2 + W^2 + UW \cos \beta_2 \quad (2.18)$$

In theory, for maximum turbine efficiency, absolute exit velocity  $C_2$  should be equal to zero giving also exit angle  $\beta_2 = 180^\circ$ . However, in practice this is never the case since the water needs to have enough kinetic energy to leave the bucket, and in the case of vertical axis Pelton turbine, enough kinetic energy to overshoot the whole wheel. This is counted as a loss of energy and it is called exit or swirling loss. In practical applications exit angle  $\beta_2$  is around  $170^\circ$ . Another reason for this, beside above mentioned, is back-splashing of the bucket that follows. The water that exits the first bucket can impinge on the following one and cause a counter torque which decreases the efficiency of the turbine.

In terms of the speed ratio, in principle, the highest efficiency is achieved for

$$k = \frac{U}{C_0} = 0.5 \quad (2.19)$$

so for maximum efficiency, Pelton turbine should work at this operating condition.

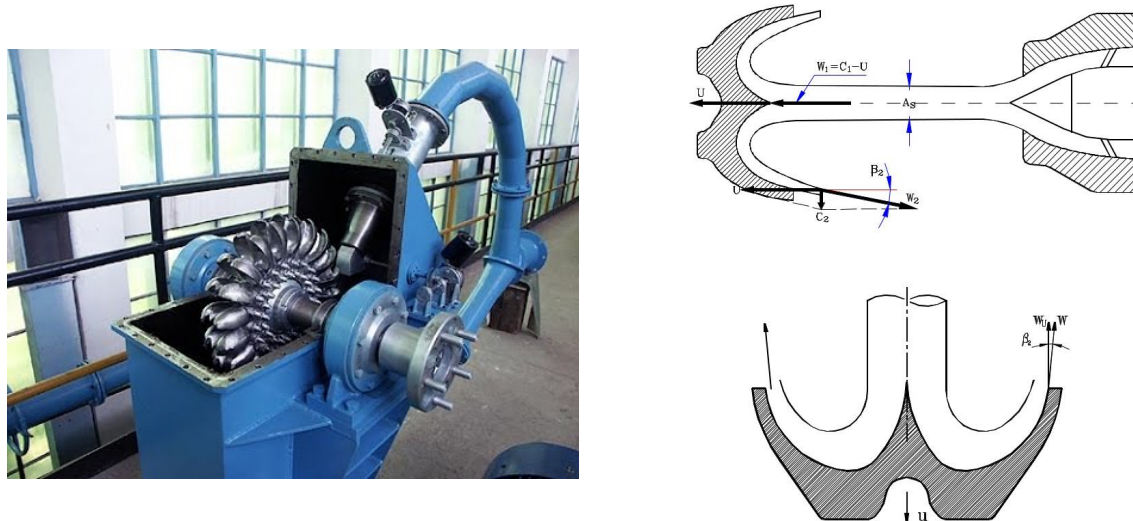


Figure 2.3: Pelton turbine with two injectors and the jet-bucket flow interaction (Taken from [4]).

Calculation of the size of the Pelton runner and size of its buckets is the first step in the design process. Few of the most important geometric parameters are: Pitch circle diameter  $D_m$ , wheel bucket inner diameter  $D_b$ , wheel diameter  $D_a$ , bucket inner width  $B$  and bucket exit angle  $\beta_2$ . These and other geometric parameters are given in figure 2.4.

Design and dimensioning of the Pelton wheel is usually based on design flow rate and net pressure head. Furthermore, rotational speed of the generator, hence number of pole pairs, represents also important parameter for the design process.

For the design of hydraulic turbines dimensionless numbers are used to determine size and flow performance of the machine. When designing Pelton turbine, few parameters play important role (Following equations are taken from Zhang[4]).

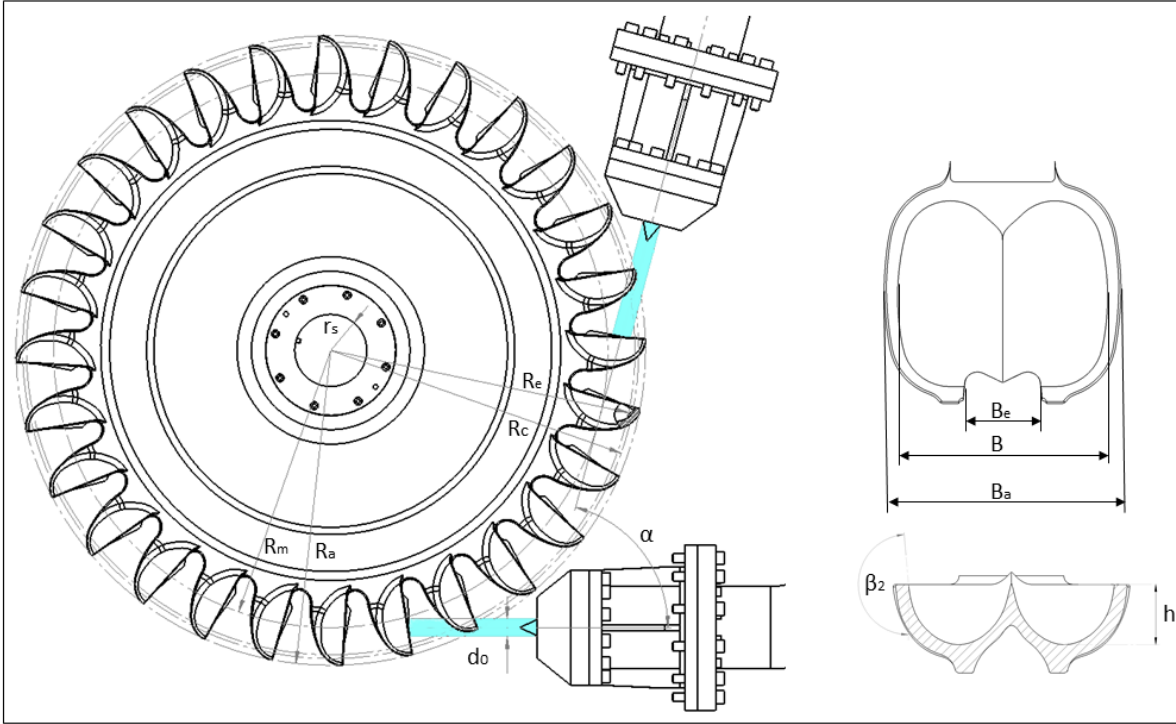


Figure 2.4: Geometric specifications of the Pelton wheel.

**Bucket Volumetric Load** represents the flow rate in the dimensionless form and also ratio between jet diameter  $d_0$  and bucket inner width  $B$ . That is why it is so convenient for determination of bucket width.

$$\varphi_B = \left( \frac{d_0}{B} \right)^2 \quad (2.20)$$

Bucket width is usually designed so that jet diameter at nominal or maximal flow rate does not exceed one-third of the bucket width. So optimum bucket volumetric load coefficient is usually between 0.09 and 0.11. [4]

**Specific Speed** is one of the most important parameters in hydraulic turbine design. It is given in dimensional form for Pelton with multiple injectors as:

$$n_q = n \frac{\sqrt{Q}}{\sqrt{z_{jet}} H^{3/4}} \quad (2.21)$$

Where  $z_{jet}$  is the number of injectors. The unit is [1/s], for normalized flow rate  $Q$  and net pressure head  $H$ .

Furthermore specific speed also represents diameter ratio

$$n_q = 2.63 k_m \sqrt{\varphi_B} \frac{B}{D_m} \quad (2.22)$$

so it is perfectly suited for dimensioning the diameter of the Pelton wheel (specifically pitch circle diameter  $D_m$ ). As specific speed can be determined from flow rate and net pressure head for nominal conditions from the last equation pitch circle diameter can be determined.  $k_m$  parameter is constant which will be explained below.

**Peripheral Speed Coefficient**  $k_m$  is the ratio between peripheral speed  $U_m$  defined on the pitch circle diameter  $D_m$  and jet speed  $C_0$  defined at the exit of the nozzle:

$$k_m = \frac{U_m}{C_0} = \frac{U_m}{\sqrt{2gH}} \quad (2.23)$$

It determines hydraulic efficiency of the Pelton turbine and for optimal conditions it should be set between 0.45 and 0.48.

**Characteristic bucket position angle**  $\alpha$ , as given in figure 2.5 is the angle where bucket cut-out edge intersects jet on the jet axis. It is determined as

$$\cos\alpha_0 = \frac{k_m\sqrt{\varphi_B}}{k_m\sqrt{\varphi_B} + 0.32n_q} \quad (2.24)$$

And for nominal conditions with  $k_m = 0.47$  and  $\varphi_B = 0.11$  it is given as

$$\cos\alpha_0 = \frac{1}{1 + 2n_q} \quad (2.25)$$

It is used for calculating real efficiency curve and runaway speed.

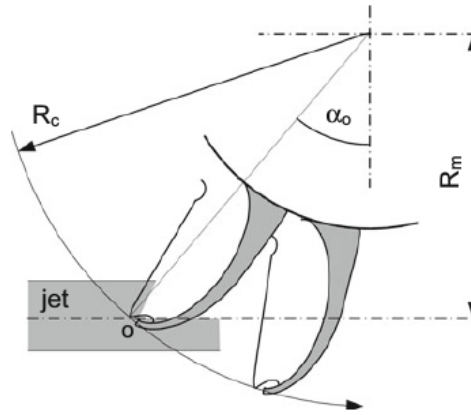


Figure 2.5: Characteristic bucket position angle (Taken from [4]).

**Peripheral speed of the bucket cut-out edge** represents the ratio between peripheral speed  $U_c$  and jet speed  $C_0$  according to:

$$\frac{U_c}{C_0} = k_m(1 + 2n_q) \quad (2.26)$$

The Pelton turbines can be installed with vertical and horizontal axis. The horizontal axis turbines are suitable for not more than two nozzles, while for multiple nozzles vertical axis Pelton turbines are used. From that reason our choice will be Pelton with vertical axis.

Number of buckets can be determined as a function of peripheral speed coefficient and specific speed:

$$N = \frac{\pi(2\lambda - 1)}{k_m\sqrt{n_q(1 + n_q)}} \quad (2.27)$$

Where  $\lambda$  is multi-bucket factor which determines how many buckets are in the same time under the impingement of a full jet. On the other hand, number of buckets can be determined using empirical formula as well:

$$N = 15 + 1.3\frac{k_m}{n_q} \quad (2.28)$$

The design and optimization of Pelton turbines has been mostly done by experimental investigations and model tests because of the flow complexity of the jet - runner interaction, which hasn't been completely understood before. Centrifugal and Coriolis forces are the main driving forces of the water flow in the Pelton turbines. Coriolis force is normal to the flow, while centrifugal force is independent of the flow (See figure 2.6).

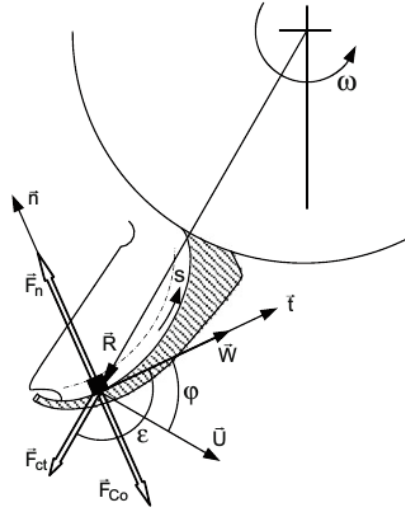


Figure 2.6: Forces exerted on the moving bucket (Taken from [4]).

Centrifugal force  $\vec{F}_{ct}$  is dependent on the radius  $r$  and rotational speed of the runner  $\omega$  and it is given

$$\vec{F}_{ct} = \vec{\omega} \times (\vec{\omega} \times \vec{r}) \quad (2.29)$$

Coriolis force  $\vec{F}_{co}$  is dependent of the flow and rotational speed of the runner  $\omega$ . It can be calculated as

$$\vec{F}_{co} = -2\vec{\omega} \times \vec{W} \quad (2.30)$$

Where  $W$  is the relative flow velocity at the bucket surface.

There is also a reaction force from the bucket surface  $\vec{F}_n$ , which is normal to the surface. Hence the governing equation for the fluid flow in the rotating bucket is derived from the momentum law:

$$\frac{d\vec{W}}{dt} = \frac{d\vec{W}_t}{dt} \vec{t} + \frac{W^2}{r_b} \vec{n} = \vec{F}_{cf} + \vec{F}_{co} + \vec{F}_n \quad (2.31)$$

It can be seen, from the equation 2.31, that the acceleration of the flow occurs in the flow direction and direction perpendicular to the bucket surface. The main driving force is the pressure force which is perpendicular to bucket surface and according to equation 2.31 it is equal to:

$$F_n = \frac{W^2}{r_b} - \vec{F}_{co} \cdot \vec{n} - \vec{F}_{ct} \cdot \vec{n} \quad (2.32)$$

Only the components in the direction of the bucket motion are contributing to the power, hence:

$$\dot{e} = F_n(-\vec{n}) \cdot \vec{U} = -\frac{W^2}{r_b} \vec{n} \cdot \vec{U} + (\vec{F}_{co} \cdot \vec{n}) \vec{n} \cdot \vec{U} + (\vec{F}_{ct} \cdot \vec{n}) \vec{n} \cdot \vec{U} \quad (2.33)$$

Specific work then can be calculated by integrating above equation

$$e = \int_0^t \dot{e} dt \quad (2.34)$$

so the power contribution is then found as

$$P_{jet} = \dot{m}_{jet} e_2 \quad (2.35)$$

In order to guarantee safe exit of the water from the bucket without back-splashing of the following bucket, which might generate counter-torque, one must satisfy the following condition:

$$\frac{h_a}{T_p \tan(\beta_2)} < 1 \quad (2.36)$$

Where  $h_a$  is the joint thickness of the water sheet and bucket wall thickness at the bucket exit,  $T_p = T_u + T_c$  is the pitch length between two buckets and  $\beta_2$  is the relative velocity exit angle. These parameters are depicted in figure 2.7. Bucket pitch length can be calculated as

$$T_p = \frac{\pi D_m}{N} \quad (2.37)$$

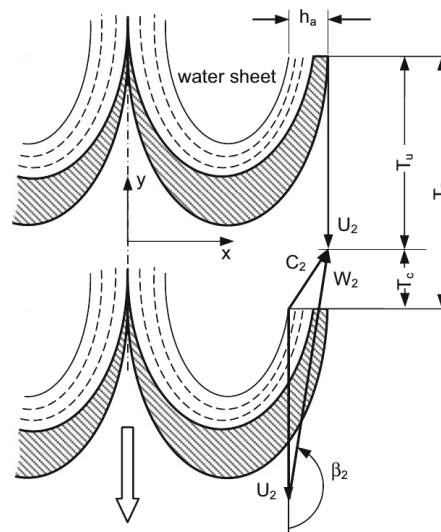


Figure 2.7: Exit flow conditions (Taken from [4])

For the vertical installations, exit flow in the upper half of the bucket acts against the gravity, so special exit conditions need to be considered in this case. Water exiting the bucket in the upper half needs to have enough kinetic energy to overshoot complete wheel and not fall back on it (Figure 2.8). Two areas can be distinguished here: bucket root area and bucket cut-out area.

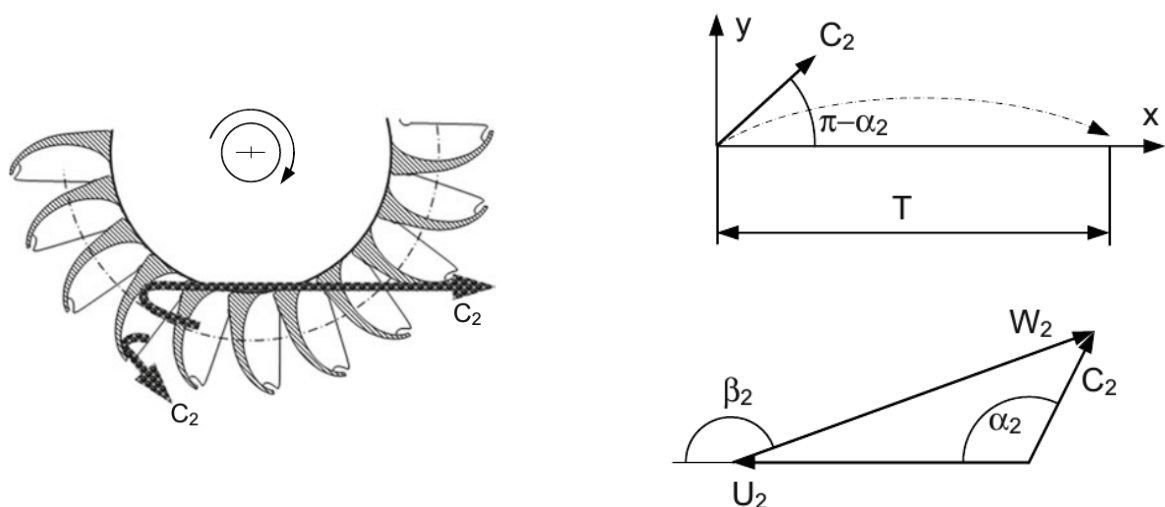


Figure 2.8: Exit flow conditions at bucket root and cut-out area and flow overshoot (Taken from [4]).

To make sure that water will leave root area, one should calculate minimum exit velocity  $C_2$ :

$$C_{2x}^2 = -\frac{gT}{2\left(\frac{h_a}{T} + \tan(\alpha_2)\right)} \quad (2.38)$$

Where  $T$  is the distance that water particle needs to travel in order to leave the runner area and  $\alpha_2$  is the angle between peripheral speed  $U_2$  and absolute velocity  $C_2$ .

To ensure that water will leave the cut-out area condition for the maximum peripheral speed coefficient should be fulfilled

$$k_{m,max} = 0.5 - 0.38n_q \quad (2.39)$$

However the loss due to water falling back on the runner is in general not higher than 1% so the value for peripheral speed coefficient can sometimes be little higher than the maximum value calculated above.

### 2.3.1. Losses in the Pelton turbine

There are several sources of losses in the Pelton turbines [4].

- **Swirling losses** - flow exit velocity is higher than zero so that water can freely leave the bucket. This unused kinetic energy is characterized as loss. These losses make up around 1% of the total power generated.
- **Bucket rear side impingement losses** - if there is a back-splashing of water on the following bucket it can cause counter-torque on the shaft and also deflection by the bucket back-side. This can result in decrease in efficiency of the turbine. Order of magnitude of these losses is over 1%.
- **Friction losses** - are losses caused by the friction between bucket surface and water flow. The friction is the source for the biggest losses in the turbine and they are around 5%. The highest turbine efficiency can be achieved by lowering the friction coefficient of the bucket surface hence making bucket as smooth as possible.
- **Air friction and windage losses** - these losses are the consequence of the friction between the buckets and air that surrounds them. They are dependent on runner size, rotational speed and turbine casing and are around 0.5%.
- **Bearing friction losses** - these losses are consequence of friction in hydrodynamic plain bearings which are commonly used in Pelton turbines.

### 2.3.2. High speed jet flow

Formation of jet and flow of water in the bucket of Pelton runner is very complex. Not until recently these two flow phenomena have been properly analyzed and understood. They are the most important pieces in understanding interaction between jet and rotating bucket of the Pelton runner. This is important for the assessment of turbine efficiency and how the jet properties influence the efficiency. Furthermore, this is necessary in order to properly dimension the runner as well as the other parts of the Pelton turbine. For example, the angle between injectors needs to be larger than a certain value so that jets from neighboring injectors don't intersect. If this happens the turbine will operate with lower efficiency and the blades can be damaged. Also minimizing force fluctuations during the jet impact is highly important not just from structural reasons but also for achieving highest efficiency. Knowing the forces that govern the flow and understanding the flow processes of jet-bucket interaction this simplifies the design procedure and calculation of design parameters for the Pelton turbine. Luckily, in recent years, there was some advancement in this area, hence design of Pelton turbines today does not solely rely on experiments and model tests but also has a solid theoretical understanding and backup. [18]

### 2.3.3. Stresses in the bucket of a Pelton turbine

Pelton turbines are generally used for pressures above 50 bar. The biggest and the most powerful Pelton turbines ever produced, as mentioned before, are turbines for Bieudron hydro power plant in Switzerland. The pressure head is 190 bar and output of each unit is 423 MW. Building of this plant has

pushed engineering to its limits and brought breakthroughs, new developments and new design tools in the field. Main parts of the Bieudron turbines, runner, distributor, injector and valves were optimized using Finite Element Analysis and the results were compared and verified by laboratory measurements. The runner stress analysis was done by measuring pressure distribution on the rotating bucket for the first time in history. [19] [20]

Design and development of Pelton turbines for pressures above 200 bar poses additional challenge for engineers and manufacturers. The upper limit for pressure comes from the structural mechanics of a Pelton turbine because of the fatigue and cracking of the buckets near the root region due to cyclic pressurizing during rotation of the runner. This can be even more expressed for the DOT concept because Pelton turbine will have to operate with variable pressure. The stresses in the bucket material are limited to around 200 MPa in order to allow the crack to penetrate the plate and cause leakage which will be detected before unstable rupture. This criterion is safety factor and it is called LEAKAGE BEFORE RUPTURE. This is applied so that crack can be detected in time before it becomes unstable and starts increasing with a speed of sound.[21]

#### 2.3.4. Influence of seawater conditions on a Pelton turbines

There is not much research about application of Pelton turbines in seawater conditions. There are some other types of hydraulic turbines which have been used in these conditions. For example, axial turbines used for harnessing tidal energy or pump-turbines used for seawater pumped-storage (e.g. the power plant in *Okinawa Island, Japan*). These examples can be very helpful in designing turbine for this project as well. The materials and anti corrosive measures for turbine and other corrosive material are already tested and applied for these projects. Problem with seawater is corrosion of the equipment caused by the salt in the water and adhesion of marine life to pipes, pumps and turbines. One possible solution suggested is using mild carbon steel coated with paint for low-speed flow parts and using stainless steel for high-speed flow parts. Cathodic protection should be used for corrosion due to cracks and paint damage.

Another problem that will be considered is adhesion of marine organisms to the pipes, pumps and turbines because it can reduce the efficiency of the system. It is found that they stick more easily if the flow speeds are low rather than high. Hence the parts of the system where water is more stagnant have higher risk in getting contaminated with marine organisms. Applying material or coating that repel water can prevent most of the organisms to stick to the surface.[22]

Since Pelton turbines require elevated water reservoir, their seawater application was never really considered. DOT wants to show that using Pelton turbines in combination with hydraulic pumps and wind turbines in offshore conditions is not just feasible but also profitable in terms of lowering the cost of electricity production. The design experience from Bieudron plant as well as from the other projects will be extremely valuable for the design of Pelton turbine for DOT concept. However, specific conditions which DOT turbine will be exposed to will require some new solutions outside standard design procedures.

### 2.4. Experimental investigation of the flows inside the Pelton turbines

In the past, Pelton turbine manufacturers have mostly relied on experiments and scaled model tests. The main reason for this was lack of theoretical knowledge about hydrodynamics of Pelton turbines. Although recent breakthroughs and technological developments, both in theory and computational fluid dynamics, gave us other tools for designing more efficient machines, we are still not quiet there to use these tools as standalone but only together with experimental validation. That is why experimental research and model tests still play important role in turbine design. This is especially the case for design of Pelton buckets.

For the bucket design, as previously mentioned, two approaches or test set-up's are mainly used:

- Fixed bucket
- Rotating bucket

Furthermore, quality of the high speed jet is of most importance for the total efficiency of the Pelton turbine. Experimental investigations of the jet can give us a better insight in the structure and the

shape of the jet as well as which parameters have the influence on its quality. All this information can be extremely valuable for the design of distributor and injector (nozzle, spear).

These three experimental approaches, mentioned above, are discussed in the following sections in more details.

#### 2.4.1. Experimental investigations on a fixed bucket configuration

Results gained from tests on a fixed bucket, in practice, can not be considered valid for the rotating bucket. However, partial optimization of the bucket edge and cutout can be carried out. In practice, results obtained from measurements on a fixed bucket are mostly used for validation of numerical stimulation models.

Some of the phenomena which are not considered with fixed bucket set-up are: Centrifugal and Coriolis forces, impingement of the following bucket and unsteady feeding.[5] Furthermore, cyclic loading of the bucket due to rotation and its influence on the fatigue of the bucket material and dynamic stability of the whole turbine can not be investigated with this configuration.

On the other hand, this kind of set-up is relatively easy to build, less time consuming and lot cheaper than set-up with rotating buckets. It can provide information on maximum jet impact force that the buckets are exposed to (maximum force is exerted when the peripheral speed of the runner is equal to zero, meaning the runner isn't rotating - usually during start-up) and thus give a fair estimate of the stresses in the bucket root area which is exposed to the highest stresses during turbine operation.

Over the years numerous studies were conducted on the fix bucket configuration. These investigations included measurements for determination of the pressure distribution at the bucket surface, maximum force on the bucket, determination of water-air interface location in the bucket or water film thickness and flow visualization. For pressure distribution measurements on a fixed bucket, pressure gauges were utilized by drilling the holes for pressure intakes at multiple locations on the inside of the bucket(Figure 2.9). The incidence angle at which jet impinges the bucket can be changed by rotating the bucket or injector.

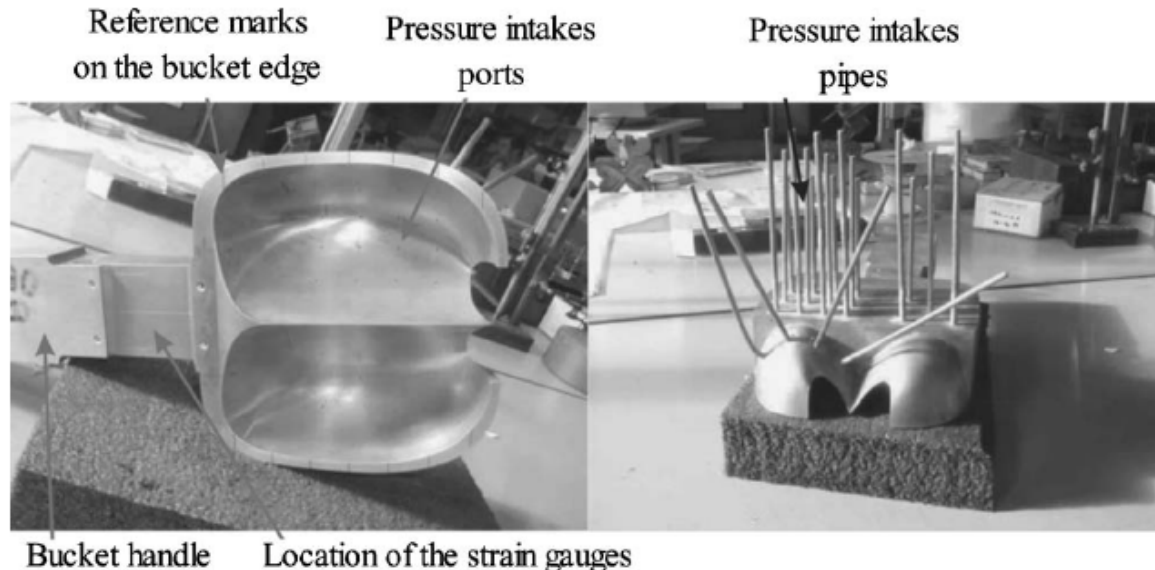


Figure 2.9: Locations of pressure intakes for pressure distribution measurements (Taken from [5])

As an example, in one paper, authors were conducting several measurements, on fixed bucket configuration, with different jet diameters and several hydraulic heads[5]. The pressure distribution and total forces on the bucket were acquired. The pressure measurements were achieved by means of pressure intakes placed on 16 locations on the left half of the bucket and 5 intakes on the right half to measure and ensure flow symmetry and jet alignment. Intakes were than connected via straight tubes with differential pressure transducers. The thrust and torque were measured by placing 8 strain

gauges on the bucket handles(4 gauges on the each side). Flow visualization was also conducted using a numerical camera. The experimental results showed that head variation doesn't have a significant influence on the pressure distribution at the bucket inner surface. Variation of the incidence angle of the jet and nozzle diameter, influences the leakage through the cutout edge. Leakage is increasing with increasing nozzle diameter and increasing incidence angle. All the measurement results were used to show the accuracy of numerical methods that were developed during previous years.

Kvicinsky also did an experimental and numerical investigation on a fixed Pelton turbine bucket by means of pressure distribution and water sheet thickness measurement [13]. First test was conducted with the single injector shooting onto the fixed plate. The advection of water was studied by changing the inclination angle of the plate. The pressure distribution on the plate was measured by means of 29 pressure taps which are drilled in the plate. The water sheet thickness is measured by means of laser and image processing. The second test was conducted with the fixed Pelton bucket. The same measurements as for the fixed plate are done here as well. However, for the first time, piezo-resistive pressure sensors, directly embedded into the bucket surface, were used for measuring the pressure distribution inside the Pelton bucket. The water sheet thickness was measured with the same technique as for the fixed plate, just with a slightly modified test rig.

Both of these tests were used for comparison and validation of numerical simulations.

#### 2.4.2. Experimental investigations on a rotating bucket configuration

For the complete bucket design optimization, tests should be done with rotating bucket (whole runner with buckets). This way Coriolis, centrifugal and inertial forces are included as well as different phenomena occurring during operation, like: bucket back splashing, unsteady feeding, Coanda effect and cyclic loading of the bucket due to rotation. Furthermore, real pressure distribution inside the bucket surface can be measured, as well as the real stresses that bucket is exposed to during impingement of the high speed jet.

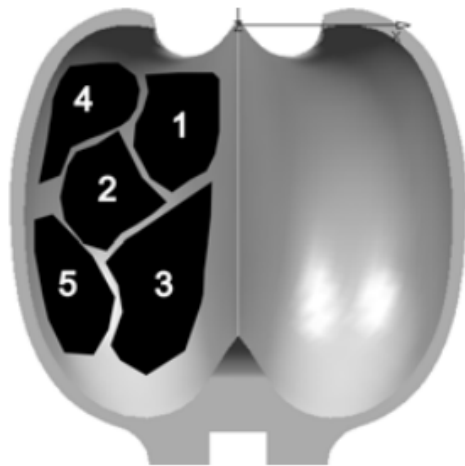


Figure 2.10: Locations of five pressure zones[6]

visualization is provided as well. Results were compared with numerical analysis and showed a good agreement.

Perrig with a group of authors[7], conducted similar numerical simulation and experimental measurements on the rotating bucket, also defining five zones with different flow pattern and different pressure signals. Furthermore, they analyzed the flow patterns in all zones and determined the zones which have most contribution to the torque. The torque contribution from each zone was calculated by projecting local surface normal pressure of elementary area  $A_k$  on the local peripheral direction. Power contribution was found by multiplying torque contribution with angular velocity.

$$P_i = \left[ \sum_{k=1}^m \vec{r}_{ik} \left( \int_{A_{ik}} p_{ik}(t) \vec{n}_{ik} dA_{ik} \right) \right] \cdot \vec{\omega} \quad (2.40)$$

It is noticeable, from figure 2.11, that most contribution to the torque or most power exchange

In the past, due to difficulty in measurements and high expenses, pressure measurements and flow visualization are mostly done on a fixed bucket. Development of new measurement techniques and instrumentation allowed that the pressure distribution and the flow inside the buckets can be measured in real conditions with rotating buckets. One of the first pressure measurements on the rotating buckets are conducted in 1998 by installing several piezo-electric sensors inside the bucket surface.[23]

In 2002, Kvicinsky[6] conducted a complete experimental analysis on a rotating bucket by means of measuring unsteady pressure distribution by placing 32 piezo-resistive sensors inside the bucket surface. Several operational points were tested and five zones which corresponds to five different signal characteristics have been spotted (Figure 2.10). The flow visualization is provided as well. Results were compared with numerical analysis and showed a good agreement.

comes from zones 1 and 2. According to the authors this is because these two zones are under direct impingement of the jet when the bucket starts cutting the jet and when the available kinetic energy is at maximum (total kinetic energy of the jet).

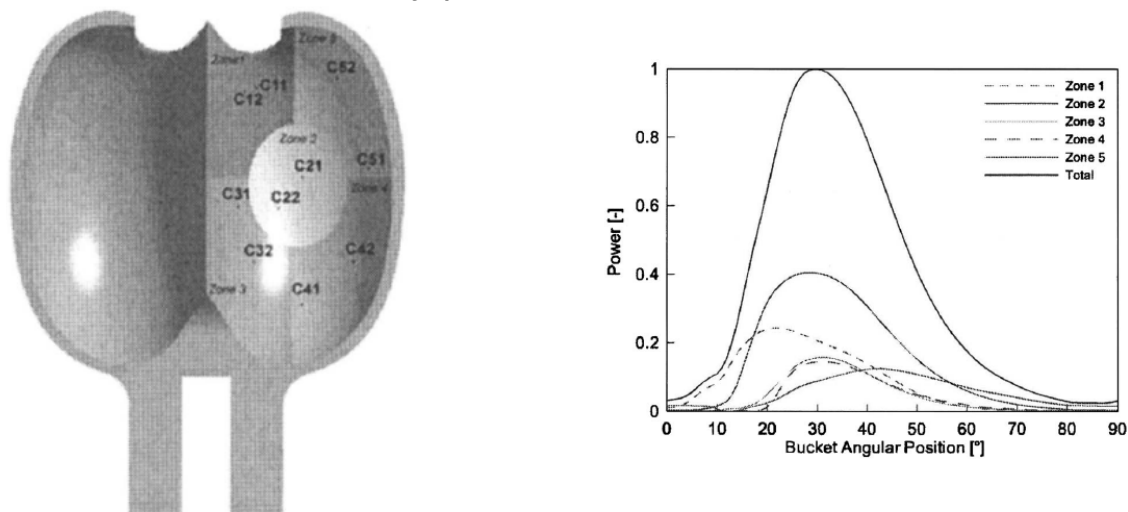


Figure 2.11: Pressure zones in the bucket and their individual contribution to the power exchange with respect to the bucket angular position [7].

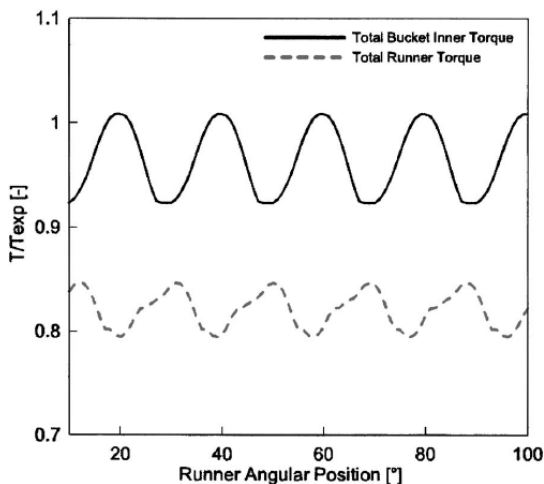


Figure 2.12: Contribution of the bucket backside to the total torque with respect to runner angular position [7].

Furthermore, zone 2 is more than 2/3 of the time exposed to pressure and contributes to more than 40% of the bucket torque. Also the most of the power exchange happens when the bucket is at angular position around  $30^\circ$ , where zones 2 – 4 have maximum power contribution.

The contribution of the backside of the bucket was investigated as well (Figure 2.12). It was concluded that close to the cutout edge, backside of the bucket contributes to the total torque of the runner. This is ascribed to Coanda effect [24], which is phenomenon emerging when jet is passing next to a convex surface. The pressure between the solid surface and surface of the jet is then reduced so jet tends to stick to the surface and follow its curvature. Although contributing to the torque, some experiments reported that lowering the pressure due to Coanda effects can cause cavitation pitting and erosion close to cutout edge, so special attention should be devoted for the design of the backside surface of the bucket in order to avoid cavitation.

In his PhD thesis [8], Alexandre Perrig, conducts three types of experimental investigations of the rotating bucket under normal operating conditions: unsteady wall pressure measurements with 43 piezo-resistive pressure sensors (embedded in the bucket inner surface, backside and on the sides), thickness of the water film and flow visualization with several endoscopes (one mounted and rotating with the bucket and others fixed with the casing, see figures 2.15 and 2.16). The test were carried out on a model Pelton turbine with a single injector. Several operating points were investigated.

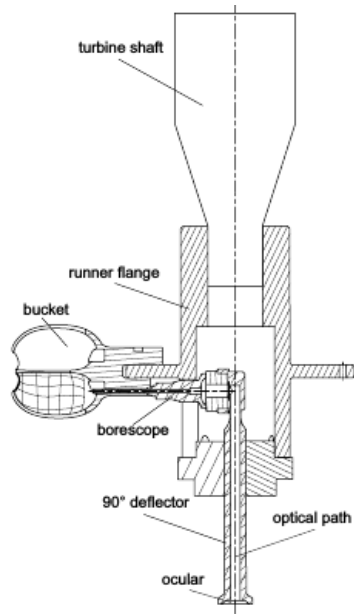


Figure 2.13: Location of endoscope for relative flow measurements [8].

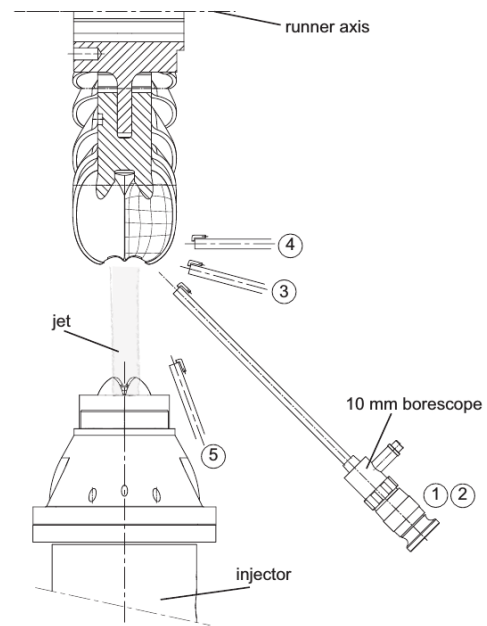


Figure 2.14: Locations of external endoscopes [8].

As in previous article, power budget and power contribution of five distinct zones are determined. Zones 1 and 2 contribute the most to the power budget, as they are under direct jet impingement at the start of the cycle when kinetic energy of the flow is the highest. Zone 2 contributes 2/3 of the power budget, while zone 5 has the highest contribution duration of over 2/3 of full cycle time.

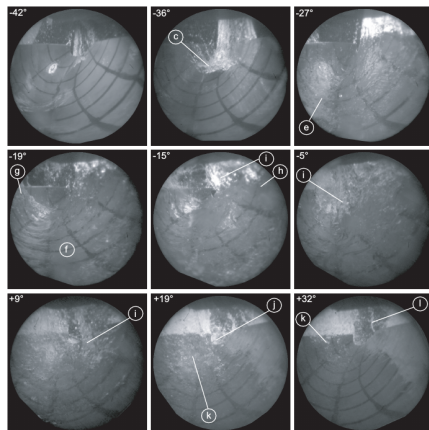


Figure 2.15: Example of onboard endoscope bucket flow visualization [8].

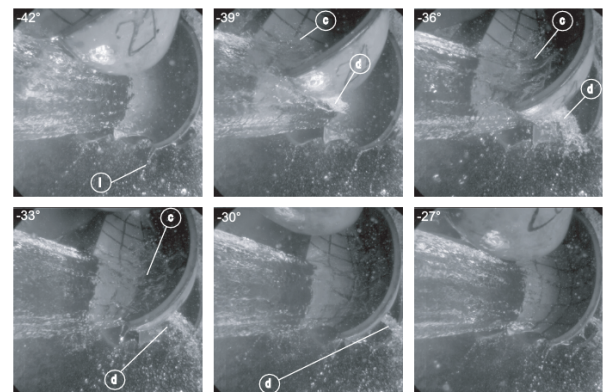


Figure 2.16: Example of external endoscope bucket flow visualization [8].

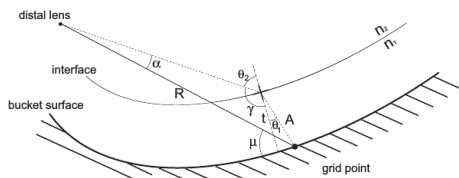


Figure 2.17: Simplified optical model [8]

Water thickness was determined from the refraction law by assuming simplified optical model 2.17. From the Sine Theorem and Snell's law, the thickness is calculated as:

$$t = \frac{R \cos \theta_1}{\sin(\theta_2 - \theta_1)} \sin \alpha \quad (2.41)$$

### 2.4.3. Experimental investigations of a high speed jet flow

Pelton turbines are high efficiency machines that can today achieve over 90% of hydraulic efficiency. Amongst other things, quality of the jet plays important role in achieving this high efficiency.[4] The

part responsible for creating a high quality jet is called an injector (figure 2.18). The role of the injector is to convert the pressure energy at the inlet to pure kinetic energy in form of a high speed jet. It mainly consists of the nozzle, spear with regulation needle and the servomotor for controlling the spear position.

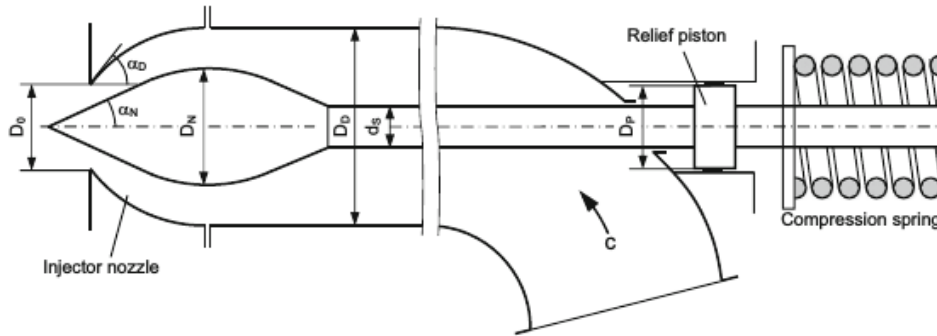


Figure 2.18: Injector with external servomotor (Taken from [4])

Servomotor can be mounted externally or internally. The later set-up is not that common because it requires mounting servomotor inside the pipe which significantly aggravates construction and makes access for maintenance or any other work more difficult. On the other hand, external set-up gives a much more control and access, thus simplifying the whole construction. However in order to put the servomotor outside the pipe, the pipe itself needs to be bent before the nozzle which influences the flow reaching the nozzle and thus the structure of the jet.

Experimental investigation of the jet, in the past, mostly relied on standard measurements of the jet axial velocity distribution by using Pitot tube or jet flow visualization using photography. In 2000, Zhang develops Dual Measurement Method (DMM) for measuring velocity distribution inside the high speed jet by using Laser Doppler Anemometry(LDA) method [?] [25] [10]. This method allows to measure axial velocity distribution in the jet more accurately, as well as the secondary flows occurring in the jet due to non-uniform flow caused by the bend before the nozzle.

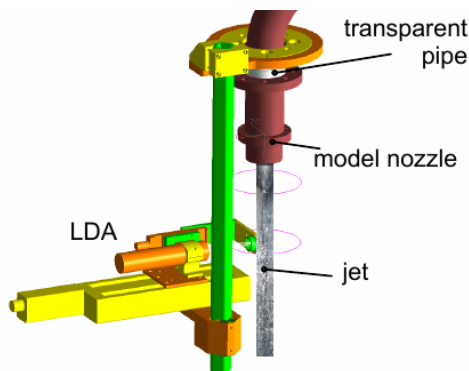


Figure 2.19: Dual measurement method set-up[9]

Zhang and Parkinson conducted measurements of the velocity distribution just behind the pipe bend and in the high speed jet using DMM method. To ensure optical access to the flow in the pipe behind the bend, they inserted a small transparent piece of pipe made from Plexiglas. For measurement of the jet velocity distribution dynamic unsteady behavior of the jet surface, due to turbulent energy exchange with surrounding air, makes the measurement with the LDA extremely difficult. For this reason, small piece of plexiglass was set next to the jet surface so to allow for the laser beam to propagate through it. The magnitude of the secondary flow in the jet is significantly lower than the primary flow (axial), so this is the main reason for

difficulty in the measurements of the jet tangential velocity field. Dual Measurement Method is based on two separate measurements with LDA in order to calculate the error in optical alignment so it can be corrected accordingly.[10]

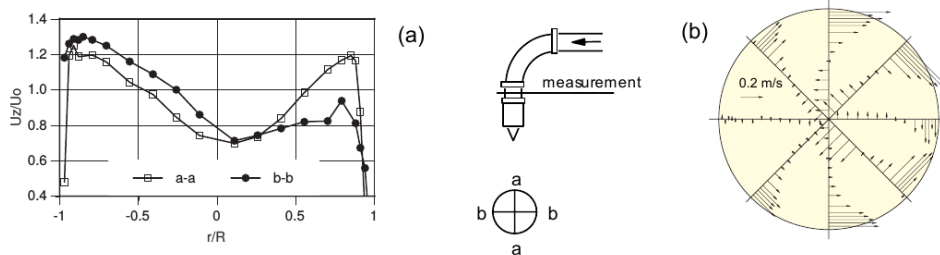


Figure 2.20: Velocity distribution in the pipe (Taken from [10])

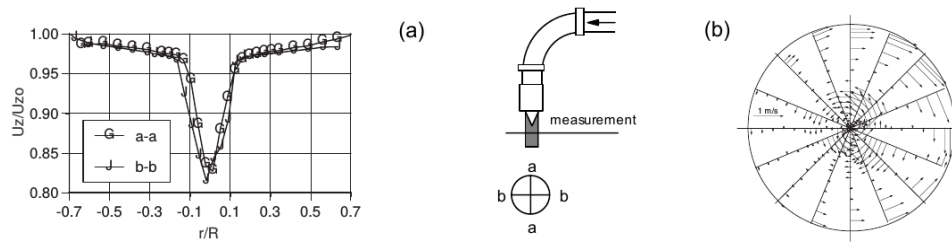


Figure 2.21: Velocity distribution in the jet (Taken from [10])

The results from both measurements are shown in the figures 2.20 and 2.21. It can be seen from the first figure that the tangential flow in the pipe after the bend has two rotational flows which are oriented in the opposite direction and thus collide on one side of the pipe. Furthermore, the existence of the core with velocity deficit is evident from the axial velocity distribution in the pipe. This is, according to authors, consequence of the nozzle influence.

The axial velocity deficit is lot more expressed in the core of the jet itself. It is a direct consequence of the wake from the needle surface. Tangential velocity distribution in the jet cross-section shows that secondary flows in the jet arise from the non-uniform velocity distribution at the injector inlet, caused by existence of the bend. The flow structure is similar to the one from the pipe with slightly increased rotational velocity in the core.

The existence of the secondary flows in the jet can cause shift of the jet core [25] which might influence the jet misalignment with the bucket cutout and thus uneven spreading of water in the bucket halves. Furthermore, it can manifest a disturbance at the jet surface in terms of water droplets spreading away from the jet. This disturbance influences the quality of the jet and hence the efficiency of the Pelton turbine.

The quality of the jet is of most importance for the efficiency of the turbine. Many things like nozzle geometry, needle geometry, roughness of both needle and nozzle surfaces, local resistance before the nozzle (bend), nozzle control, pressure variation can influence the structure of the jet and thus its quality. For the development of the accumulator system for the pulsating Pelton nozzle technology tests were conducted at the Waterpower Laboratory at the Norwegian University of Science and Technology. For this kind of technology, nozzle is configured so that it opens and closes several times per second. This in return creates high pressure pulsations between nozzle and upper reservoir through the penstock.

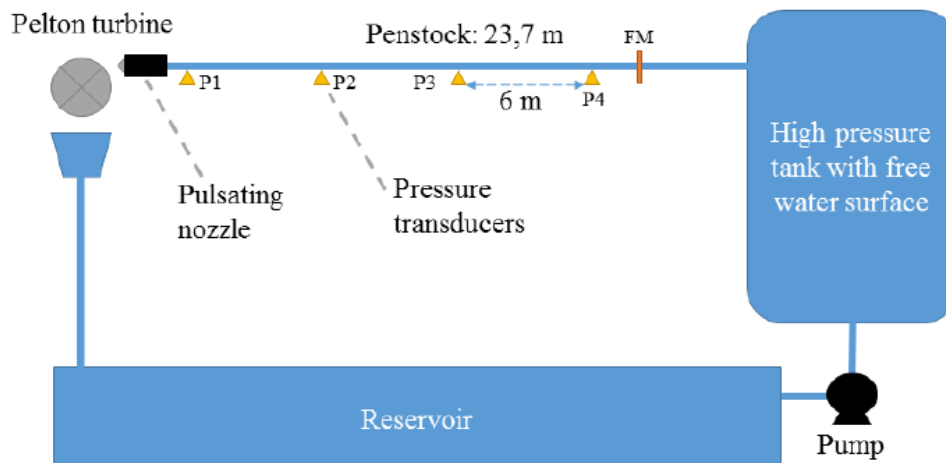


Figure 2.22: Test set-up for pulsating nozzle technology (Taken from [11])

The idea is to open the nozzle when pressure pulsation returns from the reservoir and thus creating water projectile which then hits the bucket with high speed. High speed camera is set in front of the nozzle to record the pulsating jet.

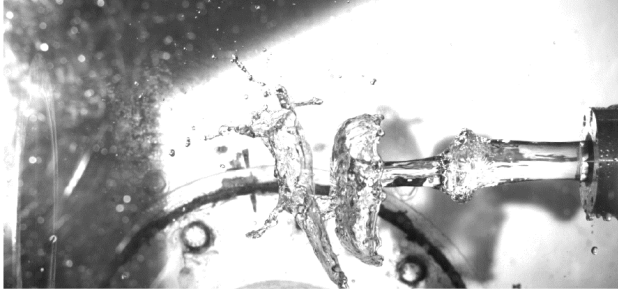


Figure 2.23: Flow visualization of the jet[11]

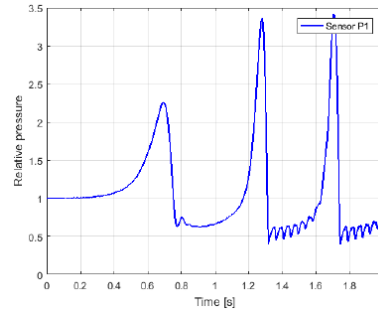


Figure 2.24: Pressure transducer signal[11]

The experiments were done with different frequencies of opening and closing of the nozzle. Figure 2.24 shows the pressure peaks and oscillations due to opening and closing of the nozzle. Authors reported a standing wave after these oscillations and identify this frequency as a dominating natural frequency of the system. The instabilities in the jet captured in the figure 2.23 are according to the authors consequence of this standing wave.[11]

These results give an interesting insight in the behavior of the jet due to pressure variation at the inlet of the injector. This might be the case for the DOT concept if the assumption of the pressure variation due to displacement pump prove to be true. Pressure measurements and jet flow visualization in the next part will give an answer if this problem exists and if so, a better understanding of how does it influence the efficiency of the turbine and how can it be mitigated.

## 2.5. Numerical investigation of the flow inside the Pelton turbines

Numerical analysis is the newest approach in scientific research. It uses numerical approximation of mathematical equations to find a solution for some physical problems described by those mathematical models. As computer technology develops, this approach becomes more important in everyday research and aims to one day completely replace expensive experimentation.

### 2.5.1. Governing equations of fluid dynamics

All equations of fluid dynamics are derived from three main laws of physics.

- CONSERVATION OF MASS
- NEWTON'S SECOND LAW
- CONSERVATION OF ENERGY

Since the main focus of this thesis isn't fluid dynamics or CFD the main equations of fluid dynamics will just be written here without any derivation. The author refers to following literature [26] and [27] for derivation and in depth explanation.

- CONSERVATION OF MASS → **CONTINUITY EQUATION**

$$\frac{\partial \rho}{\partial t} + \nabla \cdot (\rho \vec{U}) = 0 \quad (2.42)$$

- NEWTON'S SECOND LAW → **MOMENTUM EQUATION**

$$\frac{\partial \rho u}{\partial t} + \nabla \cdot (\rho u \vec{U}) = -\frac{\partial p}{\partial x} + \nabla \cdot (\mu \nabla u) + S_{M_x} \quad (2.43)$$

$$\frac{\partial \rho v}{\partial t} + \nabla \cdot (\rho v \vec{U}) = -\frac{\partial p}{\partial y} + \nabla \cdot (\mu \nabla v) + S_{M_y} \quad (2.44)$$

$$\frac{\partial \rho w}{\partial t} + \nabla \cdot (\rho w \vec{U}) = -\frac{\partial p}{\partial z} + \nabla \cdot (\mu \nabla w) + S_{M_z} \quad (2.45)$$

• CONSERVATION OF ENERGY → **ENERGY EQUATION**

$$\begin{aligned} \frac{\partial \rho e}{\partial t} + \nabla \cdot (\rho e \vec{U}) = & -p \nabla \cdot \vec{U} + \nabla \cdot (k \nabla T) + \tau_{xx} \frac{\partial u}{\partial x} + \tau_{yx} \frac{\partial u}{\partial y} + \tau_{zx} \frac{\partial u}{\partial z} \\ & + \tau_{xy} \frac{\partial v}{\partial x} + \tau_{yy} \frac{\partial v}{\partial y} + \tau_{zy} \frac{\partial v}{\partial z} \\ & + \tau_{xz} \frac{\partial w}{\partial x} + \tau_{yz} \frac{\partial w}{\partial y} + \tau_{zz} \frac{\partial w}{\partial z} + S_e \end{aligned} \quad (2.46)$$

Equations (2.43), (2.44) и (2.44) represent famous Navier-Stokes equations for incompressible flow. The last terms in these equations,  $S_{M_x}$ ,  $S_{M_y}$  and  $S_{M_z}$  represent contribution of the volume forces. Usually it is a gravity force which in most of the cases can be neglected because its magnitude is relatively small in comparison with surface forces.

If the flow is compressible, density is not constant but in fact is a function of pressure and temperature. In order to close the system of equations we need an additional equation. That equation is called equation of state.

$$p = \rho R T \quad (2.47)$$

### 2.5.2. Turbulent flow and turbulence modelling

Laminar flow is very rare in nature. Most flows are more or less turbulent. Turbulence occur when there is instability in laminar flow at high Reynolds numbers.

In turbulent flow, all flow variables are randomly changing there magnitudes and direction in time. Nevertheless, Reynolds found that they oscillate around some mean value so they can be decomposed to time averaged values and fluctuations.

$$f(t) = \bar{f} + f' \quad (2.48)$$

Where  $f$  is any flow variable.

By applying Reynolds decomposition to Navier-Stokes equations we get governing equations for turbulent flows. These equations are called Reynolds Averaged Navier-Stokes (RANS) equations.

Continuity equation:

$$\nabla \cdot \bar{\vec{U}} = 0 \quad (2.49)$$

Momentum equations are:

$$\frac{\partial \bar{u}_i}{\partial t} + \bar{u}_j \frac{\partial \bar{u}_i}{\partial x_j} = -\frac{1}{\rho} \frac{\partial \bar{p}}{\partial x_i} + \frac{\partial}{\partial x_j} (\nu \frac{\partial \bar{u}_i}{\partial x_j} - \overline{u'_i u'_j}) + S_{M_i} \quad (2.50)$$

In Reynolds momentum equations, additional stresses ( $-\overline{u'_i u'_j}$ ) appear at the right hand side. These are so called "fake" stresses, because they originate from convective part of inertial force due to Reynolds decomposition. In order to have a closed system, these stresses needs to be modelled. This is achieved by applying different turbulent models like Prandtl mixing length model, RNG  $k - \epsilon$ , Wilcox's  $k - \omega$  and  $k - \omega$  SST model.

For this project only  $k - \omega$  SST model will be used because many previous research suggest that it is best option for simulating flows in Pelton turbines.

This model uses standard  $k - \omega$  model next to the wall, while away from the wall, in turbulent region, it uses  $k - \epsilon$  model. It is worth mentioning that next to RANS there are two other method for simulating turbulent effects:

- Large Eddy Simulation (LES) - this method filters Navier-Stokes equations by passing only large vortexes. It is computationally expensive because it solves non-stationary equations.
- Direct Numerical Simulation (DNS) - this method calculates averaged flow but also all the fluctuations as well. Thus It requires large computational resources and it is less used in practice.

### 2.5.3. Computational Fluid Dynamics

Computational Fluid Dynamics (CFD) uses numerical methods and algorithms to solve the equations of fluid mechanics. It is a powerful tool that is widely used in practice. Although with recent development in computer technology it became more equal partner to theory and experiment, it is still not reliable enough to be used as standalone tool but it needs constant experimental validation.

CFD analysis implies three main steps:

- Pre-processing:
  - Geometry definition (Flow domain)
  - Mesh generation
  - Defining physical model
  - Defining fluid properties
  - Imposing boundary and initial condition
- Solving: There are three main methods of fluid domain discretization:
  - Finite differences
  - Finite volumes
  - Finite elements

The most commonly used method is Finite volume method. This method works by discretizing integral fluid dynamics equations over the whole domain (turning them into algebraic equations) and solving algebraic equations by iterative procedure.

- Post-processing: Consists of results visualization and analysis.

### 2.5.4. Previous research on application of CFD for flow modelling in Pelton turbines

Due to complexity of the flow inside a Pelton turbines, specifically free surface flow inside the buckets, application of CFD for Pelton turbines started a bit later than for the other hydraulic turbines. First CFD investigations were conducted and published near the end of 20<sup>th</sup> century.

#### **F. Avellan - 1998.[23]**

This is one of the first papers published about application of VOF (Volume Of Fluid) method for free surface flow and flow inside the injector of the Pelton turbine.

The main goal of this investigation was to find out how accurately VOF method can predict the jet interface and interface of the bucket free surface flow to be able to use this approach to see how the quality of the jet influences the efficiency of the turbine and possibly predict risk of erosion due to cavitation pitting.

Authors suggest two possible options for simulation of two phase flow. First option uses two fluids in computational domain. One fluid is represented by full elements and the other one by empty elements. In the second option, full elements represent the fluid and empty ones represent the void in the domain. The second option is applicable when the forces between the fluids at the interfaces are small, for example when domain is empty at the beginning (or filled with air) and starts filling with water. The problem with this approach is that the filling process is unsteady so it requires transient simulation which means more computational time.

As a test example, a 2D jet was simulated against an inclined wall. The second approach with filling was used. Authors recommend using quadrilateral or hexahedral meshes. The results of this test were shown to be reliable and this method possibly suitable for the predication of the flows in the Pelton turbine.

Next, numerical simulation of the flow in axisymmetric injector was conducted. The flow was defined as transient, turbulent and viscous and simulations were conducted for several nozzle openings. In the same time the experimental measurements were done under similar conditions and numerical results were validated with experimental data. The measured and calculated results showed good agreement. The final simulation was the free surface flow inside the fixed bucket configuration. The pressure measurements, for both stationary and rotating bucket, at two points inside the bucket surface are

conducted in order to validate numerical results and compare stationary and rotating configuration. It has been concluded, based on pressure measurements comparison, that the flow in the stationary bucket is similar to the flow in rotating bucket. Furthermore, numerical results showed good agreement with experiment. Although pressures measured at two points were not equal to the calculated ones; however, they were close.

**Morten Hana - 1999.[12]**

There are several things that needs to be considered when doing numerical simulation for the Pelton turbine:

- Geometry is complex
- Two phase flow
- Free surface flow
- Relative motion between the jet and the bucket

Before starting any simulation it is important to determine which physical processes are important for the considered flow and which ones can be disregarded. Three non-dimensional parameters can give us that information:

- Reynolds number - represents the ratio between inertial and viscous forces.

$$Re = \frac{UL}{\nu} \quad (2.51)$$

Where according to IEC standard  $U$  is the jet speed and  $L$  is the bucket width.

- Froude number - represents the ratio between inertia and gravity forces. Give us information if the gravity force is relevant for the flow. If its between 1 and 10 then gravity force will play important role in our flow and thus should not be disregarded.

$$Fr = \frac{U}{\sqrt{gH}} = \sqrt{\frac{H}{B}} \quad (2.52)$$

Where  $H$  is net hydraulic head and  $B$  is the bucket width.

- Weber number- represents the ratio between the inertia and surface tension forces and gives us information about importance of surface tension for our flow. If its close to one then surface tension should be taken into account as well.

$$We = \frac{\rho U^2 L}{\sigma} \quad (2.53)$$

Where  $\sigma$  is the surface tension force.

According to Hana, for surface flow in buckets, inertial forces are much more significant than gravity and surface tension.

Four flow processed can be identified in Pelton turbines:

- Internal flow inside the distributor
- Internal flow inside the injector
- High speed jet flow
- Free surface flow inside the bucket

The internal flows inside the injector and distributor have solid boundaries and are relatively easy to solve. The free surface flow has a moving boundary which needs special treatment.

In the first part of his thesis Hana developed a numerical code for particle method which gave promising results but it was dropped for further development because it was too simple. For the

second part, he compares different commercial software's: Ripple, Flow3D and Ansys CFX. First two use VOF method for modelling free surface flow, while CFX uses multiphase for tracking the free surface interface.

Since the goal of this thesis is not comparison of different numerical codes but only application for solving certain problem, only ANSYS CFX will be used, and the other software's will not be discussed any further.

There are two multiphase models available in CFX:

- Homogeneous model - The same solution for all phases, just different for volume fractions.
- Multi-fluid model - Each phase has different solution.

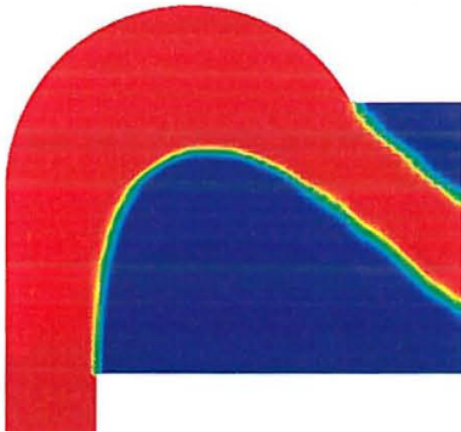


Figure 2.25: Volume fraction for a 2D bucket [12]

Author advises to use surface sharpening algorithm with homogeneous model (Note: This thesis was written 1999 and simulations were done in CFX-4. At the moment of writing the current version is CFX-19). Results from CFX showed the problem with numerical diffusion, as a consequence the water-air interface was smeared out (See figure 2.25). It is suggested that cell walls should be parallel with surface flow.

The pressure measurements were conducted in order to validate numerical results and they showed decent agreement.

Next, 3D flow was simulated with stationary and moving configuration. With stationary set-up the jet was impinging the bucket perpendicularly or at certain angle. Validation was done only with theoretical results.

The forces acting on bucket are calculated using theoretical formulas and they were compared with numerical results. Forces from numerical analysis were lower than theoretical values but still showed a good agreement.

Two approaches were used with moving configuration: fixed bucket with moving jet and sliding interface. Sliding interface was reported to give better results but it also had problems with distorting the jet and smearing the interface as for the 2D case.

#### Kvicinsky - 2002[6][13]

In 2002, Kvicinsky with group of authors, publish two papers regarding numerical and experimental analysis of 3D free surface flow in non-rotating and rotating bucket. Experimental analysis was described in section 2.4.

In the first paper, two approaches for modelling free surface flow inside the Pelton bucket were described and applied for simulation:

- Volume Of Fluid (VOF) model - This method, as mentioned before, is characteristic for filling processes. It give us the information of which cell is filled and which one is emptied. So next to the main governing equations, additional equation is required for the volume indicator function:

$$\frac{\partial F}{\partial t} + \vec{c} \cdot \nabla \vec{F} = 0 \quad (2.54)$$

When the value of volume indicator function is 1 then the cell is filled and when the value is 0 then the cell is empty. If the value is between one and zero that gives us the location of the interface between two fluids.

- Homogeneous model - This method can distinct between two phases but uses mixture when solving equations. This means, as said previously, that the solution is the same for both phases but it is different for volume fraction. Diffusion equation is used to determine the volume fraction for each phase:

$$\frac{\partial \alpha_n \rho_n}{\partial t} + \nabla \cdot (\alpha_n \rho_n \vec{c}_m) = \Gamma_n \quad (2.55)$$

Where volume fraction is defined as

$$\alpha_n = \frac{V_n}{\sum_n V_n} \quad (2.56)$$

As mentioned before, first test case was done with water jet shooting on inclined plate to study advection on the plane wall (See figure 2.27). Uniform velocity profile was used as initial condition and flow was set to be viscous with turbulent effects. For turbulence modelling,  $k - \epsilon$  model was used in CFX.

As discussed in section 2.4 the experiments were conducted to validate numerical results. The numerical and measured data showed good agreement. Only deviation was seen with the pressure measured for the case of 0 degrees. The reason for this is the velocity deficit caused by the wake from the needle tip which wasn't taken into account by using uniform velocity profile as initial condition. The real velocity profile was later measured and used as initial condition for the new simulation and it gave an excellent agreement with measured values, which can be clearly seen from figure 2.26.

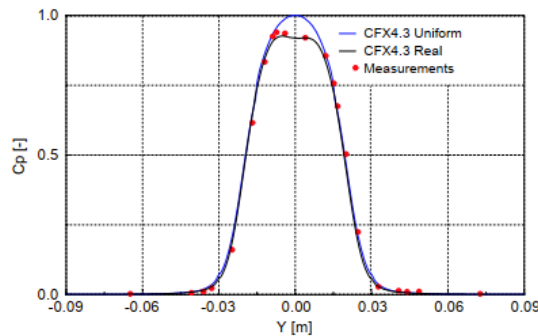


Figure 2.26: Comparison between experimental and numerical results for 0 degrees inclination angle (Taken from [13])

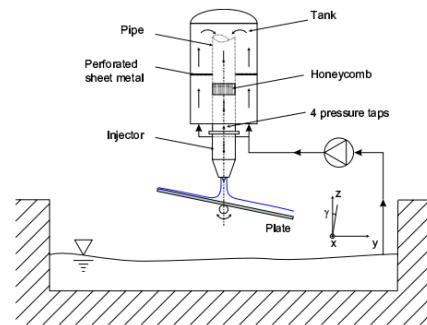


Figure 2.27: Test rig for plane wall measurements (Taken from [13])

Next, the 3D flow in non-rotating bucket was simulated. The flow was considered to be axisymmetric, steady, viscous and turbulent. The pressure distribution was measured inside the bucket and used to validate numerical results. They showed an excellent correspondence. Furthermore, the thickness of the water layer was also measured and compared. It also showed good agreement with small error margins because of the diffusion on the free surface.

Second paper deals with free surface flow in the rotating buckets. Both experimental and numerical analysis are conducted and results are compared. The numerical simulation was run in CFX 4.3 with homogeneous model for modelling free surface flow. The flow was considered to be viscous and laminar. The boundary condition at the inlet was set to be transient movement of the jet velocity profile.

As concluded by the authors, the results couldn't be compared with experiments, because jet doesn't intersect the median line as in the experimental observation.

#### Zoppe - 2006[5]

In this paper author conducts an experimental and numerical analysis of the free surface flow inside the fixed Pelton turbine bucket (See figure 2.9).

ANSYS Fluent code was used for simulation with VOF model for modelling the free surface flow. Initial test, as in previous papers, was conducted on a flat plate to test the accuracy of the Fluent VOF. Results showed an excellent agreement with the experiment.

The flow is considered to be symmetric so only flow in the half of the bucket was simulated. This is convenient in terms of the computational time because it decreases number of cells by half. Furthermore the mesh size dependence was investigated with four meshes with different number of elements. It is found that results are insensitive on further increase in number of elements above 180k.

Fluent uses Finite Volume Method for discretization of the domain. The flow is considered to be turbulent and standard  $k - \epsilon$  model was used for modelling turbulence. The free surface interface was described with value of volume fraction of 0.5 and interface is reconstructed using PLIC method.

It has been shown, in some previous research that viscous forces are relatively small in comparison with inertial forces. For that reason laminar simulations were first conducted. The results showed

some numerical instabilities which according to author do not come from near wall region but they appear due to high velocity gradients near the interface. By using turbulent models these gradients were largely reduced. Author suggests that modelling of the boundary layer and thus refining the mesh near the wall is not necessary because the viscous forces are small. This is confirmed and validated with the experiment.

The influence of the jet diameter on the flow distribution inside the bucket (Figure 2.28) and thickness of the water sheet was investigated as well. The thickness of water sheet decreases normally for smaller diameters from cutter until outlet. However after certain diameter size it comes to a build up of water at certain distance from the cutter. Author argues that this is due to over-pressure at the bottom of the bucket where water experiences reduction of velocity.

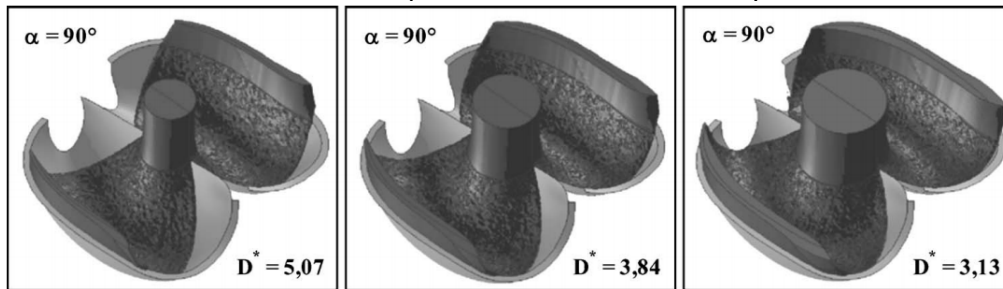


Figure 2.28: Flow distribution inside the bucket with three different jet diameters (Taken from [5])

The pressure distribution was investigated as well as the influence of the different jet diameters and impingement angles on the pressure distribution. The results identify the zones with highest pressure which contribute the most to torque of the turbine.

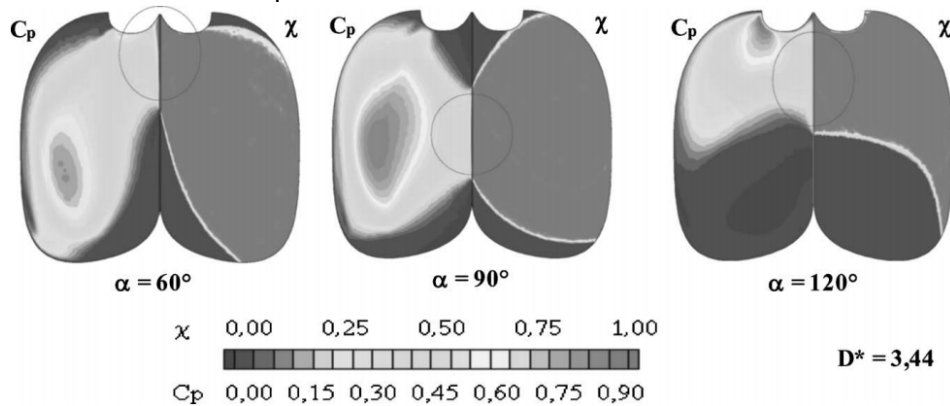


Figure 2.29: Pressure (left) and volume fraction (right) distribution inside the bucket surface for different impingement angles (Taken from [5])

The numerical pressures showed good agreement with measured ones except for certain angle of impingement which is attributed to loss of flow through the cut-out edge. Furthermore, the total torque and thrust force are calculated by applying momentum theory to the fluid domain inside the bucket. Again, numerical results showed good agreement with measurements with small differences at certain incidence angles which is again contributed to the leakage through the cut-out edge. Maximum thrust is reported at angle of incidence of 90 degrees, while maximum torque is recorded at 110 degrees.

Another thing that was observed and that is interesting to mention, is torque and thrust variation with jet diameter (Figure 2.30). It is noted that maximum thrust and torque values correspond to optimum jet diameter from the theory.

Finally, it is shown through efficiency analysis, that partial optimization of the bucket can be done through analysis of the flow in the fixed bucket.

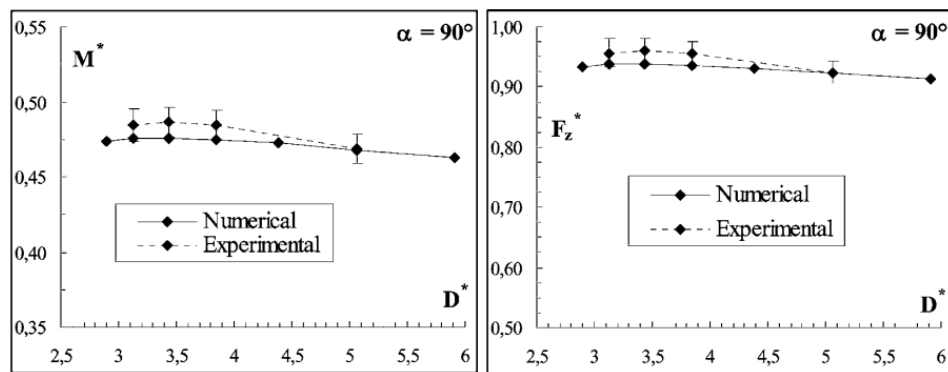


Figure 2.30: Torque and thrust force, respectively, versus different jet diameters (Taken from [5])

### A.Perrig - 2006[7]

The unsteady free surface flow inside the rotating Pelton turbine buckets is simulated. ANSYS CFX 5 code was used with two phase homogeneous model for modelling free surface flow.

High resolution upwind scheme was used for discretization of momentum and continuity equations. Transient terms were modelled with second order backward Euler scheme and turbulence was modelled with  $k - \epsilon$  model with standard wall functions. The jet was considered to be ideal and initialized with uniform velocity profile. The whole domain was meshed with unstructured mesh with around 645 nodes and 2.4 million tetrahedral elements. The mesh size solution dependence was performed as well with four different meshes.

The authors also conducted measurements and flow visualization as already discussed in section 2.4. Both experimental and simulation results show five distinct pressure zones inside the bucket, that contribute the most to the torque. It is noted that numerical and experimental results are in good agreement regarding the phase shift but there are some differences in the magnitude. These differences are explained by looking at difference in flow patterns from simulation and real flow visualization. The conclusion was that the simulation and experimental results agree pretty well in the areas where the flow is mostly dominated by the inertial forces and it is not affected by the interaction of the high speed jet and the bucket.

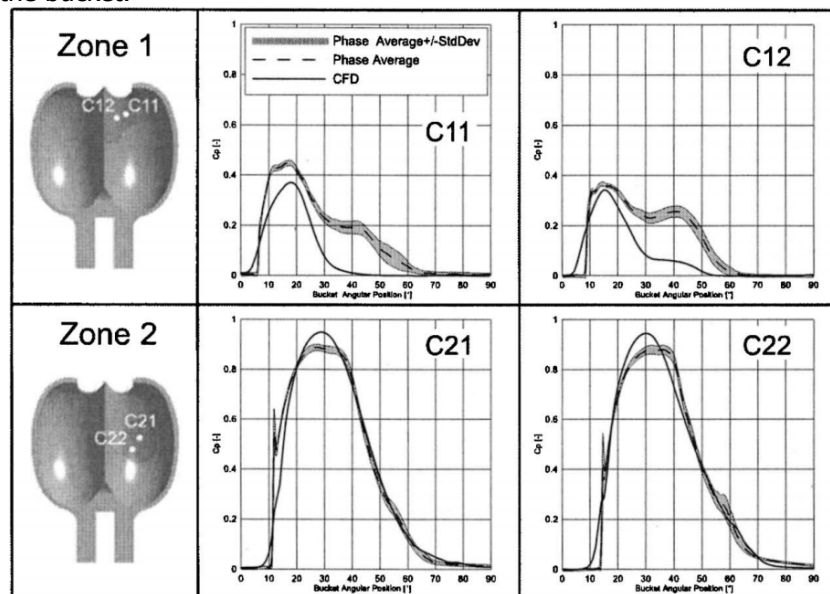


Figure 2.31: Comparison of pressure coefficients between numerical and experimental results for two pressure zones (Taken from [7])

A.Perrig in his PhD thesis [8] goes in more detailed experimental and numerical analysis with the free surface flow inside the Pelton turbine bucket. He uses two numerical models for free surface flow modelling: 2-Phase Homogeneous model and 2-Fluid model. He concludes that second one gives more

accurate results, while first one is too diffusive.

Over the past few years there has been more research on this topic. Two master theses from L.F. Barstad [28] and L.E. Klementsens [29] will be particularly useful for this thesis, because they give more detailed description about meshing and physical setup for the simulation. They will be used as a partial guideline in chapter 5.

# 3

## Preliminary design of a Pelton turbine

To be able to calculate dimensions of the Pelton wheel it is necessary to know hydraulic net head (or pressure) and design flow rate. Hydraulic net head, for classical hydraulic power plants, is determined by site location and it is roughly the height difference between lower reservoir and inlet of the injector. For DOT concept the net head is determined by the pressure created by pumps driven by the wind turbines. Thus pressure is only limited by the power of the displacement pumps and the strength of the material that can withstand that pressure. In this preliminary design the Pelton wheel will be dimensioned for pressure of 200 and 400 bar in order to get an insight on how the pressure influences the parameters of the Pelton wheel. The general calculation will be conducted for rated powers 30MW, 50MW, 100MW, 200MW and 400MW. Disregarding all the losses this will be considered as available hydraulic power.

### 3.1. Creating a tool for Pelton turbine design with Python

In order to speed up the calculation of the geometrical as well as operational parameters for Pelton turbine, with regard to different design parameters (pressure and flow rate), small program was written in Python code. Graphical User Interface (GUI) for the program, which is given in figure 3.1, allows quick calculation and visualization of the influence of different design parameters on the design of the turbine. It enables user input of all design parameters as well as physical properties of the flow.

All the equations used for calculations of geometrical and operational parameters of the Pelton turbine are already given in section 2.3 and are taken from Zhang[4].

It should be mentioned that program allows input of either pressure difference or net hydraulic head and either power or flow rate. Having this in mind, flow rate can be easily calculated from hydraulic power and vice versa (same goes for pressure difference and hydraulic head):

$$Q = \frac{P_h}{\rho g H} = \frac{P_h}{\Delta p} \quad (3.1)$$

Where  $P_h$  is hydraulic power,  $\rho$  is density of sea water and  $g$  is gravitational acceleration. (Note: For the sake of convenience, simplicity and specificity of DOT concept, pressure difference will be used instead of pressure head from now on.)

### 3.2. Design test case

By plugging in powers, for the preliminary test case, in the equation 3.1 we obtain the flow rates as given in table 3.1.

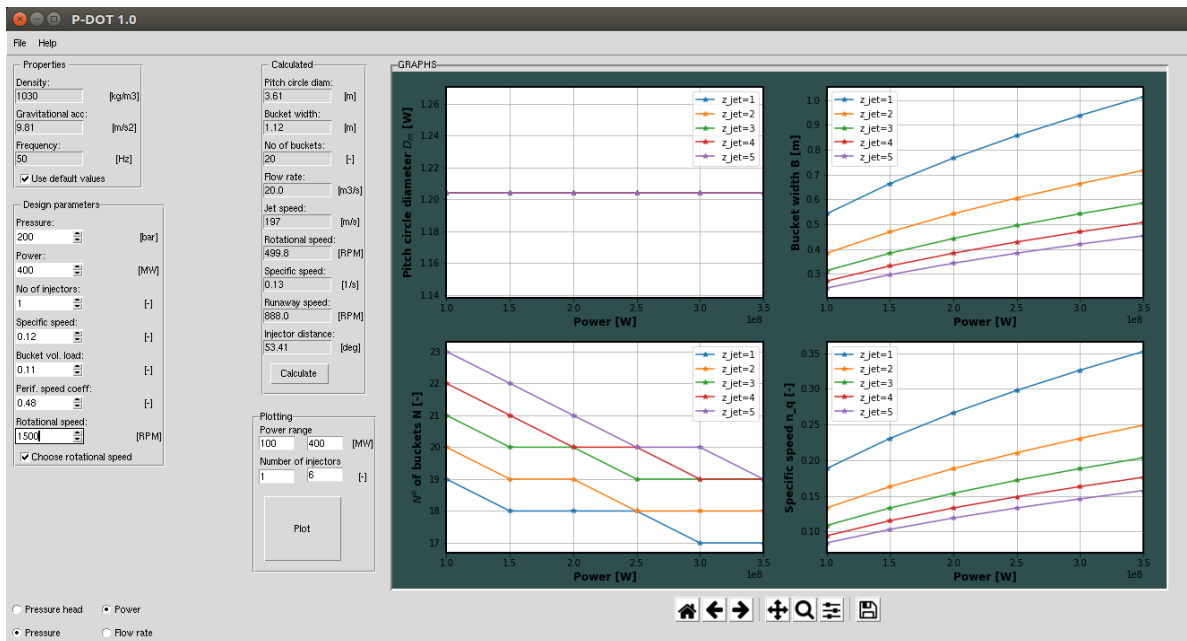


Figure 3.1: Program for dimensioning of the Pelton turbine based on main design parameters

Table 3.1: Flow rate for pressures of 200 and 400 bar

Pressure $\Delta p$	Hydraulic power $P_h$	30 MW	50 MW	100 MW	200 MW	400 MW
200 bar	Flow rate	1.5 m <sup>3</sup> /s	2.5 m <sup>3</sup> /s	5 m <sup>3</sup> /s	10 m <sup>3</sup> /s	20 m <sup>3</sup> /s
400 bar	Flow rate	0.75 m <sup>3</sup> /s	1.25 m <sup>3</sup> /s	2.5 m <sup>3</sup> /s	5 m <sup>3</sup> /s	10 m <sup>3</sup> /s

The parameters for Pelton turbine are calculated for 30 MW, 50 MW, 100 MW, 200 MW and 400 MW, for pressure difference  $\Delta p = 200$  bar and  $\Delta p = 400$  bar and for various number of injectors. For optimal operating conditions main operating parameters are chosen as follows:

- Bucket volumetric load -  $\varphi_B = 0.11$ ,
- Peripheral speed coefficient -  $k_m = 0.47$  and
- Specific speed -  $n_q = 0.12$ .

In the tables below results are shown for  $P = 100MW$  and for various number of injectors. Table 3.2 is for pressure difference  $\Delta p = 200$  bar, while table 3.3 is for pressure difference  $\Delta p = 400$  bar. Furthermore in the figures below values for pitch circle diameter and bucket width can be seen for different hydraulic powers. (Note: Results for other hydraulic powers are given in the Appendix A)

Table 3.2: Calculated parameters for  $P=100MW$  and  $\Delta p = 200$  bar

Description	$z_{jet} = 1$	$z_{jet} = 2$	$z_{jet} = 3$	$z_{jet} = 4$	$z_{jet} = 5$	$z_{jet} = 6$
Pitch circle diameter $D_m$	2.4 m	1.8 m	1.2 m	1.2 m	1.2 m	1.2 m
Bucket width $B$	0.52 m	0.39 m	0.32 m	0.26 m	0.23 m	0.23 m
Number of buckets $N$	22	22	21	22	23	23
Rotational speed $n$	750 rpm	1000 rpm	1500 rpm	1500 rpm	1500 rpm	1500 rpm
Number of pole pairs $p$	4	3	2	2	2	2
Specific speed $n_q$	0.093 s <sup>-1</sup>	0.088 s <sup>-1</sup>	0.11 s <sup>-1</sup>	0.093 s <sup>-1</sup>	0.083 s <sup>-1</sup>	0.08 s <sup>-1</sup>

Table 3.3: Calculated parameters for  $P=100$  MW and  $\Delta p = 400$  bar

Description	$z_{jet} = 1$	$z_{jet} = 2$	$z_{jet} = 3$	$z_{jet} = 4$	$z_{jet} = 5$	$z_{jet} = 6$
Pitch circle diameter $D_m$	1.67 m					
Bucket width $B$	0.33 m	0.24 m	0.2 m	0.16 m	0.16 m	0.12 m
Number of buckets $N$	23	26	28	31	31	36
Rotational speed $n$	1500 rpm					
Number of pole pairs $p$	2	2	2	2	2	2
Specific speed $n_q$	$0.08 \text{ s}^{-1}$	$0.06 \text{ s}^{-1}$	$0.05 \text{ s}^{-1}$	$0.04 \text{ s}^{-1}$	$0.04 \text{ s}^{-1}$	$0.03 \text{ s}^{-1}$

It is interesting to notice, from figures 3.2 and 3.3 as well as from tables 3.2 and 3.3, that calculated pitch circle diameter is lower for higher pressure difference and it increases with increase of hydraulic power or flow rate. The smallest diameter is limited with highest synchronous rotational speed of the generator and thus number of pole pairs. Bucket width is also lower for higher pressure differences and increasing almost linearly with power. Accordingly, rotational speed is higher for higher pressure difference and number of pole pairs is lower. However, minimum number of generator pole pairs is limited to two, hence rotational speed is limited to 1500 rpm. The trend for minimum number of buckets can not be clearly identified from figures 3.2 and 3.3. This is because it is a function of specific speed which in turn is dependent on rotational speed which is, as mentioned above, limited with number of pole pairs and it has to be synchronous in order to keep constant frequency of the grid. This can be confirmed from figure 3.4 where turbine is dimensioned by keeping the constant rotational speed. It is noticeable now that minimum number of buckets is decreasing as power increases. Specific speed trend is also hard to observe from first two figures because synchronous rotational speed is different for different powers; however, observing the figure 3.4, with constant rotational speed, it is clear that it has increasing trend with power. Furthermore, for turbine with less injectors specific speed is higher. This fact can be used for choice of the optimal number of injectors by looking for which number of injectors the value for specific speed parameter is closest to design value. Note that design value for the specific speed is chosen based on rotational speed of the generator, pressure and flow rate, as given by equation 2.21. In the figure 3.5, the influence of the number of injectors on the specific speed is clearly visualized. For the 100 MW Pelton turbine and pressure difference  $\Delta p = 200$  bar, three injectors seems to be the best choice, since the specific speed is closest to design value of  $n_q = 0.11$ , while for  $\Delta p = 400$  bar one injector, with these geometric and operational characteristics, would probably assure the most efficient solution.

These parameters can be varied and adjusted, however the change of one parameter will influence the other parameters and performance of the turbine so this should be done carefully by using the previous design experiences as well. The characteristics of the generator should be also taken into account for the design, in terms of the number of pole pairs and rotational speed which needs to be constant.

At this point, it should be mentioned that this preliminary design is standard Pelton turbine design based on the normal conditions at which these turbines are used. In the following chapters of this thesis attempts will be made to adjust and redesign the Pelton turbine for the DOT concept and for offshore applications.

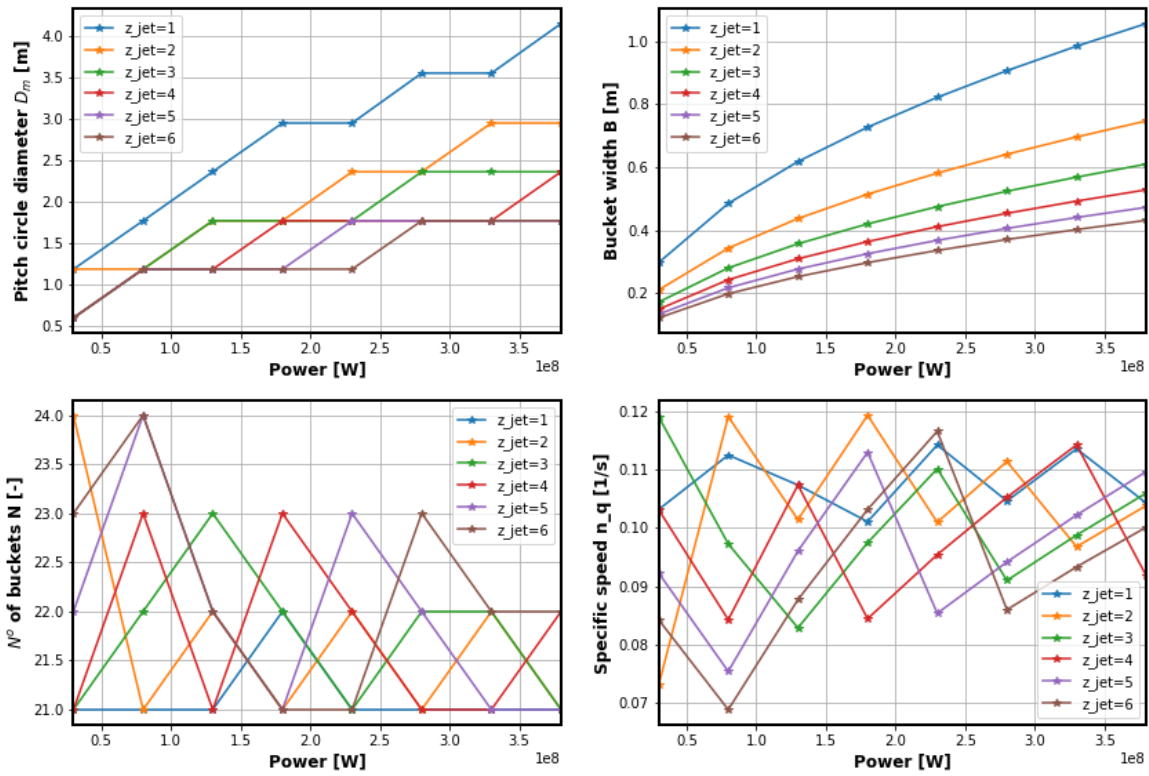


Figure 3.2: Pelton turbine size parameters for pressure difference  $\Delta p = 200$  bar

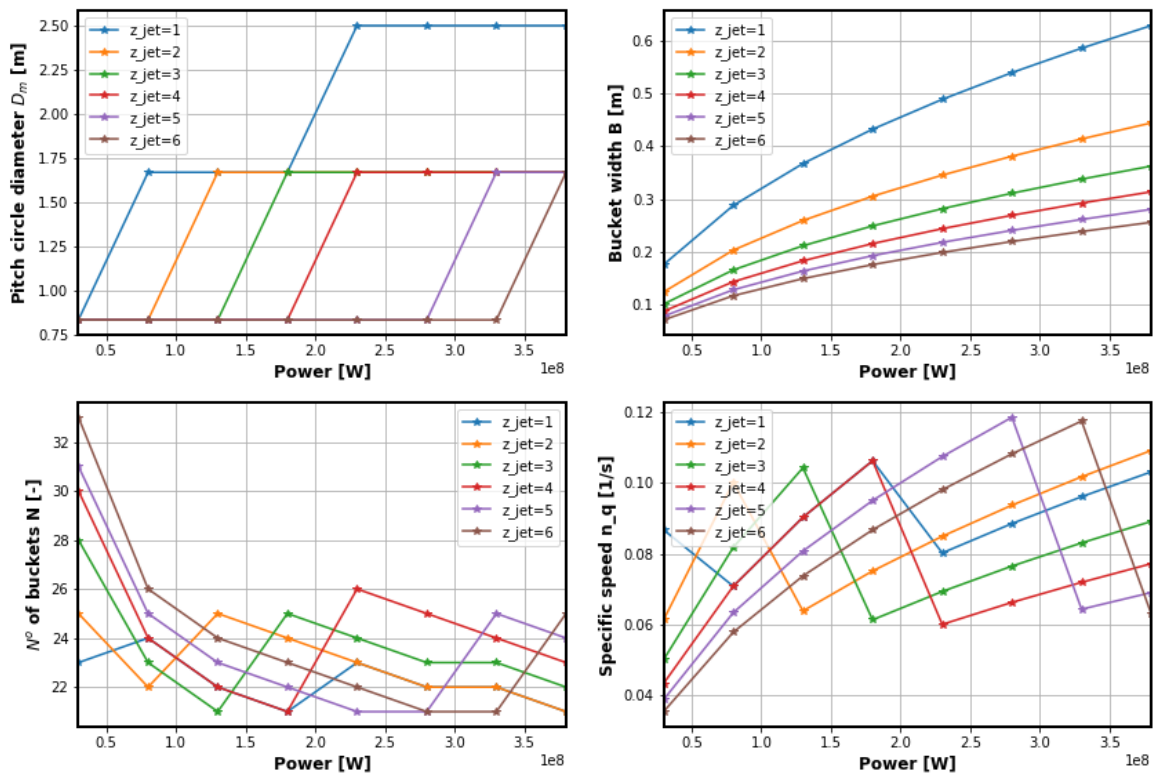


Figure 3.3: Pelton turbine size parameters for pressure difference  $\Delta p = 400$  bar

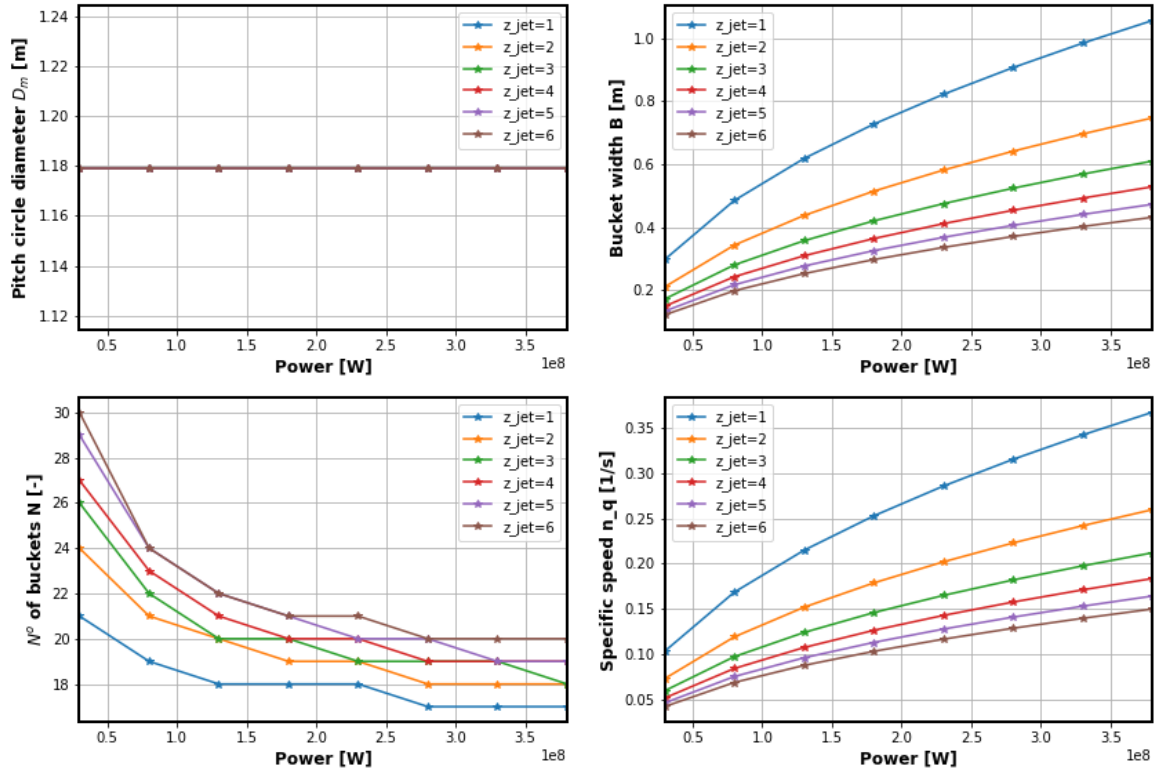
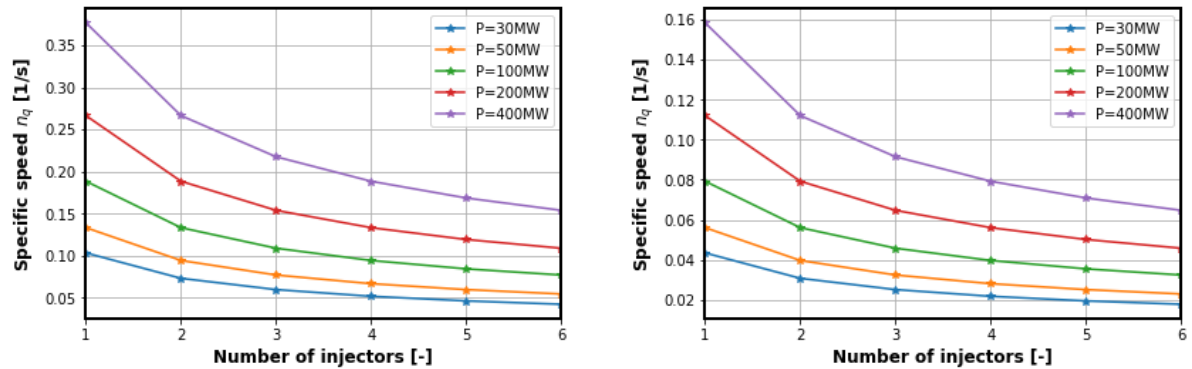


Figure 3.4: Pelton turbine size parameters for pressure difference  $\Delta p = 200$  bar and fixed rotational speed  $n = 1500$  rpm



(a) Specific Speed vs No. of injectors for pressure difference  $\Delta p = 200$  bar

(b) Specific Speed vs No. of injectors for pressure difference  $\Delta p = 400$  bar

Figure 3.5: Specific speed as a function of the number of injectors. Rotational speed is kept constant at  $n = 1500$  rpm

# 4

## Experimental analysis of the Pelton turbine jet flow

As a part of this master thesis project, experimental investigation of the Pelton turbine is going to be conducted. The main goal of the experiments is to provide an answer to two main research questions defined regarding the operational conditions of Pelton turbine for DOT concept:

- What is the influence of the pressure head and the flow rate on the efficiency of the Pelton turbine and what is the upper limit for the pressure?
- Is there a fluctuation in pressure caused by the displacement pumps and if yes how do these fluctuations influence the efficiency of the turbine?

To answer these questions, several measurements were planned to be conducted in two phases. The main reason for splitting measurements in two phases is the time management. All components for both phases are designed and prepared for the experiment, however due to lack of time only phase I of the experiment is executed. Nevertheless, design and preparation for both phases are discussed in following sections.

### 4.1. Test set-up

Complete test rig was designed by looking at some previous experimental investigations conducted by various authors and it is shown in figure 4.1. 3D model is made in SOLIDWORKS 2018 software package.

#### 4.1.1. Test equipment specifications

The full test set-up is shown in the figure 4.2. The schematic overview is given in figure 4.3.

The components described here are given in figure 4.2 and pump specifications are given in table 4.1:

- **Positive displacement pump** - Janus MB160 is bi-directional motor, which means that it can be used both as a pump and as a motor. Since for the test we use it as a pump, henceforth it will be referred to as such. This is an axial displacement pump with a single piston. The volumetric displacement of the piston is 225 cc/rev which means that maximum flow rate at maximum rotational speed of 2000 RPM can be 450 l/min. The maximum power that needs to be provided in order to achieve maximum pressure of 160 bar, is around 110 kW. However since the two generators used in this setup can provide maximum power of 27.5 kW each and boost pumps require one generator, the expected power for PD pump is around 45 kW with batteries included. From the pump performance curves (Figure 4.4) it can be seen that for input power of 45 kW the maximum pressure of around 80 bar can be achieved at rotational speed of 1500 rpm. This gives the maximum allowable flow rate of around 340 l/min.

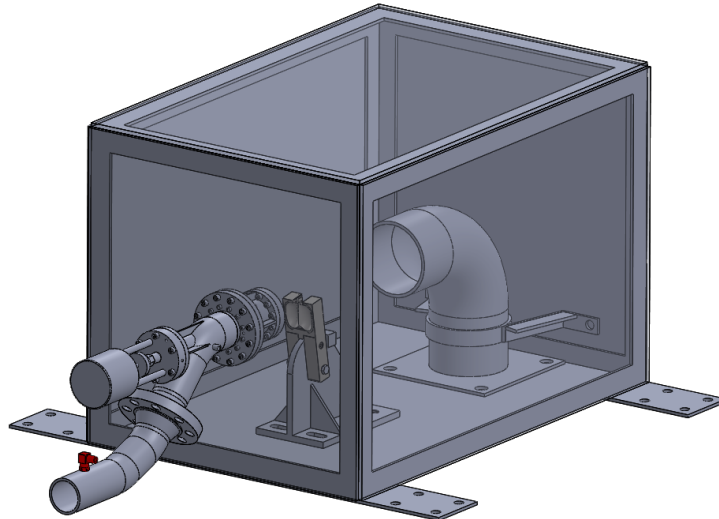


Figure 4.1: 3D model of the test rig designed for the experiment. Two polycarbonate transparent plates are placed from one side and on top of the steel cage to enable optical visibility. Thick steel plates are placed on other sides. The detailed technical drawings for the test rig are given in the Appendix B.

Table 4.1: Axial PD pump characteristics

Description	PD Pump
Type	Janus MB160
Displacement [cc/rev]	225
Rot. speed [RPM]	2000
Max. power [kW]	120
Max. pressure [bar]	160

- **Booster pumps** - Pleuger NB64-23 + M6-600-2 is a submersible multistage centrifugal pump with submersible motor. It is placed inside of the water reservoir and it is used to boost the pressure at the inlet of the PD pump. This is necessary because PD pump needs minimum 12 bar of pressure at the inlet, for the starting torque, to be able to rotate unloaded shaft. The pump characteristics are given in table 4.2. As mention before, motor for the booster pump runs at rated power of 27 kW. There are two booster pumps placed inside the reservoir, however only one pump is used for the tests.

Table 4.2: Main characteristics of the boost pump

Description	Booster Pump
Type	Pleuger NB64-23
Max. flow rate [l/min]	259
Rot. speed [RPM]	3440
Motor rated power [kW]	27
Max. pressure [bar]	30

- **Injector (Spear valve)** - Injector is one of the most important components for the Pelton turbines. It is used to convert pressure energy to kinetic energy of the high speed jet. For the DOT concept, as previously explained, it is also used for the passive control of the wind turbine. By changing the position of the spear valve the pressure at the inlet of injector is changed. This information of the pressure change then propagates, via hydraulic circuit, all the way to wind turbine rotor which has to respond to change in counter torque.

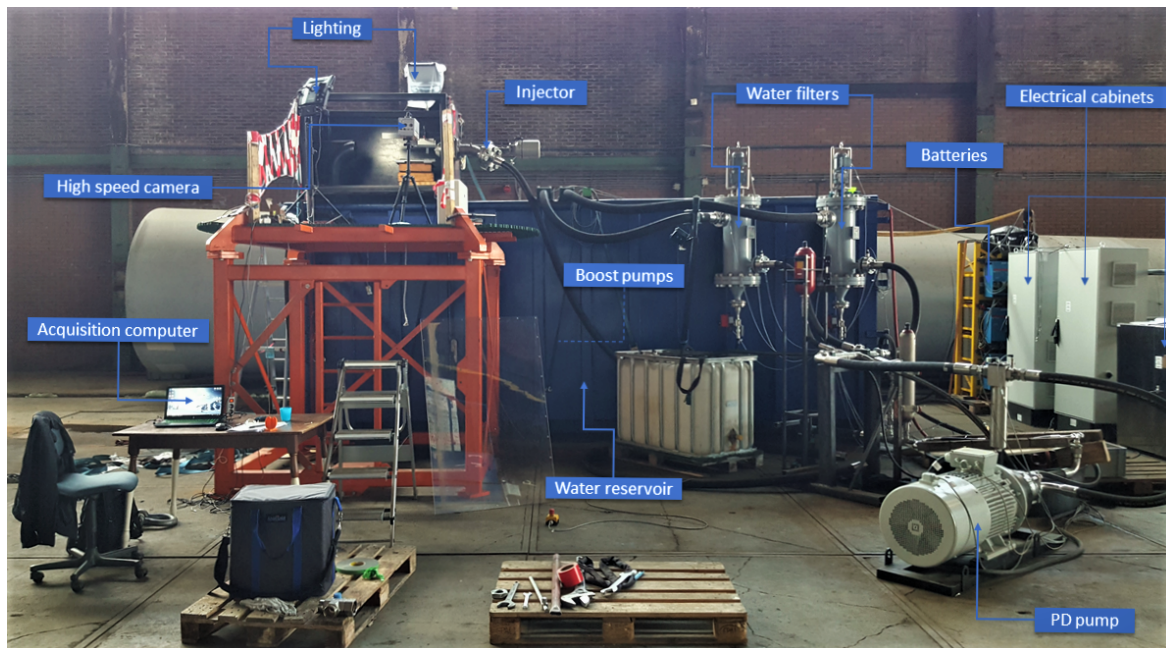


Figure 4.2: Complete set-up for the experiment, assembled and placed in DOT testing hall. Test rig is placed at the top of the water container.

Pressure in the injector can be calculated with equation 2.11 and it is dependent of the flow rate and effective nozzle area (Equation 2.10). For the injector used in this experimental set-up the effective nozzle areas for different nozzles are given in figure 4.5. Nozzle used in this set-up has head diameter of 25 mm. It can be seen from the figure 4.5 that spear range for this nozzle from fully closed to fully open, is 0 to 25 mm. However, during the tests, by measuring the spear position, it is noticed that it can go up to 28.7 mm from fully closed position. The reason for this is probably that spear retracts 3.7 mm beyond the fully open position before the limit switch is activated. Nevertheless, since all measuring points were defined for the small opening of the spear valve, this isn't considered to be important for this thesis.

#### 4.1.2. Phase I: Investigation about influence of different parameters on quality of the high speed jet

Phase I of the experiment is the investigation of the influence of the pressure fluctuations, pressure head and flow rate on the quality of the high speed jet. The measurements will be conducted for a range of pressures and a range of flow rates. The flow rate will be controlled by changing the rotational speed of the PD pump.

$$Q = \frac{V}{1000} \cdot n \text{ [l/min]} \quad (4.1)$$

Where  $V$  [cc/rev], is the volumetric displacement of the piston, and  $n$  [RPM] is the rotational speed of the pump. Pressure will be controlled by changing the position of the spear valve needle.

Following type of measurements will be conducted:

- Pressure measurements before the injector - this is to confirm the existence and magnitude of the pressure fluctuations caused by the displacement pump.
- Flow rate measurements - this will be done indirectly by multiplying the rotational speed of the pump with the volumetric displacement of the piston and subtracting the measured water leakage.
- Flow visualization of the high speed jet - this is to see the influence of the fluctuations (if exists), pressure head and flow rate on the structure of the high speed jet and thus its quality.

Instrumentation necessary for the phase I measurements:



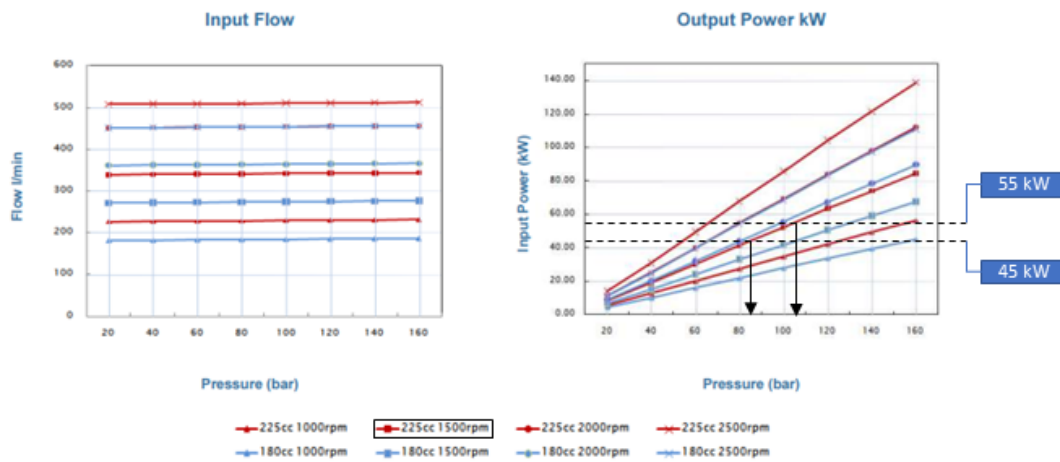


Figure 4.4: Performance curves of the axial PD pump. Left: Flow rate for range of rotational speeds of the pump. Right: Required power input for different flow's and different pressures.

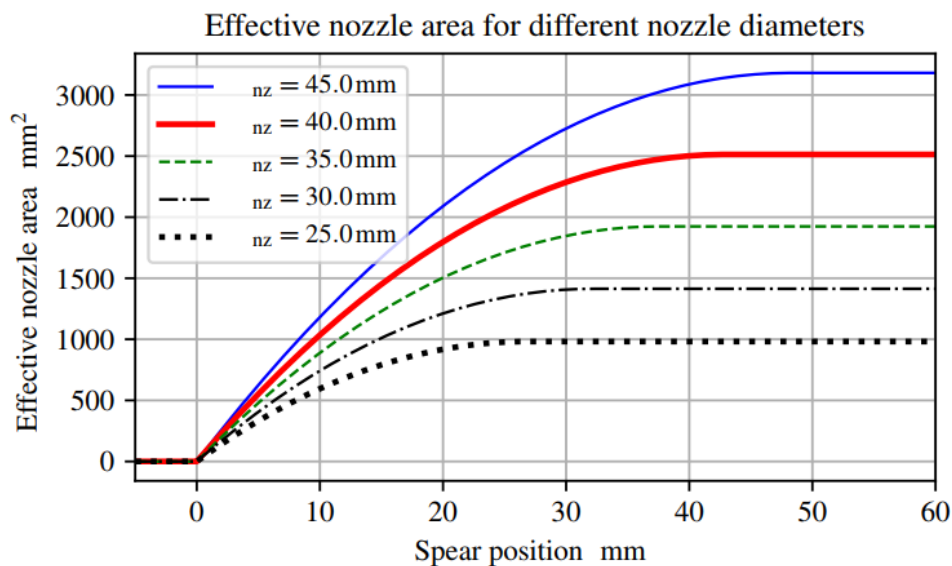


Figure 4.5: Effective nozzle area as a function of spear position for different nozzle diameters. Taken from [14]. Note: For the test, 25 mm nozzle will be used.

- **Lighting system** - In order to be able to capture images at high frame rate and high shutter speed (short exposure), proper lighting system is necessary. Standard light sources that work on AC power and are connected to the grid, do not have continuous light but instead have the light flicker at the frequency of the grid (50 or 60 Hz). There are few options for light sources that are used in high speed imaging to overcome the problem with flicker. Some of them include:
  - Battery powered lamps - don't produce any flicker because batteries use DC current so there is no frequency shift.
  - Laser - can produce both continuous and pulsed light.
  - Tungsten lamps - are high power lamps with Tungsten filaments. Since they are big they need more time to cool down, so during the power down cycle they don't have time to dim so they reduce the frequency flicker.
  - Flicker free LED lights - these lights convert AC to DC power which is, as mentioned before, flicker free.

For the experiment, Astra LED light panels (Figure 4.8) were used since they were cheapest op-

tion, easiest to acquire and don't require any training nor supervision to work with. The main characteristics of these lights are summarized in table 4.5. According to manufacturer the output of these lamps is comparable with 1000 Watts of softlight. In order to ensure the best image contrast, the lights were not pointed directly at the jet but at the reflective surface that is placed below the jet so that light doesn't illuminate the background.



Figure 4.8: Astra LED light-panels used as light source for the flow visualization of the high speed jet.

Table 4.5: Astra LED light-panel main characteristics.

Description	Lighting system
Model	Astra 1x1 EP bicolor 1000W
Power draw	55 W
Exposure Value	11,3 = 6303 lux
Flicker	Flicker-free
Quantity	2

#### 4.1.3. Phase II: Investigation about influence of different parameters on pressure distribution inside a Pelton turbine bucket

The Phase II of the experiment is meant to investigate the influence of all parameters from the Phase I but on the pressure distribution inside the fixed Pelton turbine bucket. The reason why fixed configuration is chosen, as elaborated in section 2.4, is because it is cheaper and easier to set up. Fixed configuration can, nevertheless, provide valuable information about influence of different parameters and help to identify main constraints for the design of a Pelton turbine for DOT concept. The angle of the jet impingement on the bucket cutout can be changed by rotating the bucket as shown in the drawing 1.2 in the Appendix. Furthermore, the stresses in the root of the bucket will be measured in order to confirm that they are within the limit. Although not representative of the real rotating wheel, the torque will be calculated as well in order to assess the efficiency of the turbine. The results from these measurements will be used for validation of the numerical simulations.

Following type of measurements will be applied, besides ones already defined in Phase I:

- Visualization of the flow inside the bucket - in order to visually observe how pressure and flow rate influences the spreading of water inside the bucket. Furthermore it would be interesting to see if the pressure fluctuations (if exists) have an effect on the jet misalignment with the bucket cutout.
- Measurements of the pressure distribution inside the bucket - to quantitatively describe the influence of aforementioned parameters on the pressure distribution inside the bucket and thus identify the parts of the bucket which contributes the most to the torque.
- Measurements of the stresses at the root of the bucket - to determine the magnitude of the stresses in the bucket root, the part of the bucket which is exposed to the highest stresses during the operation (and start and stop).

Instrumentation necessary for the phase II measurements are given in table 4.6.

Two ways for measuring the pressure distribution inside the Pelton turbine bucket are found in literature. One option is embedding multiple piezo-resistive sensors inside the bucket surface, as explained in [6], [13], [7] and [8]. Second one is drilling the multiple pressure taps inside the bucket surface and connecting the taps through pressure scanner (Ex. Scanivalve) with single pressure transducer as outlined in [5]. The second method is only applicable for the stationary bucket (which is our case), but it is lot cheaper, simpler and easier to implement. Also since time is limiting factor it has been decided to continue planing with second method for measuring pressure distribution.

Table 4.6: Summary of the required instruments for the both test phases. Note that for pressure distribution two solutions are mentioned, however only one will be used.

Name	Type of measurement	Range	Quantity
Pressure sensor	pressure	0 – 200 bar	1
High speed camera	flow visualization	1 – 10 · 10 <sup>3</sup> fps	1
Strain gauges	stresses	-	8
1. Piezo-resistive sensors	pressure distribution	0 – 200 bar	21
2. Pressure sensor with scanivalve	pressure distribution	-	1

To be able to have correlation between the stationary and rotating bucket it is necessary to determine the angles and positions at which jet interacts with the bucket. Furthermore, this is also important for the phase I because it will give us the information about the length of the jet which interacts with single bucket and thus the observation length. In order to be able to determine bucket position relative to the jet, an explanation of the bucket cycle is necessary.

Visualization of the bucket cycle steps during the operation of the Pelton turbine is shown in figure 4.9. We will follow the bucket one (marked with red color) while it rotates with the Pelton wheel and bucket two (marked with blue color) which follows it. As can be seen from the top drawing of figure 4.9, bucket one begins its cycle by starting to cut the upper surface of the jet at point A. Once it cuts through the whole jet diameter, it will be under full jet impingement until following bucket starts cutting the jet and enters its own cycle. This happens at point B in the middle figure. The time or exposure of the bucket to impingement of the full jet is determined by the size of the wheel, number of the buckets, distance and angle of the injector and diameter of the jet (determined by the pressure, flow rate and position of the spear). The bucket cycle continues up to the point where following bucket (blue) cuts through the whole jet (Point C; Note: This is not completely true, because even after the following bucket cuts through the whole jet there is still water passing the cut-out edge. Nevertheless, this is disregarded in this analysis). The cycle of the bucket one is marked with angle  $\gamma$  in the bottom figure.

The length of the jet, from the nozzle exit up to the bucket cutter, at the end of the bucket cycle is marked with  $L_{jet}$ . This value is very important for both experiment and CFD because it determines the part of the jet that interacts with turbine buckets and thus the part that is most important for observation. Furthermore, together with bucket cycle  $\gamma$ , it determines the position and angle range of the bucket for the stationary configuration, relative to the nozzle exit. This is clearly shown in the figure 4.10. Since the radius of rotation of the stationary bucket  $R_c - R_d$  is smaller than radius of rotation of the Pelton wheel  $R_c$ , than in order to have the same angle of incidence between the jet and the bucket, as well as the same distance from the nozzle, position of the bucket center of rotation needs to be changed for every angular change in the bucket cycle. As bucket cycle is defined with angle  $\gamma$ , bucket center of rotation should move along the blue arc (4.10) of the radius  $R_d$ , and the bucket should be rotated so the tip of the bucket cutter is coincident with the intersection point of the circle of radius  $R_c$  and line that goes through center of the bucket rotation and center of the runner rotation (Note: This is the center of circles of radius  $R_d$  and  $R_c$ ). The fixed bucket configuration for the experiment is designed so that it allows vertical and horizontal translation and rotation of the bucket in order to properly position the bucket with respect to the jet. This is achieved by means of bolts and threaded holes positioned at the base plate of a bucket holder (See the Appendix).

In order for phase II to be conducted, bucket needs to be manufactured first. Impact of the high speed jet of water on the fixed object can cause extremely high forces and thus high stresses of the material. That being said, preliminary stress analysis needs to be conducted before sending bucket for manufacturing.

Real turbine is meant to operate with the design pressure of 420 bar, which gives jet speed:

$$C_0 = \phi \sqrt{2gH} = 289.8 \text{ m/s} \quad (4.2)$$

where  $H = 4280$  is equivalent net pressure head. Efficiency of the nozzle is considered to be 100%. Although in practice this is never true, for the stress estimation it can act as a safety factor.

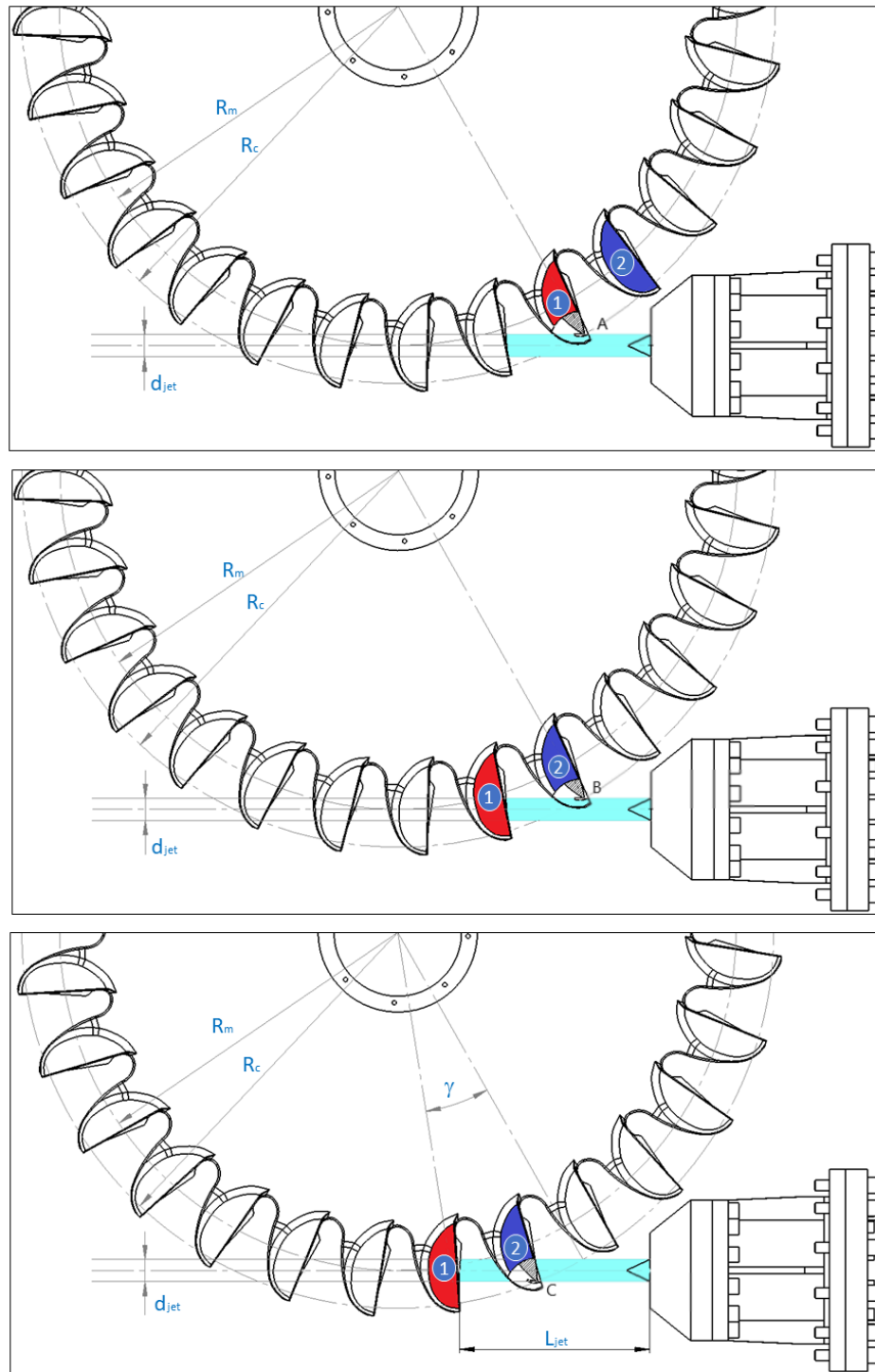


Figure 4.9: Graphical explanation of the Pelton turbine bucket cycle: top: Start of the jet-bucket interaction; middle: End of the full impingement; bottom: End of the bucket cycle.

Peripheral speed coefficient is given as:

$$k_m = \frac{U}{C_0} \approx 0.5 \quad (4.3)$$

where  $k_m$  is the peripheral speed coefficient, and for maximum efficiency it should be around 0.5. This gives the value for peripheral speed  $U = 144.9$  m/s.

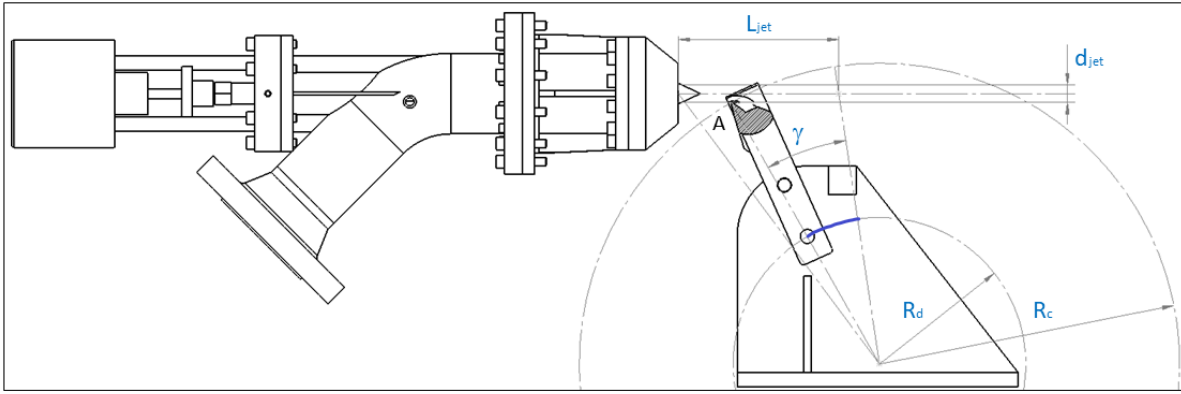


Figure 4.10: Stationary jet-bucket configuration designed for the experiment. Note: All dimensions and positioning are based on existing Pelton turbine manufactured for DOT.

However that design pressure refers to the rotating bucket. In order to calculate equivalent pressure and force for the fixed bucket we first need to determine equivalent jet speed. Having in mind that relative velocity seen by the rotating bucket (see figure 2.3) is given as:

$$W_1 = C_0 - U = 144.9 \text{ m/s} \quad (4.4)$$

For the fixed bucket peripheral speed  $U$  is equal to zero, thus peripheral speed coefficient is zero as well. This gives the value for jet speed  $C_0 = 144.9 \text{ m/s}$ . From this, the equivalent design pressure is:

$$H = \frac{C_0^2}{2g} = 1070 \text{ m} \rightarrow p = 105 \text{ bar} \quad (4.5)$$

To design the bucket to withstand the stresses during tests, the maximum jet impact force will be estimated and used as input parameter for stress analysis. Largest jet impact force is calculated as:

$$F_{bucket} = 2\dot{m}_c C_0 (1 - k_m) = 2\dot{m}_c C_0 = \pi g \rho \varphi_B H B^2 \quad (4.6)$$

where  $g$  is the gravitational acceleration,  $\rho$  is the density of water,  $\varphi_B$  is bucket volumetric load,  $H$  is the net hydraulic head and  $B$  is the width of the bucket. The maximum flow rate that can be achieved with available displacement pumps is limited to 800 l/min so the tests will be conducted at partial loads. However, in order to be able, in the future, to do the test at full loads for which the bucket is designed, the maximum jet force and stresses will be calculated for design flow rate of 3500 l/min or 0.06 m<sup>3</sup>/s.

The diameter of the jet, assuming no losses, is calculated as:

$$d_0 = \sqrt{\left(\frac{4Q}{\pi C_0}\right)} = 0.023 \text{ m} = 2.3 \text{ cm} \quad (4.7)$$

This gives the bucket volumetric load

$$\varphi_B = \left(\frac{d_0}{B}\right)^2 = 0.044 \quad (4.8)$$

where width of the bucket is  $B = 0.11 \text{ m}$ .

Returning this value to equation 4.6, maximum jet impact force on the bucket is estimated to be  $F_{bucket} = 17548 \text{ N}$ .

The bucket itself is redesigned for purpose of the test, to make it cheaper and easier to manufacture. This is done by removing complex surfaces at the backside of the bucket since they will not influence the pressure distribution in a fixed configuration. 3D model along with main dimensions of the redesigned bucket are shown in the appendix. Material properties for the bucket and bucket holder are given in the table below:

Static structural analysis was conducted in ANSYS Mechanical and the results are shown below.

As it can be seen from the figures, maximum stress is 105.9 MPa which is much lower than the yield strength of both materials. This means that we are in elastic region and pieces will not deform.

Table 4.7: Material properties

Part	Material	Elastic Modulus	Tensile strength	Yield strength
Bucket holder	Structural steel	200e+03	460	250
Bucket	Stainless steel	200e+03	600	400

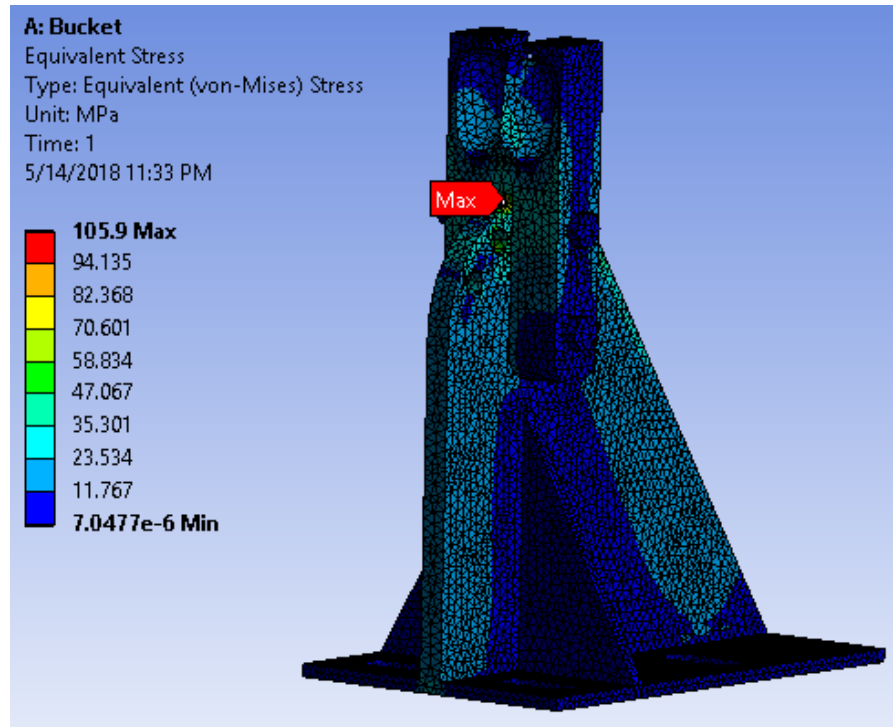


Figure 4.11: Results of FEA (Finite Element Analysis) for Von-Mises stresses in the bucket with normal force of  $F = 20 \text{ kN}$  applied on the bucket surface.

## 4.2. Result analysis of the Phase I: High speed jet flow visualization

As mentioned before, the phase I of the tests is meant to show how pressure, pressure fluctuations from displacement pump and the flow rate, influences formation of the high speed jet, its quality and thus efficiency of the turbine. The test set-up is configured as explained in section 4.1 and the instrument specifications are given. The measurement campaign is conducted for the operating points given in table 4.8.

Major difference in operating conditions of the Pelton turbine for the DOT concept and standard hydro power plants with these turbines is that standard turbine will operate with constant pressure, determined by the height difference between the upper and lower reservoir. The flow rate is then regulated by the spear valve. For the DOT concept, flow rate is dictated by the rotational speed of the displacement pump, thus rotational speed of the wind turbine and therefore wind conditions at the wind farm site. In this case the pressure has to be regulated and kept constant by control of the spear valve. This implies that, at below rated wind conditions, Pelton turbine will have to operate with lower pressures and lower flow rates than it is designed for. Since stability and the structure of the jet are extremely important parameters that influence the flow distribution inside the Pelton bucket and in the end term total efficiency of the turbine, investigating these parameters at **partial loads** might be really important part of the hydraulic turbine design for DOT.

All operating points, given in table 4.8 correspond to partial loads of the existing turbine used for these experiments.

As it can be seen from the table 4.8 measurements are performed for ten flow rates and for the range

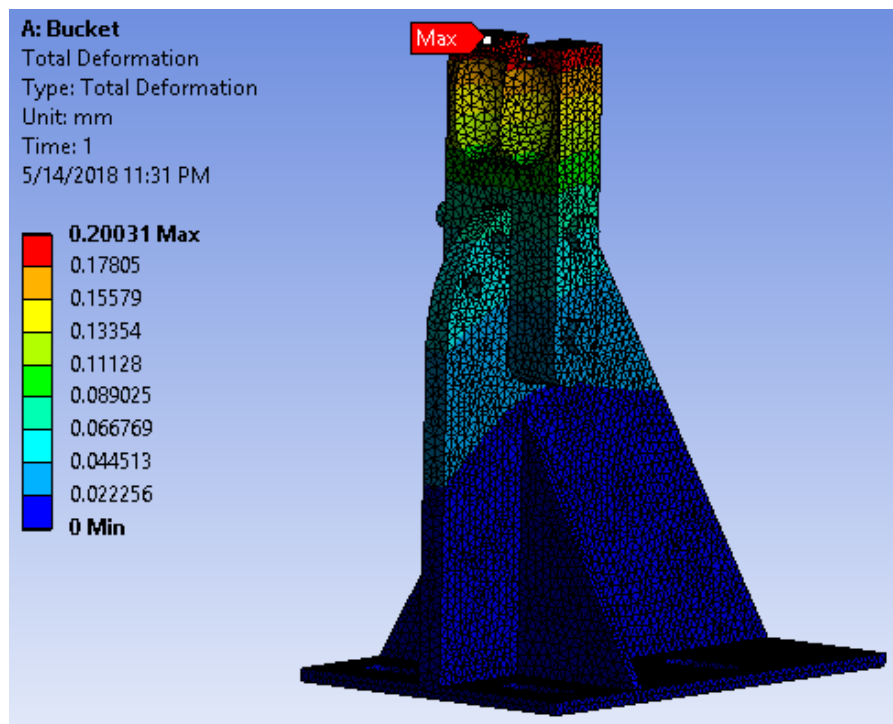


Figure 4.12: Results of FEA (Finite Element Analysis) for total deformation of the bucket with normal force of  $F = 20 \text{ kN}$  applied on the bucket surface.

Table 4.8: Pressure/flow measurement points for the phase I of the test. Note: First number in the pressure range column also defines the pressure step.

Rotational speed	Flow rate	Pressure range	Pressure measurements	Flow visualization
500 rpm	112.5 l/min	2 - 16 bar	✓	✓
600 rpm	135 l/min	2 - 22 bar	✓	✗
700 rpm	157.5 l/min	4 - 24 bar	✓	✗
800 rpm	180 l/min	5 - 40 bar	✓	✓
900 rpm	202.5 l/min	5 - 45 bar	✓	✗
1000 rpm	225 l/min	5 - 55 bar	✓	✓
1100 rpm	247.5 l/min	5 - 65 bar	✓	✗
1200 rpm	270 l/min	5 - 80 bar	✓	✓
1300 rpm	292.5 l/min	5 - 75 bar	✓	✗
1400 rpm	315 l/min	5 - 70 bar	✓	✓

of pressures. The reason why the pressure ranges are different is because pressure is a function of flow rate and resistance in the system. At lower flow rates it was impossible to achieve higher pressures as the spear valve is very close to fully closed position so the spear valve couldn't be controlled accurately enough to prevent it from completely closing. It should be mentioned that the flow visualization was not performed for the whole pressure range.

Also another interesting phenomenon is noticed during the tests. When test rig is fully enclosed from all sides, it is noticed that the front poly-carbonate plate is vibrating due to the air movement caused by the water jet interacting with surrounding air. In order to prevent the vibrations the top plate was removed from the test rig. That allowed the air to freely leave the box and no further vibrations were noticed. This also gave additional perspective in realizing the importance of Pelton turbine casing design, not just from standpoint of windage losses (efficiency) but also dynamic loading caused by the air movement inside the turbine casing.

### 4.2.1. Pressure at the inlet of the injector

These measurements are performed in order to confirm the existence of the pressure fluctuations caused by the PD pump and determine its magnitude and frequency. Furthermore, the measured pressure signal will be used as the inlet boundary condition for the CFD simulation in the next step.

The results from the pressure measurements for three different flow rates are shown in figures 4.13, 4.14 and 4.15. As can be seen from the time series in the left column, the fluctuations of pressure can reach over 6 bar, however this can be also the consequence of noise from the system. In order to see if these fluctuations originate from the discrete movement of the piston of axial displacement pump, spectral analysis of the signal is conducted. Results are shown in the right column. We can clearly identify frequencies that correspond to rotational velocity of the pump and thus the movement of the piston. Frequency of 10 Hz correspond to rotational speed of 600 rpm, 16.6 Hz corresponds to 1000 rpm and 23.3 Hz is the frequency of the PD pump rotating at 1400 rpm. Also, interesting to notice is the frequency of 17 Hz which is common for all measuring points, however its origin was not identified. In the end it should be said that piston frequency wasn't identified for all measuring points. The reason for that can be because the signal was too noisy and the total acquisition time was too low.

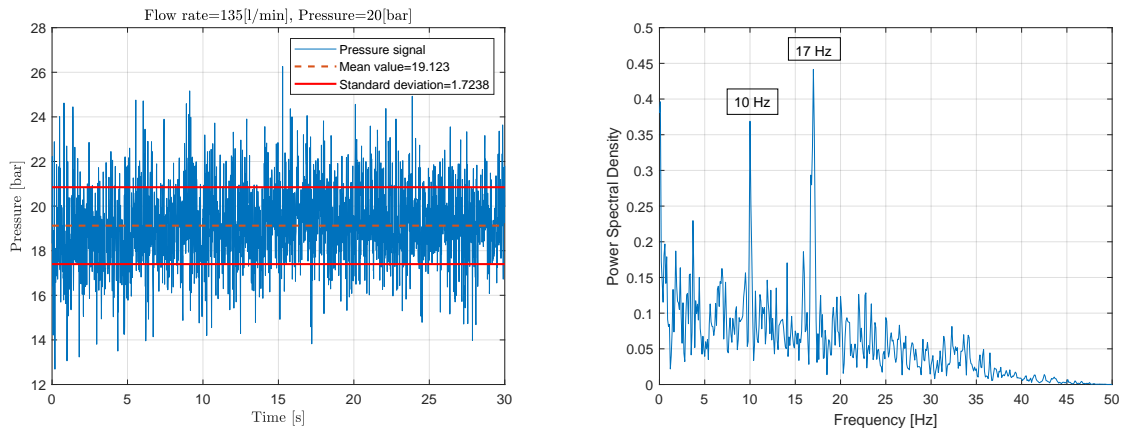


Figure 4.13: Pressure time series signal and its power spectrum at pump motor speed of 600 rpm and set pressure of 20 bar.

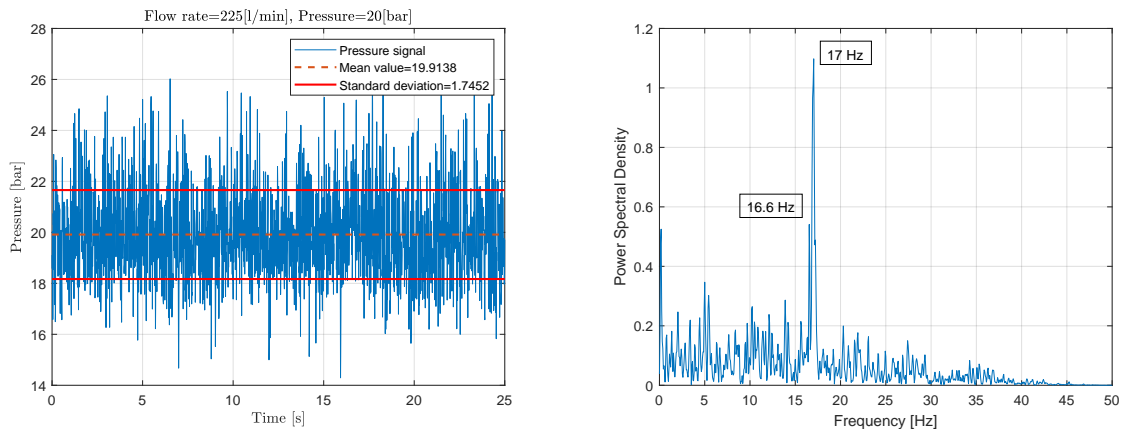


Figure 4.14: Pressure time series signal and its power spectrum at pump motor speed of 1000 rpm and set pressure of 20 bar.

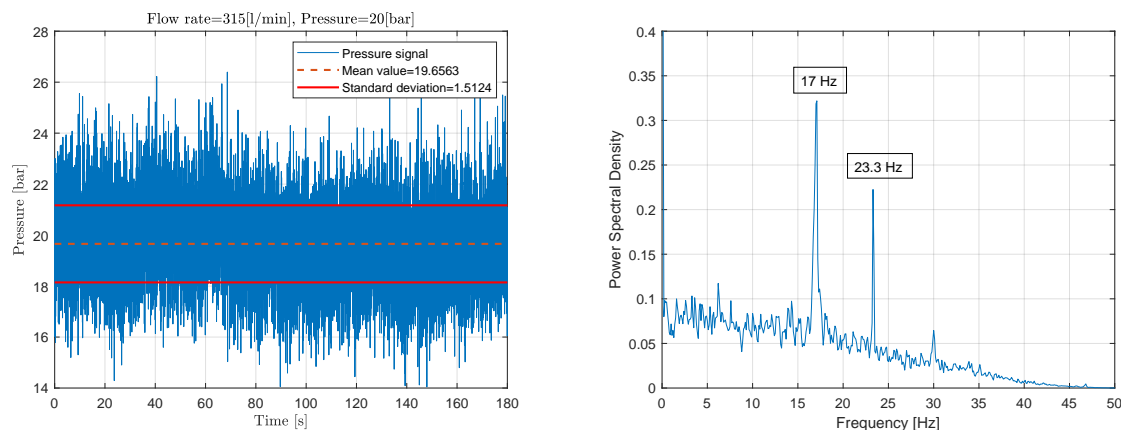


Figure 4.15: Pressure time series signal and its power spectrum at pump motor speed of 1400 rpm and set pressure of 20 bar.

#### 4.2.2. Flow visualization

Flow visualization was performed for different flows, as given in table 4.8, but not for the whole pressure range at a given flow. There are several reasons for this. Firstly, test time window was very limited. Since camera had only one 10 Gb memory card, the data from the card had to be transferred first and saved on local hard drive before starting with next measurement point. This was a very time consuming process. Secondly, one second of recording, at speed of 5400 fps and maximum resolution of  $1024 \times 1024$  pixels, contains around 10 Gb of data and there were over a hundred operating points observed. Nevertheless, jet flow visualization was performed successfully and the results are given below.

One of the assumptions, that the pressure fluctuations from the PD pump will influence the quality of the jet, could not be backed up. By pure visual inspection of the recorded images for different operating points, no visible disturbances - in terms of water bulges - were noticed, as in case of pulsating nozzle (figure 2.23) and reported in [11].

Nevertheless, some other interesting information can be obtained by visual inspection of the recordings. In the figure 4.17, images for four different pressures at maximum flow rate of 315 l/min are shown. What can be noticed from these recordings is the large instability in the jet flow, in terms of flow separation or dispersion at the upper side of the jet. This separation comes from the fact that there are two secondary flows in tangential direction caused by the existence of the bend before the injector. These two flows are rotating in opposite direction and collide in the jet on the side of the bend. This is shown in subsection 2.4.3 and investigated and reported by Zhang and Casey in [25]. Furthermore, in order to achieve high pressures at low flow rates, the spear needle had to be moved very close to fully closed position where the effective nozzle area is very small (See figure 2.18). This is an additional condition which might have influenced stability of the jet flow at higher pressures. This is visualized in figure 4.17, where it can be clearly seen that instability is increasing with increase in pressure.

As it can be seen from the figure 4.17, the distance of separation from the injector nozzle is decreasing with increase in the pressure. Furthermore, it also decreases with decrease in the flow rate. This is clearly depicted in the figures 4.16 a) and 4.16 b) where distance of the points of separation are acquired with Photron FASTCAM software. The scale calibration was done prior to the measurements by using, as reference, the meter scale placed above the jet in the same plane as the jet, with respect to the camera depth of field. It should be noted that the exact point of separation is hard to define especially because the injector bend is under certain angle with respect to camera field-of-view plane. As mentioned before, secondary flows collide at the side of the pipe bend, therefore the dispersion starts at that point, which is not located in the camera plane. This can be confirmed by noticing the portion of the jet where its transparency is completely blocked by dispersed flow in the back side, as marked with blue arrows in figure 4.17. In the first image, at the 20 bar pressure, the dispersion can be clearly noticed in the back of the jet but the divergence is not noticeable from the camera plane

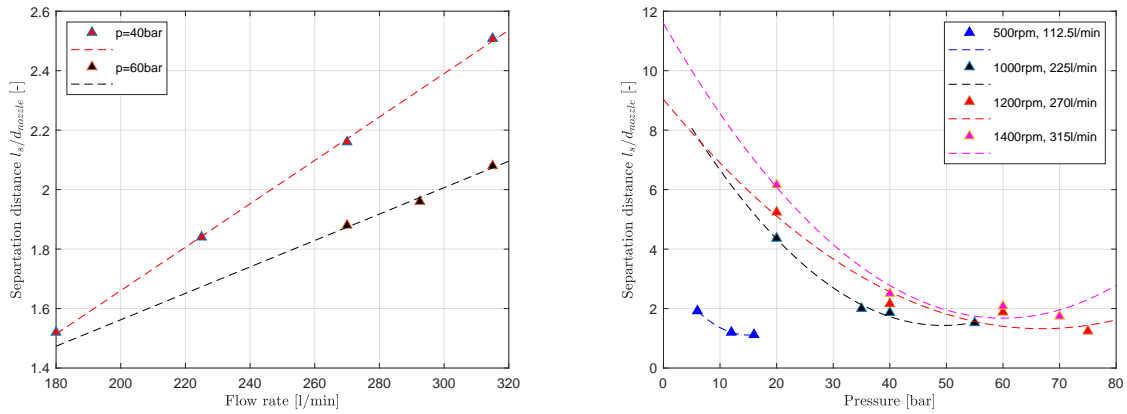


Figure 4.16: Distance of separation (dispersion) of the water jet as a function of the flow rate (left) and pressure (right) normalized with the nozzle diameter.

and more severe instability probably starts at the distance larger than the cameras field-of-view. Although the points of separation are not precise, the trend of change in distance is what is important because it gives the idea about the flow rate necessary at certain operating pressure to have the highest quality jet and thus ensure the most efficient energy exchange between the turbine and the jet. This might be one of the most important challenges in the Pelton turbine design for the DOT concept.

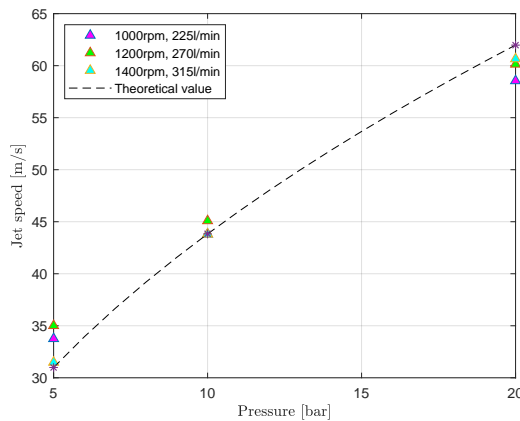


Figure 4.18: Jet speed as a function of pressure measured at different flow rates.

There are two other parameters that can be obtained from the flow visualization of the jet. These are jet speed and jet diameter. Jet diameter is determined for different operating points in the same way as for the distance of separation. The example of the procedure for determination of the jet speed is shown in figure 4.19. Four consequent frames are observed at the maximum flow rate and 20 bar pressure. The small structure at the surface of the jet was noticed and marker was placed to follow it as it propagates downstream. As the structure remains coherent during the four frames, the distance that it travels during that time was measured. Since the frame rate is known, the speed of the jet is calculated as follows:

$$C_0 = \frac{\delta x}{N_f / fps} \quad (4.9)$$

Where  $\delta x$  is distance of travel,  $N_f$  is number of frames travelled and  $fps$  is the frame rate. The jet speed is calculated for three different flow rates and three different pressures as shown in figure 4.18. Since the jet speed is only dependent on the pressure as given with Torricelli formula (Eq. 2.16) the value should be the same for all flow rates. However there is a small difference in measured values and theoretical value which is also given in the same figure. There could be several reasons for this: uncertainty in measurements, difference between real pressure and observed one, water leakage, non-uniform velocity profile etc.

It should be noted that it was possible to determine the speed of the jet only for the pressures up to 20 bar. At higher pressures it is difficult to find structures that remain coherent for two consequent frames to be able to measure distance travelled. It might be possible to do this by increasing the frame rate and shutter speed but this would require more powerful lighting system in order for camera to receive enough light with such a short exposure time.

Regarding the jet diameter, the values for different flow rates and at different operating pressures are given in figure 4.20 a). It should be noted that jet diameter is measured in front of the *vena contracta*

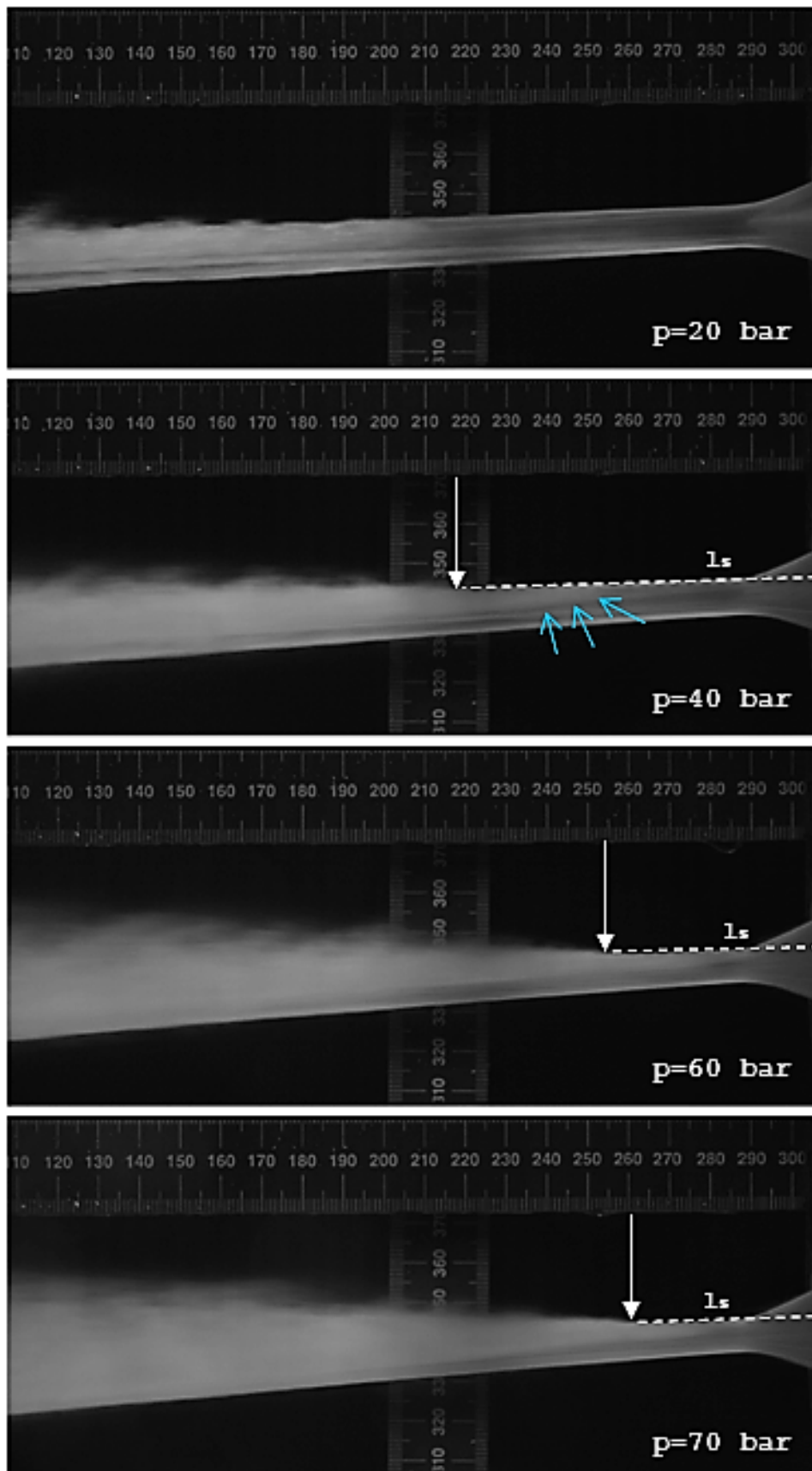


Figure 4.17: Flow visualization of the high speed jet at the flow rate  $Q = 315$  l/min and rotational speed 1400 rpm. Dispersion of the water droplets and separation distance from the injector nozzle. Note: Dashed line represent distance of the separation point from the nozzle exit ( $l_s$ ); Blue arrows indicate the region where jet transparency is blocked by dispersed flow behind the jet.

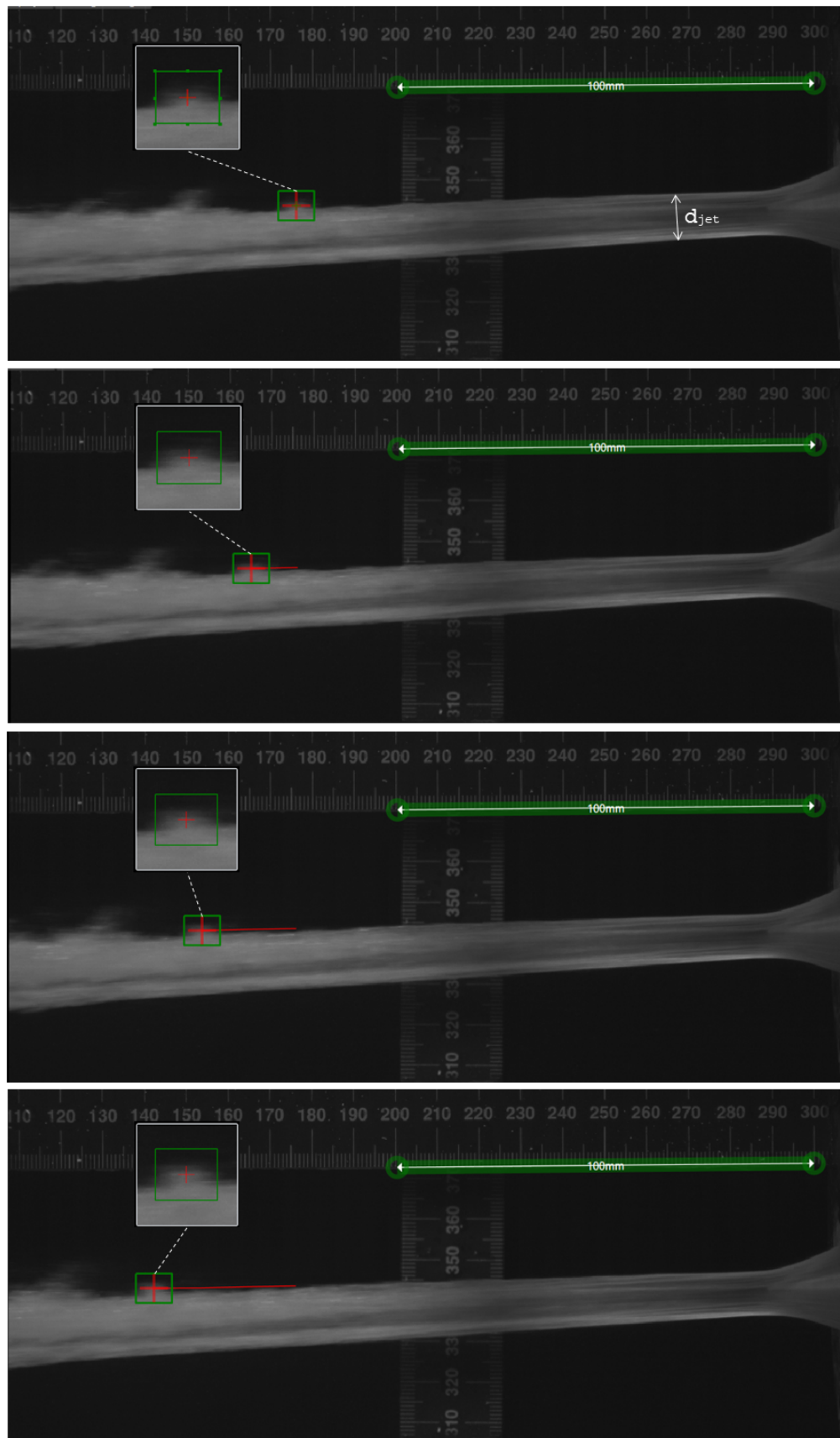


Figure 4.19: Flow visualization of the high speed jet at the flow rate  $Q = 315$  l/min and rotational speed 1400 rpm. Procedure for determination of the jet speed.

(narrowest diameter), where it has constant value. As expected from theory, clear decreasing trend is depicted when decreasing the flow rate and increasing pressure. The value of jet diameter, or rather the ratio between the jet diameter and the width of the bucket, from a stand point of the efficiency, is very important for the design of the Pelton turbine. The square of this ratio, as already explained, is called the bucket volumetric load (Eq. 2.20) and the highest efficiency is achieved for  $\varphi_B = 0.11$ , or when the jet diameter is around one third of the bucket width [4], [21], [30]. Bucket volumetric load as a function of pressure and flow rate is shown in figure 4.20 b). Since the existing Pelton turbine and its bucket are designed for much higher flow rates, the bucket volumetric load is way below optimal value. But the trend can give us indication of what flow rate is necessary at certain pressure in order to have the highest efficiency.

What is also interesting to notice, from figures 4.20 and 4.16, is that separation distance and jet diameter have similar trend relative to pressure and the flow rate.

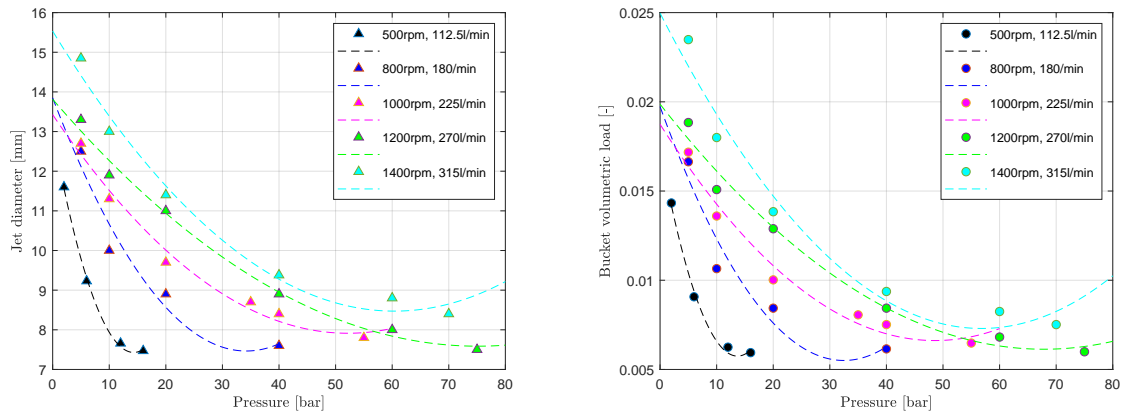


Figure 4.20: Jet diameter (left) and bucket volumetric load (right) as a function of pressure and the flow rate.

# 5

## CFD analysis of the flows inside a Pelton turbine

In this chapter numerical simulations and analysis of the flow inside the injector, flow of the high speed jet and flow inside the bucket will be performed. Simulations are done for single bucket position and three different spear positions and thus three pressure set points. Set points correspond to the conducted tests which are discussed in previous chapter.

### 5.1. CFD software and simulation set-up

ANSYS CFX and ANSYS Fluent are two commercial codes that are most used in the previous studies of the flow in Pelton turbines. They were validated and they showed good agreement with experimental measurements. This, and the fact that there are vast online resources for learning this software, is the reason why are they considered for this thesis project as well. Furthermore, student licence for this software is available at TU Delft and DTU.

Both solvers use control volume method to discretize the flow domain. The main difference is that CFX uses finite element with vertex-centered numerics, where all the solution variables and flow properties are written at element vertices. Control volume is created around the element vertex by joining surrounding cell and edge centers, as shown in figure 5.1. On the other hand, Fluent uses finite volume method with cell-centered approach, where all the variables and fluid properties are stored at the element center.

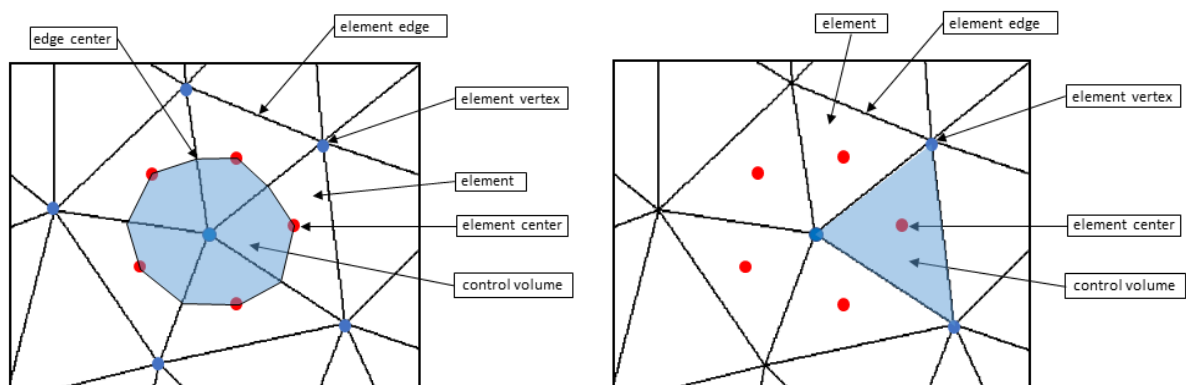


Figure 5.1: CFX vertex-centered FV discretization scheme (left) and Fluent cell-centered FV discretization scheme (right).

These two codes also differ in the way they solve governing equations. Fluent uses both segregated and coupled solver, while CFX offers only coupled solver. The difference between these solvers is in the order in which momentum and continuity equations are solved. The pressure and velocity are strongly coupled through main governing equations, meaning in order to solve for the velocity field it is neces-

sary to know the pressure field. A segregated solver at the start uses a guess for the pressure field and then solves the momentum equations in order to get the velocity field. Next, velocity field is checked to see if it satisfies the continuity equation. If not, pressure correction is used for the pressure field and momentum equations are recalculated. This is continued until velocity field satisfies the continuity equation. Since only single equation at a time is solved, this solver requires less memory for storage but needs more time to converge. On the other hand coupled solver requires more memory but less time for convergence since it solves both, continuity and momentum, equations at the same time.

Another characteristic of the flow in Pelton turbines is that, after the nozzle, the flow has to be considered as two-phase flow. Liquid phase is the water jet coming from the nozzle and gaseous phase is the surrounding air. The existence of more phases complicates numerical modelling of the flow. Nevertheless, there are several models that are created to deal with multi-phase flows. Most widely used and validated model for multi-phase flow is Volume-Of-Fluid (VOF), which is also offered in Fluent solver. The 2-phase homogeneous model is the equivalent model to VOF offered by CFX solver. More information about these models is given in chapter 2.

It has been reported before that CFX 2-phase homogeneous model is more accurate than Fluent VOF for simulating two phase flow in Pelton turbines [13]. From this reason and also better familiarity, Ansys CFX solver is used for numerical analysis of the flow in this thesis project.

Before starting with simulation, it is important to determine which forces are relevant for the investigated flow and which ones can be disregarded as having only minor influence on the flow. As mentioned before in section 2 and taken from Hana[12], influence of certain forces on the flow in Pelton turbines can be assessed by calculating three dimensionless parameters:

- Reynolds number - addresses importance of viscous and inertial forces,
- Froude number - addresses importance of gravity vs inertial forces,
- Weber number - addresses relevance of surface tension vs inertial forces,

These number are calculated for the investigated flows and given in table 5.1.

*Table 5.1: Dimensionless parameters for investigated flows. Characteristic lengths for injector, water jet and bucket are, respectively: internal diameter of the injector pipe, diameter of the jet and bucket width; Characteristic speeds are: water speed inside the injector and jet speed for both jet and bucket domain.*

Description	Injector	Water jet	Bucket
Characteristic length	0.1 m	0.0103 m	0.11 m
Characteristic velocity	0.67 m/s	63.24 m/s	63.24 m/s
Pressure	20 bar	20 bar	20 bar
<b>Reynolds number</b>	6.7e03	6.5e05	6.96e06
<b>Froude number</b>	0.68	198.9	43
<b>Weber number</b>	616.6	5.66e05	6.04e06

It can be concluded from the table that inertial forces are dominant for all the flows. Gravity force doesn't have significant effect on water jet or bucket flow but it might have the influence on the flow inside the injector. on the other hand surface forces can be disregarded for all flows but according to Hana they are important for the scaling effect, so they are taken into account in these simulations as well. Surface tension coefficient is set to  $\sigma = 0.0728$  [28].

## 5.2. ANSYS Workbench project schematic and workflow

Complete simulation set-up is conducted through ANSYS Workbench environment (Figure 5.2). Workbench allows modularization of different parts of numerical analysis. Geometry definition, mesh generation and solver can be defined separately and then connected. This means that one geometry can

have different mesh or same model can be simulated with different settings or different solvers. This greatly simplifies and speeds up set-up for different cases investigated.

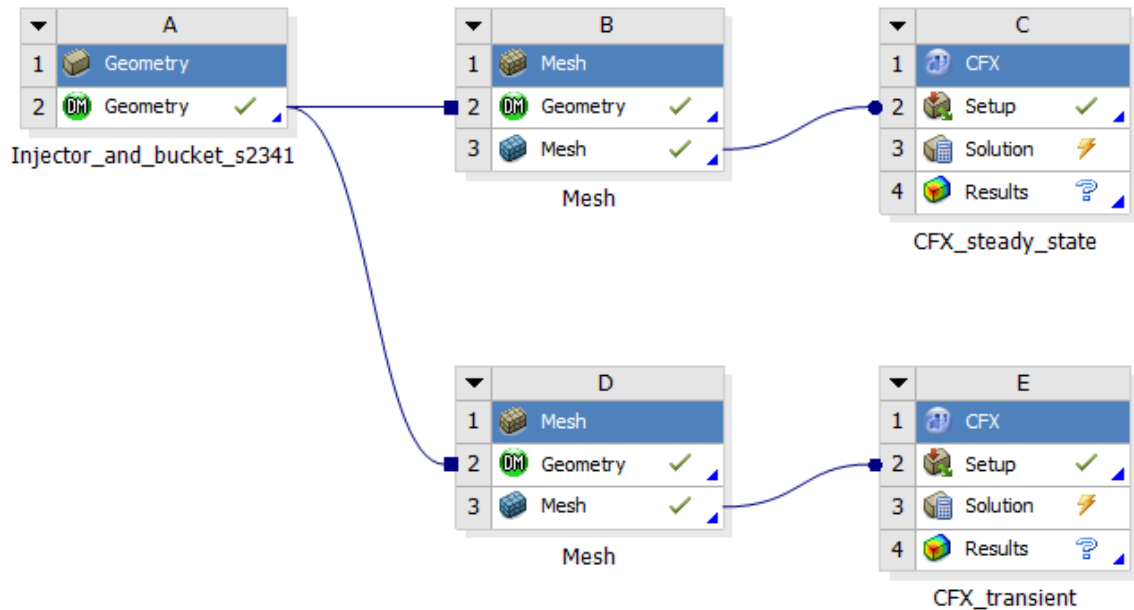


Figure 5.2: Example of workbench project schematic. Steady state and transient simulation for 60 bar case.

### 5.3. Model and test operating points

Same model for the experiment is used for numerical simulations (See figure 5.3). Only one bucket position will be considered for three different spear positions and thus three set pressures. Operating points investigated with numerical analysis are given in table 5.2. Bucket is set, with respect to bucket cycle (Figure 4.10), to the position at which it is under the full impingement of the high speed jet. It is the position just before following bucket starts cutting the jet as illustrated in the middle figure 4.9.

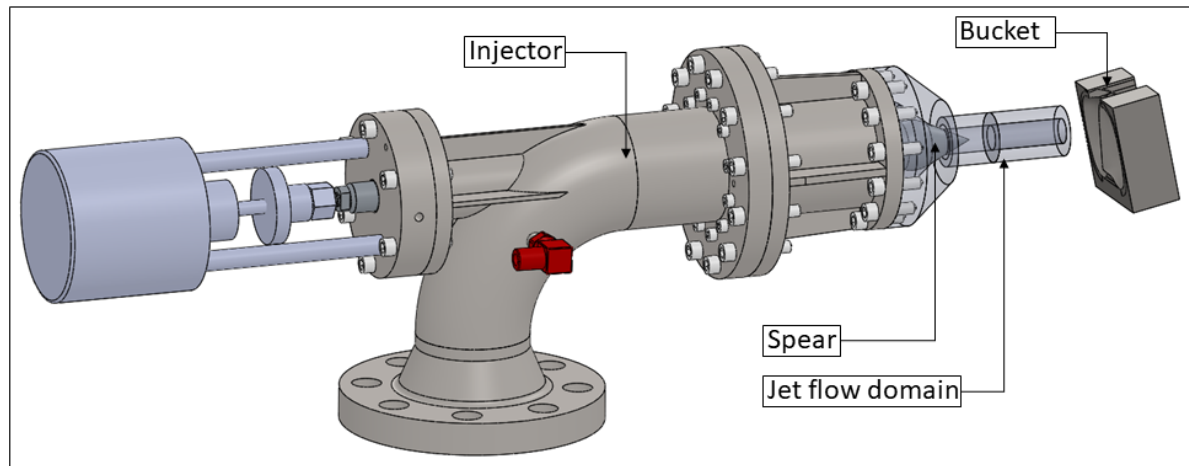


Figure 5.3: Injector-bucket configuration for the numerical analysis. Note that three cylinders are created to represent jet flow domain.

For each case, defined in table 5.2, new 3D model (Figure 5.3) is generated with different spear position and it is saved as .step file and imported to *Ansys Design Modeler*. The complete flow domain is extracted from the solid model and it is given in figure 5.4. Injector fluid domain is created by putting the caps at the inlet of the injector and the nozzle exit and filling the cavity. Bucket fluid domain is

Table 5.2: Operating points simulated with Ansys CFX. Each case correspond to different spear position which is given by the percentage of the spear valve opening. Fully opened position is at 100 %. Note: Correct spear position is acquired from the experiments for the corresponding set pressure. Furthermore, pressure at the inlet of the injector is also acquired from the measurements and it is not constant but varies with time.

Description	Case 1	Case 2	Case 3
Bucket angle	13°	13°	13°
Flow rate	315 l/min	315 l/min	315 l/min
Set pressure	20 bar	40 bar	70 bar
Spear position	13.04 %	9.32 %	6.36 %

gained by enclosing the bucket with cubical body and using Boolean operation to subtract the bucket from this body.

In order to decrease the number of cells in the computational grid, the plane of symmetry is defined. The flow is considered to be symmetrical with respect to  $yz$  plane or the plane that divides the bucket in two, along the jet cutter. After generating flow domain all boundaries are defined and are given in figure 5.4. It should be mentioned that whole flow domain is divided in two domains. Injector domain (Figure 5.4 - inlet and injector wall boundary) is defined from the inlet boundary until nozzle exit and rest of the domain is defined as the jet-bucket domain. The main reason for domain separation is because the flow in the injector can be considered as single phase flow, while jet flow and free surface bucket flow is two phase flow. Furthermore, this way injector can be initialized as completely filled with water which will decrease time necessary for simulation.

## 5.4. Meshing

Numerical mesh for simulation is generated using Ansys automatic meshing tool. Example of the mesh is shown in the figures 5.5 and 5.6. Firstly, whole domain is meshed uniformly with default settings for CFX solver and only maximum size of the element is chosen. Next, global mesh control is overridden by using body sizing method with bodies of interest to refine mesh at regions of interest. Three main regions of interest are identified as most important for the flow and mesh is refined in those regions.

Firstly, as it is shown in *Detail A* of the figure 5.5, passage between the spear needle and injector wall has the finest mesh. The reason for this, as mentioned before, is because in order to generate high pressure with low flow rate, spear has to be very close to fully closed position so that the effective nozzle area is extremely small. This and the fact that CFX uses vertex-centered discretization scheme (See beginning of section 5.1), requires that cell size in this region be several times smaller than the passage itself in order to have enough vertex points for the solution. Since the passage width is the order of millimeters this means that minimum cell size has to be at least quarter of a millimeter. The effect of this on choice of simulation time step will be explained in the subsection 5.5.

The number of cells and nodes as well as minimum cell size for three investigated cases are given in table 5.3. It should be mentioned that mesh convergence investigation is generally conducted in order to determine the number of elements after which further increase does not influence solution anymore. However since computational time was limited and smallest cell size is determined by the passage between spear and injector wall, mesh convergence is not investigated in this thesis.

Secondly, jet flow domain is constructed from two main regions: middle, jet region and outer surrounding region (See figure 5.6). This is so that jet region can be meshed separately and with smaller cells. Furthermore middle jet region is also divided in two sub-regions. This was necessary because the spear needle was sticking outside injector domain so in order to extract fluid domain, as discussed before, extension of injector nozzle is added before closing the domain with caps and filling the cavity. Thus, due to existence of needle tip this part is meshed with unstructured tetrahedral mesh. This, as it will be shown later, will have the influence on sharpness of the jet interface. Rest of the jet domain is meshed with structured hexahedral mesh.

Finally, the bucket domain, due to complexity of the geometry, is meshed also with unstructured tetrahedral mesh. Spherical body of influence allowed to refine the mesh in front of the bucket and near the bucket surface.

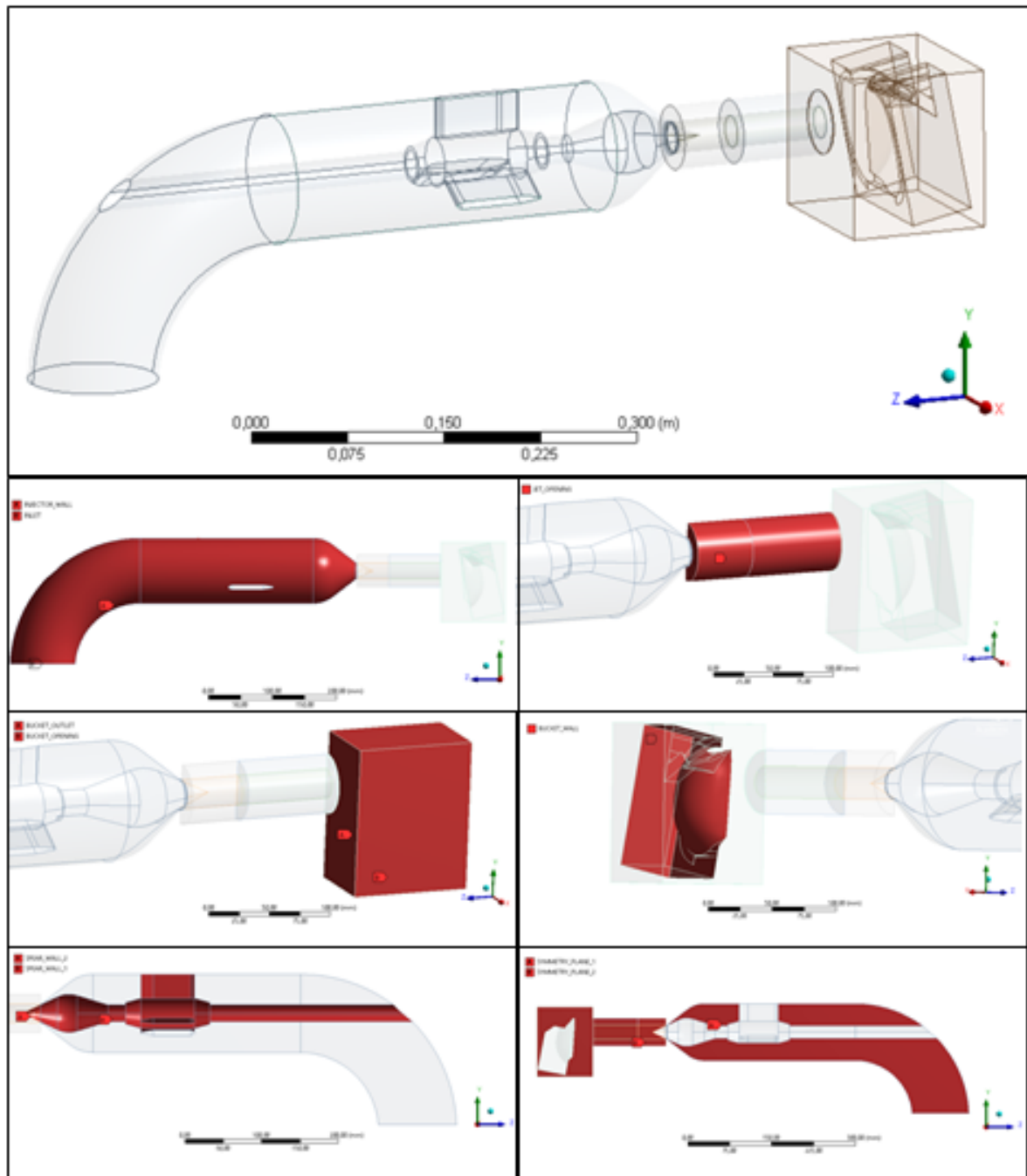


Figure 5.4: Boundaries at the domains defined for the simulation.

## 5.5. Solver set-up

In this subsection, solver set-up in Ansys CFX for investigated cases is explained in more detail.

### 5.5.1. Analysis type

The first part that has to be defined in Ansys CFX solver is the type of analysis we are conducting. This can be either transient or steady state analysis. Since we are interested in investigating pressure fluctuations and their influence on the jet and free surface flow inside the bucket thus time signal from pressure measurements is used to define time dependent inlet boundary condition, so transient simulation is chosen for the analysis.

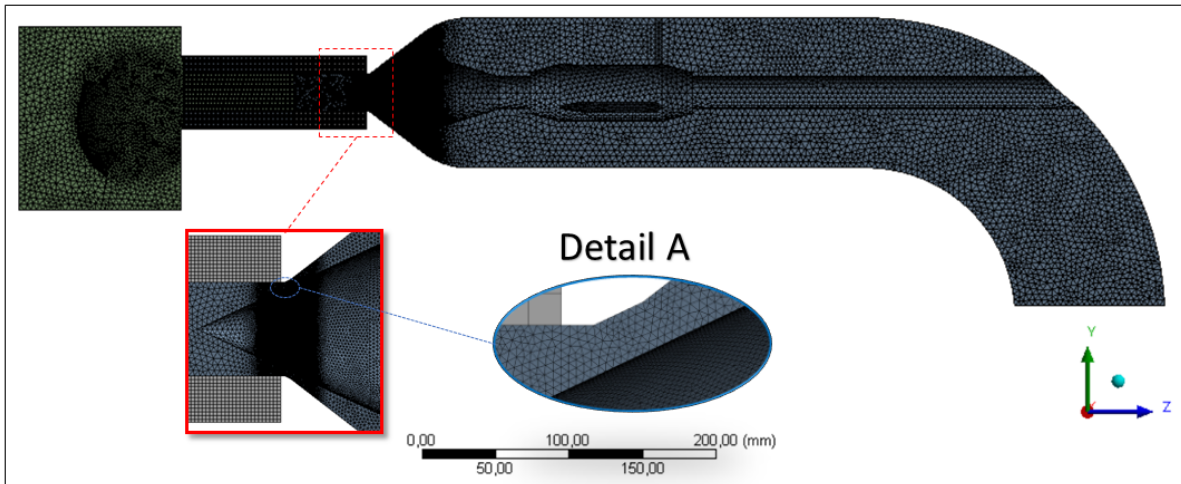


Figure 5.5: Mesh generated using Ansys automatic meshing tool shown at the symmetry plane.

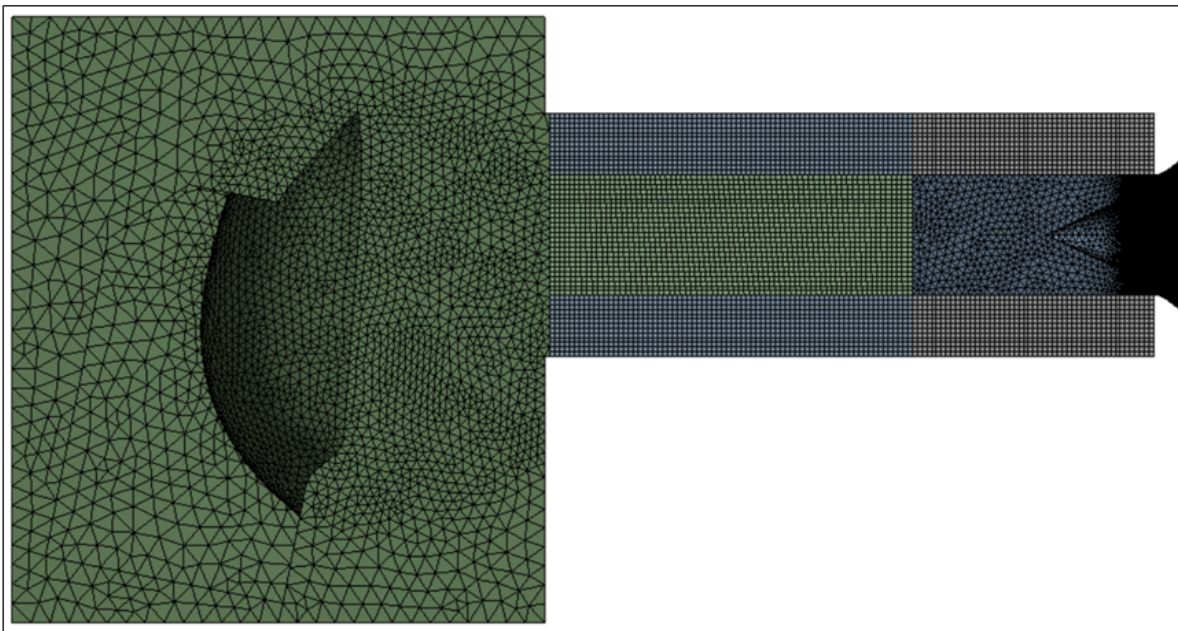


Figure 5.6: Mesh for the jet and bucket flow domain shown at the symmetry plane.

For transient simulation it is extremely important to set proper time step. As stated before, time step is related to spatial step or the cell size. Specifically minimum cell size dictates time step according to Courant–Friedrichs–Lewy criteria (Equation 5.1) so if minimum cell size is small, the value of time step has to be very small as well in order for solution to converge. Furthermore, time step also depends on the magnitude of characteristic velocity of the flow which in this case is the water jet speed.

$$\frac{u\Delta t}{\Delta x} \leq C o_{max} = 1 \Rightarrow \Delta t \leq \frac{\Delta x}{u} \quad (5.1)$$

Where  $\Delta t$  is the time step,  $\Delta x$  is spatial step,  $u$  is characteristic velocity and  $C o_{max}$  is the Courant number.

It should be noted here that value of maximum Courant number depends on type of solver used. Explicit solvers require that maximum Courant number be set to one. Implicit solvers, like CFX, does not have this requirement but sometimes is desirable to have smaller time step, especially for the

Table 5.3: Mesh statistics for investigated cases.

Description	Case 1	Case 2	Case 3
Set pressure	20 bar	40 bar	70 bar
N <sup>o</sup> of Nodes	3052965	3538307	3444546
N <sup>o</sup> of Elements	2094632	2166755	2379155
Min. cell size	0.25 mm	0.25 mm	0.25 mm

Table 5.4: Time steps for investigated cases.

Description	Case 1	Case 2	Case 3
Set pressure	20 bar	40 bar	70 bar
Jet speed	63.2 m/s	89.4 m/s	118.3 m/s
Time step	$3.95e - 06$ s	$2.85e - 06$ s	$2.28e - 06$ s
Min. time step	$3.0e - 06$ s	$2.0e - 06$ s	$2.0e - 06$ s
Max. time step	$6.2e - 05$ s	$2.2e - 05$ s	$1.0e - 05$ s
Total time set	0.05 s	0.05 s	0.05 s

multiphase flow, so the same criteria can be used. Otherwise sensitivity analysis should be carried out to determine proper time step which will give satisfying accuracy. For this thesis,  $Co_{max} = 1$  is used as criterion for calculating time step and adaptive time stepping was applied. Values for investigated cases are given in table 5.4.

### 5.5.2. Domain definition

As previously explained, two flow domains are defined for simulation: injector domain, from the inlet to nozzle exit, and jet-bucket flow domain (See figure 5.7). In principle, flow inside the injector can be considered as single phase flow and can be simulated independently, which was the initial idea. However, tip of the needle spear is inside the jet flow domain where two-phase flow has to be considered. Because of this, both domains are simulated simultaneously as two phase flow. But dividing domain in two allowed to set the initial condition for the injector domain as completely filled with water. This was important because total simulation time was extremely limited and by excluding filling process from the simulation helped focus only on the development of the jet and bucket flow.

Two fluids - water and air - are defined, with water being primary fluid. CFX homogeneous model for multiphase flow is applied with standard free surface model. Turbulence is modeled by  $k - \omega$  SST turbulent model with automatic wall functions. Domains are initialized with Cartesian velocity components set to zero and relative pressure set to zero. Water volume fraction was set to one and air volume fraction was set to zero for injector domain (injector is initially filled with water), while for jet-bucket domain it is opposite.

### 5.5.3. Boundary definition

All boundaries and their basic settings are defined according to table 5.5. It should be mentioned that inlet boundary condition set as total pressure is actually static pressure at the inlet of injector which is measured during the experiment plus dynamic pressure calculated as:

$$p_d = \frac{\rho v^2}{2} \quad (5.2)$$

Where  $v$  is the water velocity inside the injector calculated from volumetric flow rate:

$$Q = v \frac{D^2 \pi}{4} \Rightarrow v = \frac{4Q}{D^2 \pi} \quad (5.3)$$

Where  $D$  is the internal diameter of the injector inlet pipe. Volumetric flow rate is known, as rotational speed of pump and piston volumetric displacement are known as well. Although water losses in the

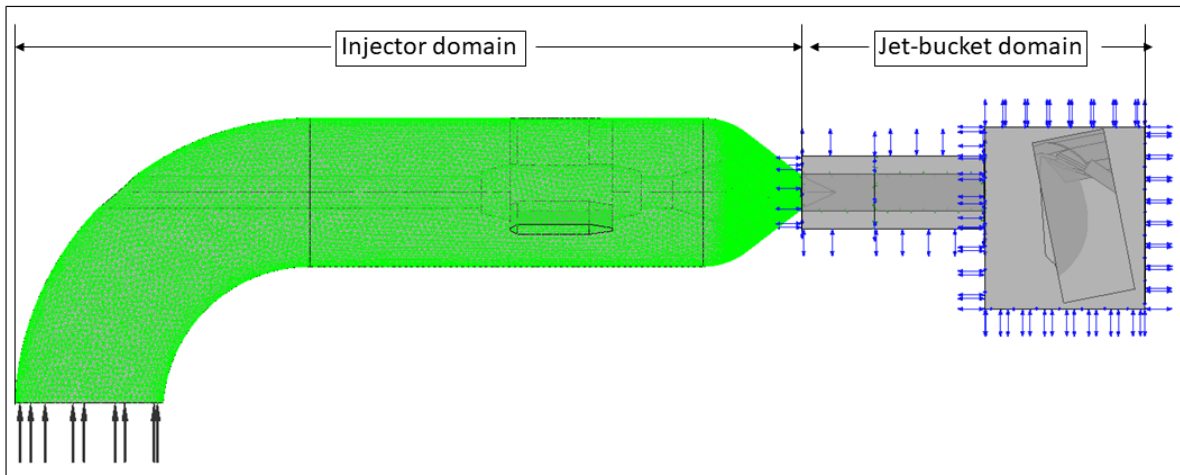


Figure 5.7: Flow domains defined for the simulation.

pump, due to leakage, are present, water velocity inside the injector is very small hence dynamic pressure is also relatively small and thus its contribution to total pressure.

Table 5.5: Boundary properties and initial boundary condition. Note: ID - Injector Domain; JBD - Jet-Bucket domain.

Description	Domain	Boundary type	Boundary details	Volume fraction
Inlet	ID	inlet	total pressure	air=0, water=1
Injector wall	ID	wall	no slip condition	-
Bucket wall	ID	wall	no slip condition	-
Bucket opening	JBD	opening	opening pressure	air=1, water=0
Jet opening	JBD	opening	opening pressure	air=1, water=0
Spear wall	ID and JBD	wall	no slip condition	-

All bucket domain boundaries are defined as *opening*, as it can be seen in the figure 5.7 marked with blue arrows. The reason for this, especially front boundary where jet enters bucket domain, is because fluid can freely enter or exit domain. If it is defined as *outlet*, water which is exiting the bucket would be able to go out of the domain, but the air that is accelerated with the jet would not be able to enter the bucket domain.

#### 5.5.4. Solver and output control

For solving advection term in finite volume equations, high resolution advection scheme is used. For temporal discretization, Second Order Backward Euler scheme is used. This is implicit time stepping scheme which is second order accurate[31]. Turbulent numerics are modeled with first order accurate scheme. Residual convergence criteria is set to  $RMS 1e - 05$ . The output control is set to save the transient results every 0.5 ms.

## 5.6. Analysis of the simulation results

Three cases were simulated with a single bucket position as given in table 5.4. Note that although total time was set to 0.05 s, this is only achieved for case 1 because higher pressures and thus higher jet speed required smaller time step. Since run time in computer cluster was limited to 48 hours this also limited total time as well. Cases 2 and 3 had total simulated time of 0.029 s and 0.015 s, respectively. Nevertheless, simulations were long enough for the flow to develop and reach the bucket. This is clearly shown in figure 5.8 where it can be seen that jet already reaches the bucket at 4.9 ms. This is the case 1 where pressure at the inlet is 20 bar. As pressure increases, jet speed increases as well,

therefor, for cases 2 and 3, jet speed is higher so flow develops even faster. On the other hand, in order to investigate the effects of pressure fluctuations at the inlet of injector it would require at least 0.5 s, since the pressure fluctuations frequency, at tested speed of 1400 rpm, is around 23 Hz. This would give at least 10 pressure cycles for simulation.

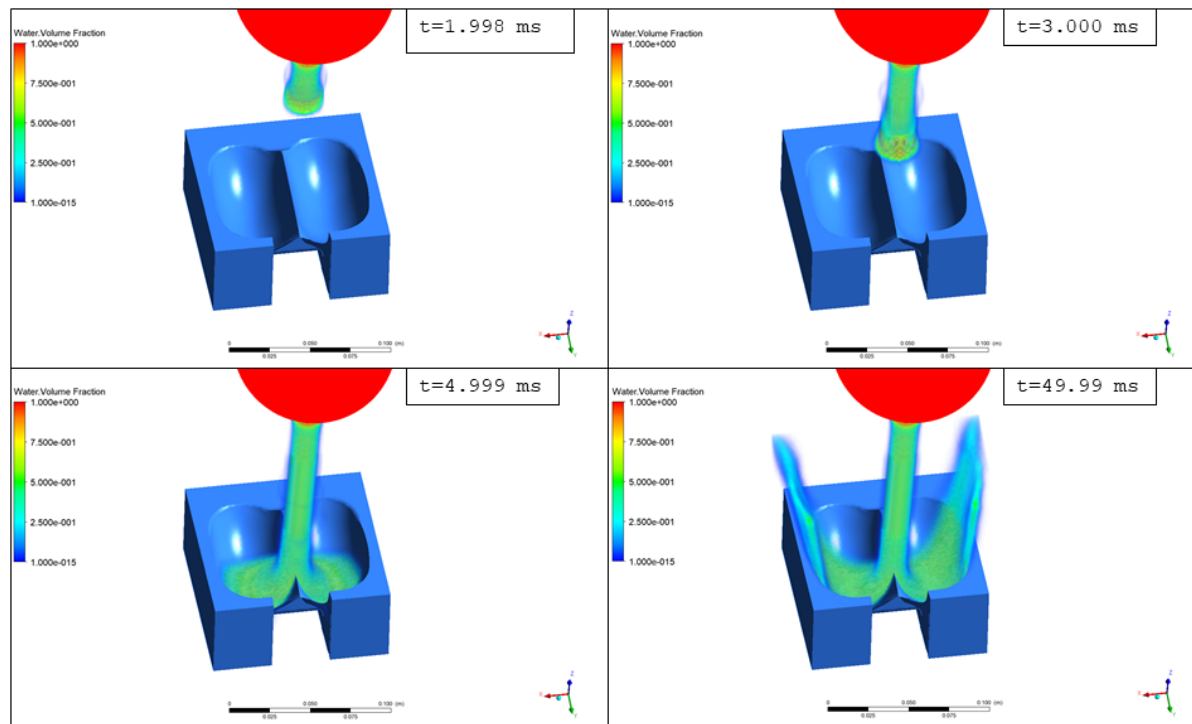


Figure 5.8: Example of the development of high speed jet at pressure of 20 bar and constant flow rate of 315 l/min.

Pressure distribution at the surface of the bucket, for all three cases investigated, is given in figure 5.10. As can be seen from the figure, the flow distribution pattern for all cases is quiet similar. This is logical because flow rate is the same for all cases.

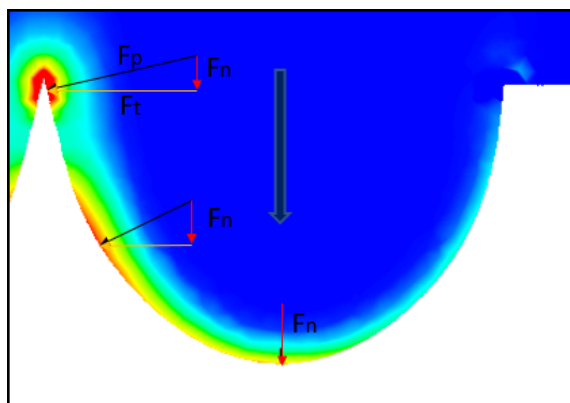


Figure 5.9: Analysis of pressure forces exerted on the bucket surface. Note: Double black arrow represents direction of rotation. Pressure force is marked with  $F_p$ , force acting in the direction of runner rotation is  $F_n$  and force normal to direction of rotation is marked with  $F_t$ .

bucket is symmetric. If there is misalignment of the jet axis, relative to the bucket cutter, this force will not be fully canceled and it might create unbalance in rotation of the runner. This, in return, will be followed by vibrations, noise and forces exerted on the shaft bearings and thus decrease lifetime of

Three pressure zones can be distinguished clearly in the figure. Zone 1 is the area where jet first comes in contact with bucket cutter. It is colored red and this is the zone of highest pressure. Of the three pressure zones, this is the one that contributes the least to the total torque of the Pelton runner. The reason for that, as shown in the figure 5.9, is because pressure always acts normal to the surface, so if the surface is under angle much smaller than 90 degrees relative to direction of rotation, component of the pressure force that contributes the most to the torque ( $F_n$ ) is relatively small. The biggest part of the pressure force, in this zone, goes to the force that is normal to the direction of rotation ( $F_t$ ). This force is parallel to the shaft axes and it can exert force on the shaft bearings. However, it is canceled by the symmetric force acting from the other half of the bucket. Nevertheless, this is only true if the flow inside the

the turbine or require frequent maintenance.

Zone 2 is larger, but the pressure is smaller than in zone 1. Finally zone 3, is the largest zone but with the smaller pressure than other two zones. However, pressure force at this zone is almost parallel with direction of bucket rotation which means that the most part of this force contributes to total torque of the Pelton runner.

Although the influence of the centrifugal and Coriolis forces are disregarded, analysis of pressure distribution in the fixed bucket configuration can be used for partial design optimization of the bucket.

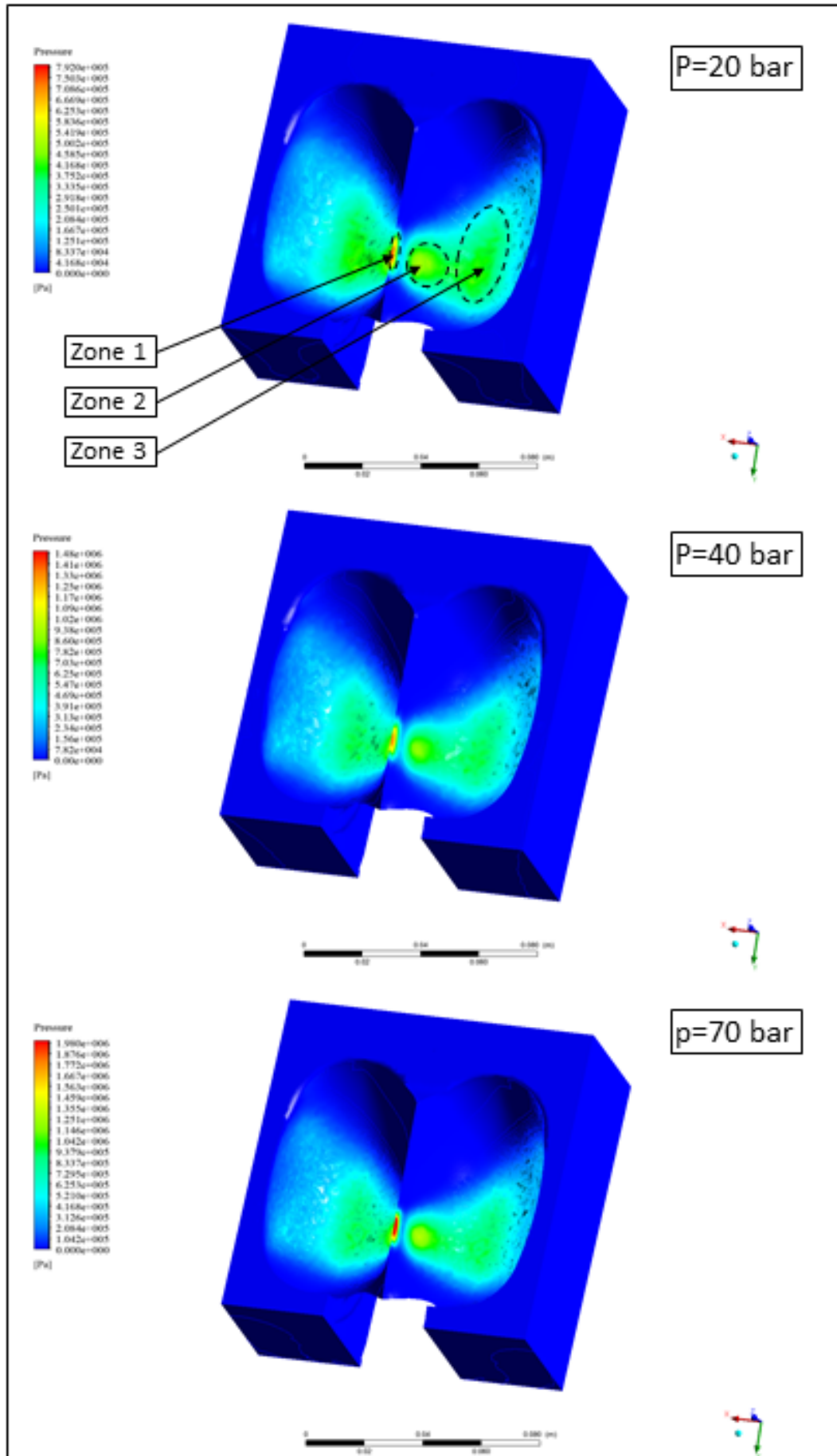


Figure 5.10: Pressure distribution inside the bucket at final timestep for different positions of the spear valve and constant flow rate of 315 l/min.

The thickness of the water layer inside the bucket, for case 1 is represented in figure 5.11. The water air interface is determined by finding the value of water volume fraction of 0.5. It can be observed from the figure that height of water layer is gradually decreasing from the tip of the bucket cutter until the bucket outlet edge. This is due to the spreading of water over the bucket surface.

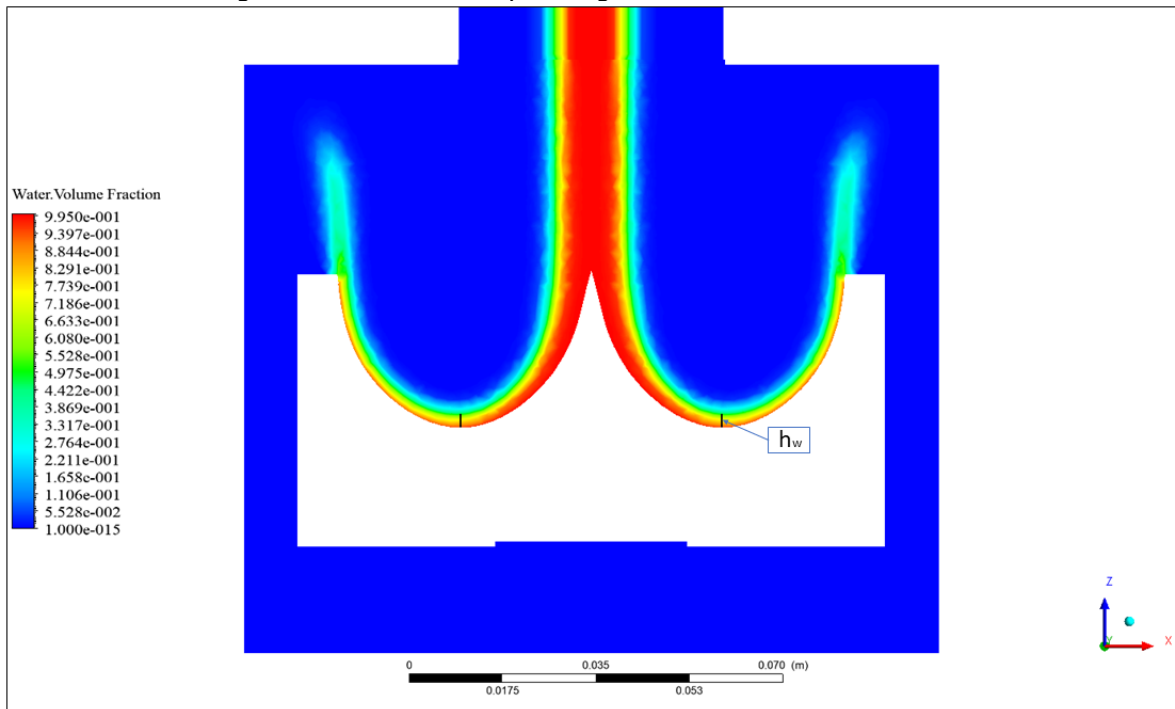


Figure 5.11: Water layer thickness at deepest point in the bucket at pressure of 20 bar and constant flow rate of 315 l/min.

The height of the water layer, for all investigated cases, is determined at the bucket's deepest point and values are given in table 5.6. It can be clearly seen that thicker water sheet corresponds to lower pressure.

Table 5.6: Water layer thickness for investigated cases at the bucket deepest point.

Description	Case 1	Case 2	Case 3
Set pressure	20 bar	40 bar	70 bar
Water layer thickness	2.5385 mm	2.176 mm	1.595 mm

Overpressure in water layer comes as a consequence of curved streamlines below the water sheet and it is most expressed at the deepest point of the bucket. This pressure gradient influences velocity distribution inside the water layer [4]. Water layer pressure distribution, for investigated case 1, is shown in figure 5.12.

Pressure distribution over the height of water sheet, at deepest point of the bucket, is given at the figure 5.13 for all investigated cases. Similar increasing trend can be noticed for all cases, going from the water sheet surface until the bucket surface, with clear difference in magnitude.

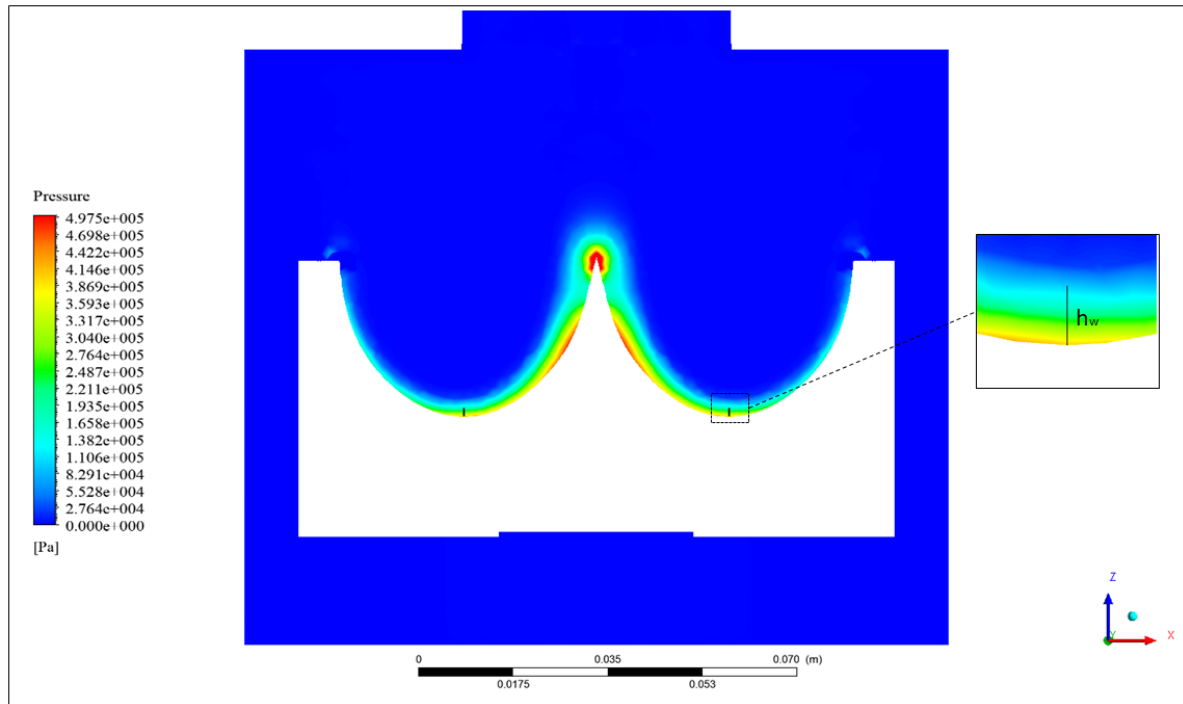


Figure 5.12: Water layer pressure distribution in the bucket at pressure of 20 bar and constant flow rate of 315 l/min.

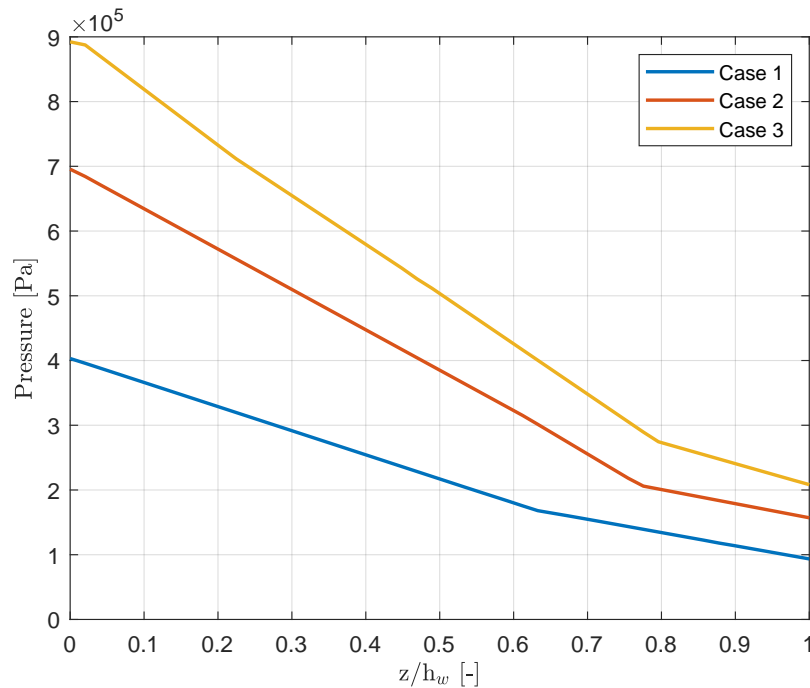


Figure 5.13: Water layer pressure distribution at deepest point in the bucket at constant flow rate of 315 l/min.

Simulated high speed water jet for three positions of the spear valve at constant flow rate is given in the figure 5.14. Position of the interface between the air and water jet is determined by the 0.5 value of the water volume fraction. As it can be seen from the figure, at the part of the jet domain close to the nozzle and in the bucket flow domain, interface is smeared out, while at the part of the jet in front of bucket domain it is more sharp. The reason for this, as shown in detail view, is because different

type of meshing used for these domains. Smearred jet interface domain is meshed with unstructured mesh with mostly tetrahedral elements, while sharper interface is meshed with structured hexahedral elements. Hexahedral elements gave better interface because they were oriented in the direction of the flow.

It can be noted that in simulated case there is no visible divergence of the jet or separation at the upper surface of the jet as observed in the experiment. There could be several probable reasons for this:

- Continuous fluid model used for the simulation is not able to model particle separation
- Flow inside the injector is not symmetric in reality
- Inlet is too close to the injector bend for velocity profile to develop

Nevertheless, this requires further investigation to narrow down the exact cause of this problem and set-up the solver properly.

Diameter of the jet is measured at the beginning of the jet domain with structured mesh, as shown in figure 5.14. Speed of the jet is recorded at the same position, at the jet center. Theoretical speed of the jet is found by first reading the value of the static pressure inside the injector and then calculating speed of the jet by using Torricelli formula.

$$C_0 = \phi \sqrt{\frac{2p}{\rho}} \quad (5.4)$$

Where the efficiency of the nozzle  $\phi$  is considered to be 100% and  $p$  is static pressure expressed in Pascals.

In order to determine real nozzle efficiency, simulated and calculated jet speeds are compared. All calculated and acquired values are given in table below. Furthermore, experimental jet diameter for three cases is given as well. It can be clearly seen that there is a difference between simulated and real value of jet diameter which is a result of difference in flow rate. The possible reason for difference in flow rate between experiment and simulation is because total pressure is set for simulation at the inlet of injector without actual knowledge about velocity inside the injector. Velocity is only calculated based on experimental set flow rate and internal diameter of the injector pipe.

*Table 5.7: High speed jet parameters and efficiency of the nozzle. Note: Simulated flow rate is calculated using simulated jet speed and simulated jet diameter.*

<b>Description</b>	<b>Case 1</b>	<b>Case 2</b>	<b>Case 3</b>
Realized pressure	19.75 bar	39.76 bar	69.72 bar
Experimental jet diameter	11.4 mm	9.38 mm	8.4 mm
Simulated jet diameter	13.775 mm	12.489 mm	10.683 mm
Simulated jet speed	61.39 m/s	87.61 m/s	115.29 m/s
Theoretical jet speed	62.849 m/s	89.174 m/s	118.08 m/s
Simulated flow rate	548.7 l/min	643.6 l/min	619.7 m/s
Nozzle efficiency	0.977	0.982	0.976

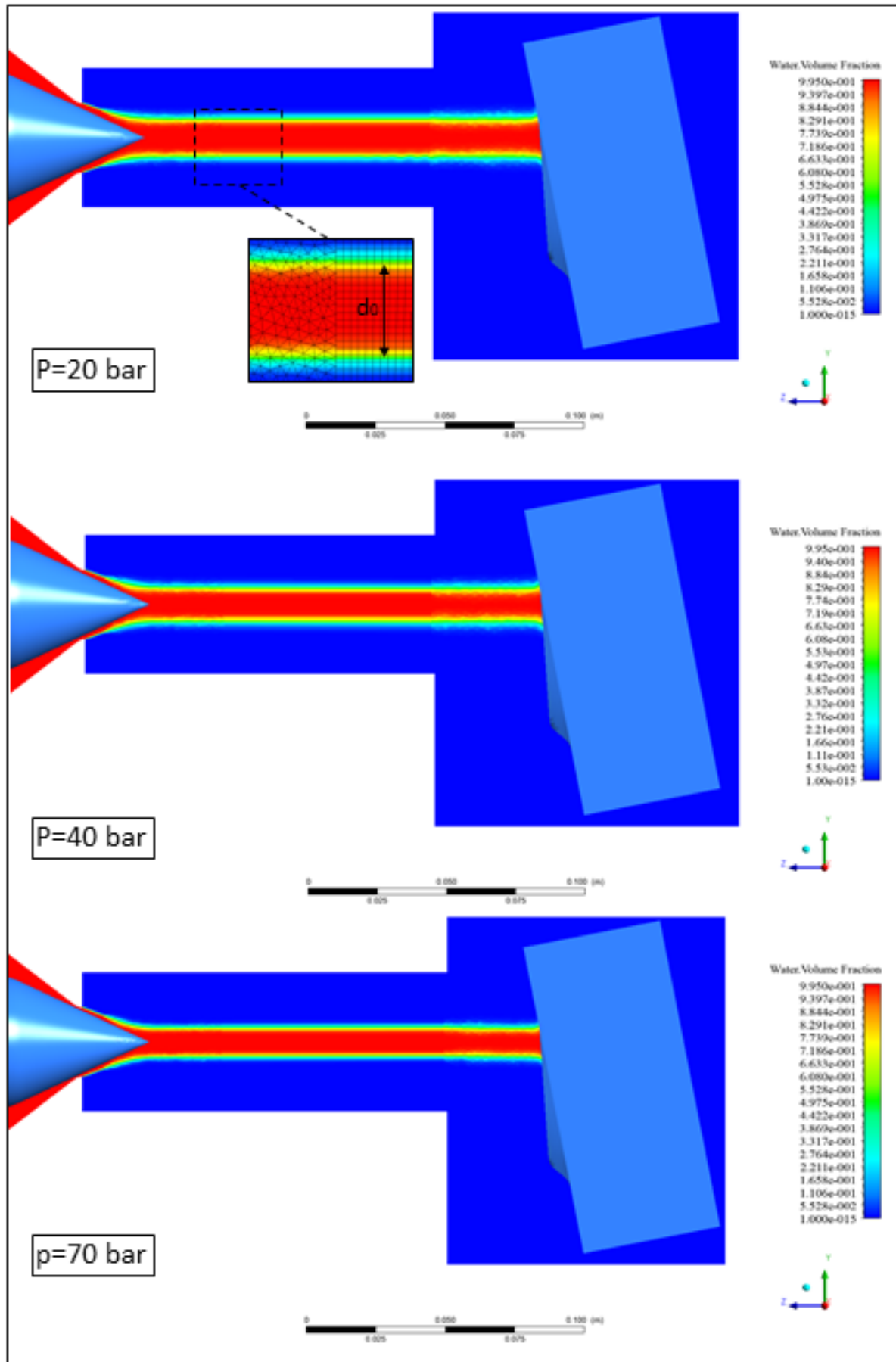


Figure 5.14: Diameter of the high speed jet and water/air interface for different positions of the spear valve and constant flow rate of 315 l/min.

# 6

## Conclusions and recommendations

### 6.1. Conclusions

Delft Offshore Turbine (DOT) company is developing centralized power production system for offshore wind farms by combining wind turbine and hydraulic turbine technology. The goal of this thesis was to identify problems and try to overcome challenges in design of Pelton turbine for DOT concept. Three methodologies were used: theory, experiment and numerical analysis.

First, **theoretical approach** was used to develop a tool for preliminary design of Pelton turbine by using Python programming language. Input parameters, pressure and flow rate, together with optimal values for peripheral speed coefficient and bucket volumetric load represent main design parameters used for the initial turbine design. Furthermore, since they are mutually dependent, either specific speed or generator rotational speed can be set as well. For given input parameters, program can calculate turbine parameters like: pitch circle diameter, bucket width, number of buckets, rotational speed, runaway speed, injector distance etc. Several test cases for different pressures and different power outputs were used to observe the influence of "site conditions" on Pelton turbine design. It is noticed that diameter of the runner has decreasing trend with increase in pressure or decrease in flow rate, but the smallest diameter is also limited with highest synchronous speed of the generator. The width of the Pelton turbine bucket is also decreasing with increase in pressure and decrease in flow rate. This is the consequence of fixed bucket volumetric load which is dependent on flow parameters through the jet diameter. If pre-set, specific speed can be used for adjusting diameter of the runner. This parameter is a function of flow rate, pressure and rotational speed of the generator. With standard hydro power plants pressure is fixed and determined by height difference between upper reservoir and inlet of the injector, so specific speed is determined by synchronous speed of the generator. For DOT concept pressure can take any value and it is limited only by power of the wind turbine. Thus it is important to identify Pelton turbine design operating points, for a given wind farm and given site conditions, which will give design solution of maximal efficiency.

For the second part **experimental approach** was used and tests were conducted to assess the influence of flow rate and pressure on efficiency of a Pelton turbine. Furthermore, indirect influence of the pressure fluctuations, caused by the discontinuous flow from the positive displacement pump, on Pelton turbine efficiency is investigated.

No influence of the pressure fluctuations on quality of the jet is noticed. However, flow separation at the surface of the jet is observed. This separation is a consequence of the secondary flows inside the jet due to existence of the bend before the nozzle. Effect of the pressure and flow rate on the distance of separation from the nozzle is investigated. It is found that distance of separation is increasing with increase of flow rate and decrease of pressure. If this distance is smaller than length of the jet that interacts with bucket during its cycle, then separation might influence not just efficiency of the Pelton turbine but also dynamic loading of the runner. Having in mind that flow rate and pressure for the DOT concept are dependent on wind conditions at which wind turbine operates, this analysis at partial

loads can be very useful for the proper choice of the operating point for which a Pelton turbine will be designed for.

Jet speed was determined by measuring a distance in two or more subsequent frames covered by a certain coherent structures found inside or at the surface of the jet and dividing by time of travel. Jet speed could not be measured for all operating points as frame rate was not high enough for higher pressures. Although it showed relatively good agreement with theoretical values this method is not very reliable as many variables can influence uncertainty in measurements.

Diameter of the jet was measured just after *vena contracta* for all operating points, and bucket volumetric load was calculated. Extremely low values of bucket volumetric load found, indicate that tested turbine would work with low efficiency at these operating points. Furthermore, the trend of bucket volumetric load and jet diameter as a function of pressure and flow rate is similar to separation distance trend. This suggests that separation distance is closely correlated with jet diameter.

It should be also noted that spectral analysis of the measured pressure signal is conducted and the frequency of the PD pump piston is identified for several operating points. Reasons for not being able to see the piston frequency for all operating points is possibly because signal was too noisy and total acquisition time was low. Also it is possible that boost pressure at the inlet of the PD pump was insufficient at certain flow rates so that piston chambers were not filling fast enough for each piston stroke.

Phase II of the experiment, due to lack of time, was not conducted. However it is designed and prepared for the future work. The results of phase I were able to give better understanding of the influence of flow rate, pressure and pressure fluctuations on development of the high speed jet and provide qualitative answer on research questions being investigated. Phase II aims to give quantitative confirmation and way to validate numerical results.

For the final part of the thesis **numerical approach** was used for simulation of the flow inside the injector, high speed jet flow and flow inside the Pelton turbine bucket. The aim of this part is to set-up a CFD model that will be able to properly simulate the flow inside the Pelton turbine and to be used after for investigation of different preliminary designs defined in the first stage.

Results of the analysis identified three pressure zones at the surface of the modelled bucket. Zone 1 is located at the tip of the bucket cutter and it is the zone with the highest pressure. However this zone contributes the least to total torque of the turbine because projection of the pressure force on direction of bucket rotation is relatively small. Zone 3 is the largest zone and it is located at the bottom of the bucket. This zone has the lowest pressure of all other zones but it contributes the most to torque because the pressure force is oriented in direction of bucket rotation. Zone 2 is between two other zones and it is located at the side of the cutter.

Water layer thickness inside the bucket was investigated as well and it is noticed that layer is thicker for higher pressures and at constant flow rate. Furthermore, pressure distribution over the height of water layer showed the existence of overpressure below the water sheet as reported by Zhang [4].

For tracking the water-air interface standard 2-phase homogeneous model was used. Interface between the water jet and surrounding air, at the part of the jet domain which is meshed with unstructured mesh, was smeared out while at the part which is meshed with structured hexahedral elements was sharper. Nevertheless, separation of the jet flow was not obtained with this model. Diameter of the jet was measured as well for all simulated cases and jet speed was found and compared with theoretical value in order to determine efficiency of the nozzle.

Results from the numerical analysis showed relatively good agreement with theoretical results, however in order to be fully reliable they need to be validated with experimental measurements. Furthermore, this model has not been able to simulate the effects like separation of the flow at the surface of the jet hence different fluid models or different solvers have to be used.

## 6.2. Recommendations

The aim of this thesis was to define and construct a complete process of Pelton turbine design for DOT concept and to try to answer some important research questions. Three research methodologies or approaches are used in this thesis and each of them plays an important part in the design process. However, these approaches are investigated independently so additional research is necessary

to connect them together and form an iterative design loop. Following future work is recommended:

- Measurement of the pressure distribution at the surface of Pelton bucket and stresses at the bucket root - this is phase II of the experiment and it is already designed and prepared as part of this thesis. The goal of this research should be investigation of the influence of flow rate, pressure and pressure fluctuations, at operating conditions of DOT concept, on the efficiency and dynamic loading of a Pelton turbine. Furthermore, these measurements can be used to validate numerical model.
- Design of the Pelton turbine bucket - proper design of the Pelton turbine bucket is of paramount importance for achieving highest efficiency of the hydraulic turbine. However, turbine manufacturers keep the design procedure confidential and there is almost no detailed guidelines available (only one freely available by the author's knowledge is a PhD thesis by Bjørn Winther Solemslie [32]). This was initially planned to be done as part of this thesis but after some research and careful consideration it was decided that it is outside of the scope.
- Improve CFD model and conduct Finite Element Analysis - Although numerical simulations showed relatively good agreement with theoretical results they still need to be validated with experimental measurements. Also, model failed to simulate jet flow separation as observed in the experiment, therefore different models need to be tested. Furthermore, FEA analysis should be conducted with data obtained from the CFD simulation.

# Bibliography

- [1] A. Jarquin Laguna, *Centralized electricity generation in offshore wind farms using hydraulic networks*, Ph.D. thesis (2017).
- [2] N. Diepeveen, *On the application of fluid power transmission in offshore wind turbines.*, Ph.D. thesis (2013).
- [3] <https://www.globalspec.com>, .
- [4] Z. Zhang, *Pelton turbines* (Springer International Publishing Switzerland, 2016).
- [5] B. Zoppe, C. Pellone, T. Maitre, and P. Leroy, *Flow analysis inside a pelton turbine bucket*, (2006).
- [6] S. Kvicinsky, J.-L. Kueny, F. Avellan, and E. Parkinson, *Experimental and numerical analysis of free surface flows in a rotating bucket*, (2002).
- [7] A. Perrig, F. Avellan, J. Kueny, E. Parkinson, and M. Farhat, *Flow in a pelton turbine bucket: Numerical and experimental investigations*, *Journal of Fluids Engineering*, **128** (2006).
- [8] A. Perrig, *Hydrodynamics of the free surface flow in pelton turbine buckets*, , 242 (2007).
- [9] Z. Zhang, *Dual-measurement-method and its extension for accurately resolving the secondary flows in lda (laser doppler anemometry) applications*, , 57 (2005).
- [10] Z. Zhang and E. Parkinson, *Lda application and the dual-measurement-method in experimental investigations of the free surface jet at a model nozzle of a pelton turbine*, (2002).
- [11] T. T. Bergflødt, B. W. Solemslie, and O. G. Dahlhaug, *Development of an accumulator system for a pulsating pelton nozzle*, (2016).
- [12] M. Hana, *Numerical analysis of non-stationary free surface flow in a pelton bucket*, (1999).
- [13] S. Kvicinsky, J.-L. Kueny, and F. Avellan, *Numerical and experimental analysis of free surface flow in a 3d non rotating pelton bucket*, (2002).
- [14] S. P. Mulders, N. F. B. Diepeveen, and J.-W. van Wingerden, *Control design, implementation and evaluation for an in-field 500 kw wind turbine with a fixed-displacement hydraulic drivetrain*, *Wind Energy Science Discussions* **2018**, 1 (2018).
- [15] M. O. L. Hansen, *Aerodynamics of Wind Turbines*. (Earthscan Publications Ltd., 2015).
- [16] EWEA, <https://windeurope.org>, (2017).
- [17] A. WindEurope, <https://windeurope.org/confex2017/>, (2017).
- [18] Z. Zhang, *Flow interactions in pelton turbines and the hydraulic efficiency of the turbine system*, *Proceedings of the Institution of Mechanical Engineers, Part A: Journal of Power and Energy* **221**, 343 (2007).
- [19] R. Angehrn, *Safety engineering for the 423 mw-pelton- runners at bieudron*, Proceeding of the 20th IAHR Symposium, Charlotte, NC. (2000).
- [20] M. Sick, G. Vullioud, H. Keck, and E. Parkinson, *New challenges in pelton research*, (2007).
- [21] H. Brekke, *Hydraulic turbines: Design, Erection and Operation* (2011).
- [22] T. Fujihara, H. Imano, and K. Oshima, *Development of pump turbine for seawater pumped-storage power plant*, *Hitachi Review*, **47**, 199 (1998).

- [23] F. Avellan, P. Dupont, S. Kvicinsky, L. Chapuis, E. Parkinson, and G. Vuilloud, *Flow calculations in pelton turbines - part 2: Free surface flows*, Proceedings of the 19th IAHR Symposium .
- [24] R. Wille and H. Fernholz, *Report on the first european mechanics colloquium, on the coanda effect*, *Journal of Fluid Mechanics* **23**, 801–819 (1965).
- [25] Z. Zhang and M. Casey, *Experimental studies of the jet of a pelton turbine*, *Proceedings of The Institution of Mechanical Engineers Part A-journal of Power and Energy - PROC INST MECH ENG A-J POWER*, **221**, 1181 (2007).
- [26] J. David Anderson, *Computational fluid dynamics : the basics with applications / john d. anderson*, (1995).
- [27] H. Versteeg and W. Malalasekera, *An introduction to computational fluid dynamics : the finite volume method / h. k. versteeg and w. malalasekera*. (2018).
- [28] L. F. Barstad, *Cfd analysis of a pelton turbine*, (2012).
- [29] L. E. Klemetsen, *An experimental and numerical study of the free surface pelton bucket flow*, (2010).
- [30] M. Nechleba, *Hydraulic turbines: Their design and equipment* (Prague: Artia, 1957).
- [31] <https://www.sharcnet.ca>, .
- [32] B. Solemslie, *Experimental methods and design of a pelton bucket*, (2016).



## Preliminary design

Table A.1: Calculated parameters for  $P=30\text{MW}$  and  $\Delta p = 200 \text{ bar}$

Description	$z_{jet} = 1$	$z_{jet} = 2$	$z_{jet} = 3$	$z_{jet} = 4$	$z_{jet} = 5$	$z_{jet} = 6$
Pitch circle diameter $D_m$	1.18 m	1.18 m	1.18 m	1.18 m	1.18 m	1.18 m
Bucket width $B$	0.3 m	0.21 m	0.17 m	0.15 m	0.13 m	0.12 m
Number of buckets $N$	21	24	26	27	29	30
Rotational speed $n$	1500 rpm	1000 rpm	1500 rpm	1500 rpm	1500 rpm	1500 rpm
Number of pole pairs $p$	2	2	2	2	2	2
Specific speed $n_q$	$0.1032 \text{ s}^{-1}$	$0.073 \text{ s}^{-1}$	$0.06 \text{ s}^{-1}$	$0.052 \text{ s}^{-1}$	$0.046 \text{ s}^{-1}$	$0.042 \text{ s}^{-1}$

Table A.2: Calculated parameters for  $P=30\text{MW}$  and  $\Delta p = 400 \text{ bar}$

Description	$z_{jet} = 1$	$z_{jet} = 2$	$z_{jet} = 3$	$z_{jet} = 4$	$z_{jet} = 5$	$z_{jet} = 6$
Pitch circle diameter $D_m$	1.67 m					
Bucket width $B$	0.18 m	0.12 m	0.1 m	0.09 m	0.08 m	0.07 m
Number of buckets $N$	30	35	40	44	47	50
Rotational speed $n$	1500 rpm	1000 rpm	1500 rpm	1500 rpm	1500 rpm	1500 rpm
Number of pole pairs $p$	2	2	2	2	2	2
Specific speed $n_q$	$0.043 \text{ s}^{-1}$	$0.031 \text{ s}^{-1}$	$0.025 \text{ s}^{-1}$	$0.021 \text{ s}^{-1}$	$0.019 \text{ s}^{-1}$	$0.018 \text{ s}^{-1}$

Table A.3: Calculated parameters for  $P=50\text{MW}$  and  $\Delta p = 200 \text{ bar}$

Description	$z_{jet} = 1$	$z_{jet} = 2$	$z_{jet} = 3$	$z_{jet} = 4$	$z_{jet} = 5$	$z_{jet} = 6$
Pitch circle diameter $D_m$	1.77 m	1.18 m	1.18 m	1.18 m	1.18 m	1.18 m
Bucket width $B$	0.38 m	0.27 m	0.22 m	0.19 m	0.17 m	0.16 m
Number of buckets $N$	22	22	23	25	26	27
Rotational speed $n$	1000.2 rpm	1500 rpm	1500 rpm	1500 rpm	1500 rpm	1500 rpm
Number of pole pairs $p$	3	2	2	2	2	2
Specific speed $n_q$	$0.089 \text{ s}^{-1}$	$0.094 \text{ s}^{-1}$	$0.077 \text{ s}^{-1}$	$0.067 \text{ s}^{-1}$	$0.06 \text{ s}^{-1}$	$0.054 \text{ s}^{-1}$

Table A.4: Calculated parameters for  $P=50\text{MW}$  and  $\Delta p = 400 \text{ bar}$ 

Description	$z_{jet} = 1$	$z_{jet} = 2$	$z_{jet} = 3$	$z_{jet} = 4$	$z_{jet} = 5$	$z_{jet} = 6$
Pitch circle diameter $D_m$	1.67 m	1.67 m	1.67 m	1.67 m	1.67 m	1.67 m
Bucket width $B$	0.23 m	0.16 m	0.13 m	0.11 m	0.1 m	0.09 m
Number of buckets $N$	26	31	34	37	40	42
Rotational speed $n$	1500 rpm	1500 rpm	1500 rpm	1500 rpm	1500 rpm	1500 rpm
Number of pole pairs $p$	2	2	2	2	2	2
Specific speed $n_q$	$0.056 \text{ s}^{-1}$	$0.04 \text{ s}^{-1}$	$0.032 \text{ s}^{-1}$	$0.028 \text{ s}^{-1}$	$0.025 \text{ s}^{-1}$	$0.023 \text{ s}^{-1}$

Table A.5: Calculated parameters for  $P=200\text{MW}$  and  $\Delta p = 200 \text{ bar}$ 

Description	$z_{jet} = 1$	$z_{jet} = 2$	$z_{jet} = 3$	$z_{jet} = 4$	$z_{jet} = 5$	$z_{jet} = 6$
Pitch circle diameter $D_m$	2.95 m	2.36 m	1.77 m	1.77 m	1.18 m	1.18 m
Bucket width $B$	0.77 m	0.54 m	0.44 m	0.38 m	0.34 m	0.31 m
Number of buckets $N$	21	22	21	22	21	21
Rotational speed $n$	600 rpm	750 rpm	1000.2 rpm	1000.2 rpm	1500 rpm	1500 rpm
Number of pole pairs $p$	5	4	3	3	2	2
Specific speed $n_q$	$0.107 \text{ s}^{-1}$	$0.094 \text{ s}^{-1}$	$0.103 \text{ s}^{-1}$	$0.089 \text{ s}^{-1}$	$0.12 \text{ s}^{-1}$	$0.108 \text{ s}^{-1}$

Table A.6: Calculated parameters for  $P=200\text{MW}$  and  $\Delta p = 400 \text{ bar}$ 

Description	$z_{jet} = 1$	$z_{jet} = 2$	$z_{jet} = 3$	$z_{jet} = 4$	$z_{jet} = 5$	$z_{jet} = 6$
Pitch circle diameter $D_m$	1.67 m	1.67 m	1.67 m	1.67 m	1.67 m	1.67 m
Bucket width $B$	0.46 m	0.32 m	0.26 m	0.23 m	0.2 m	0.19 m
Number of buckets $N$	21	23	25	26	28	29
Rotational speed $n$	1500 rpm	1500 rpm	1500 rpm	1500 rpm	1500 rpm	1500 rpm
Number of pole pairs $p$	2	2	2	2	2	2
Specific speed $n_q$	$0.112 \text{ s}^{-1}$	$0.079 \text{ s}^{-1}$	$0.065 \text{ s}^{-1}$	$0.056 \text{ s}^{-1}$	$0.05 \text{ s}^{-1}$	$0.046 \text{ s}^{-1}$

Table A.7: Calculated parameters for  $P=400\text{MW}$  and  $\Delta p = 200 \text{ bar}$ 

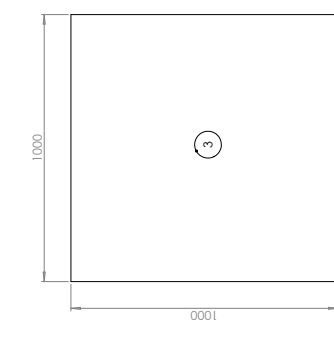
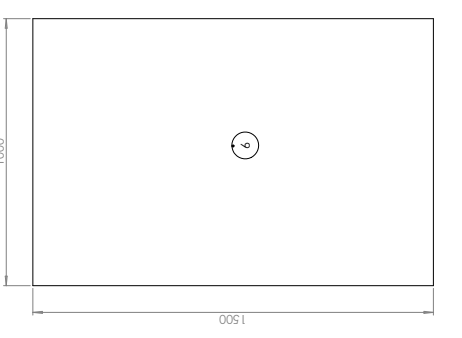
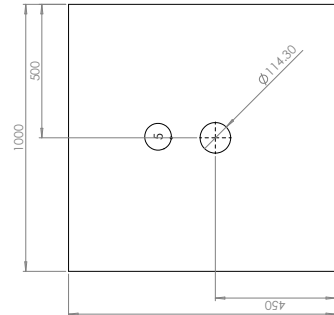
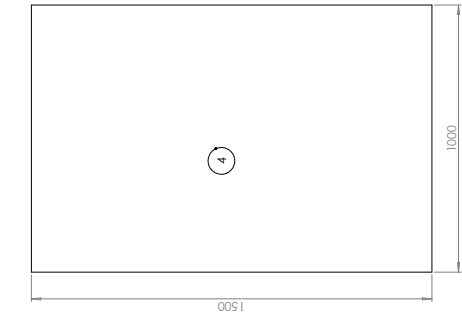
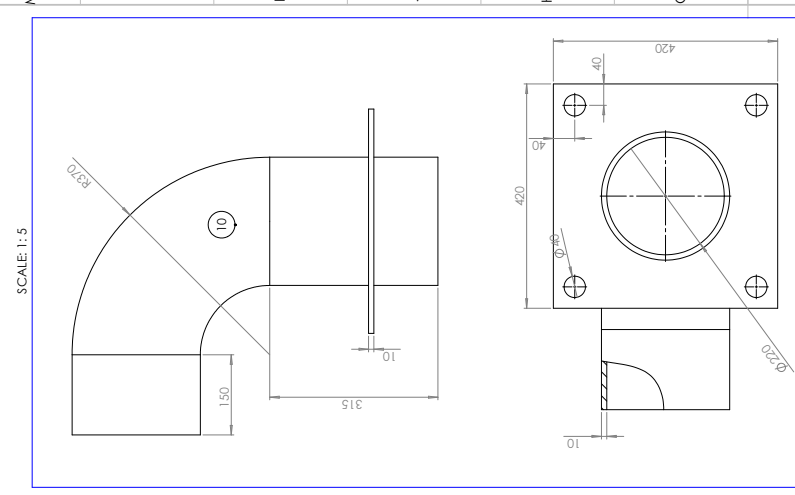
Description	$z_{jet} = 1$	$z_{jet} = 2$	$z_{jet} = 3$	$z_{jet} = 4$	$z_{jet} = 5$	$z_{jet} = 6$
Pitch circle diameter $D_m$	4.13 m	2.95 m	2.36 m	2.36 m	1.77 m	1.77 m
Bucket width $B$	1.08 m	0.77 m	0.63 m	0.54 m	0.48 m	0.44 m
Number of buckets $N$	21	21	21	22	21	21
Rotational speed $n$	428.4 rpm	600 rpm	750 rpm	750 rpm	1000.2 rpm	1000.2 rpm
Number of pole pairs $p$	7	5	4	2	3	3
Specific speed $n_q$	$0.107 \text{ s}^{-1}$	$0.106 \text{ s}^{-1}$	$0.108 \text{ s}^{-1}$	$0.094 \text{ s}^{-1}$	$0.11 \text{ s}^{-1}$	$0.10 \text{ s}^{-1}$

Table A.8: Calculated parameters for  $P=400\text{MW}$  and  $\Delta p = 400 \text{ bar}$ 

Description	$z_{jet} = 1$	$z_{jet} = 2$	$z_{jet} = 3$	$z_{jet} = 4$	$z_{jet} = 5$	$z_{jet} = 6$
Pitch circle diameter $D_m$	2.5 m	1.67 m	1.67 m	1.67 m	1.67 m	1.67 m
Bucket width $B$	0.64 m	0.46 m	0.37 m	0.32 m	0.29 m	0.26 m
Number of buckets $N$	21	21	22	23	24	25
Rotational speed $n$	1000.2 rpm	1500 rpm	1500 rpm	1500 rpm	1500 rpm	1500 rpm
Number of pole pairs $p$	3	2	2	2	2	2
Specific speed $n_q$	$0.105 \text{ s}^{-1}$	$0.11 \text{ s}^{-1}$	$0.09 \text{ s}^{-1}$	$0.08 \text{ s}^{-1}$	$0.071 \text{ s}^{-1}$	$0.065 \text{ s}^{-1}$

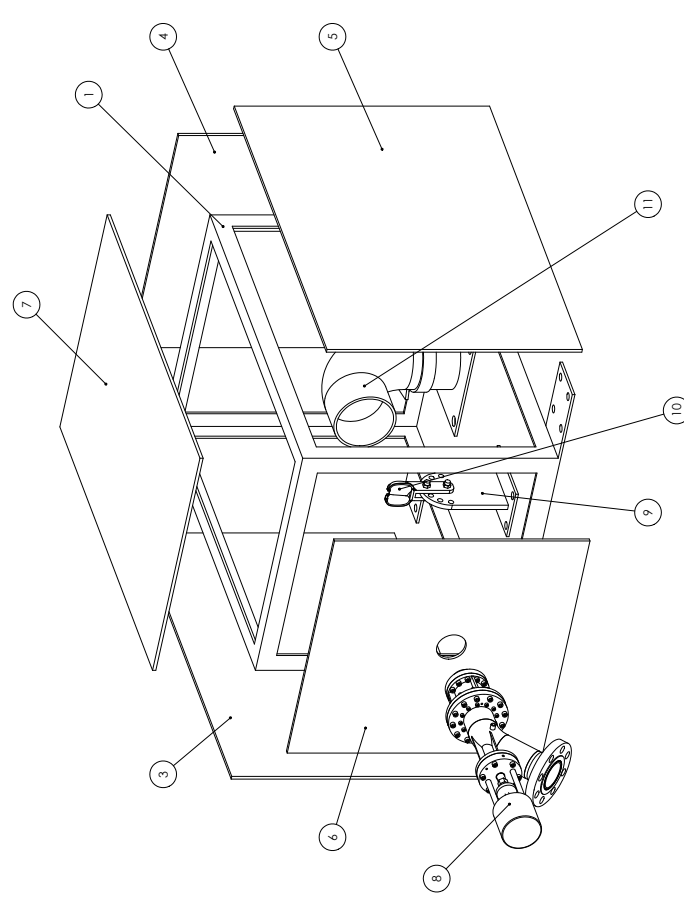
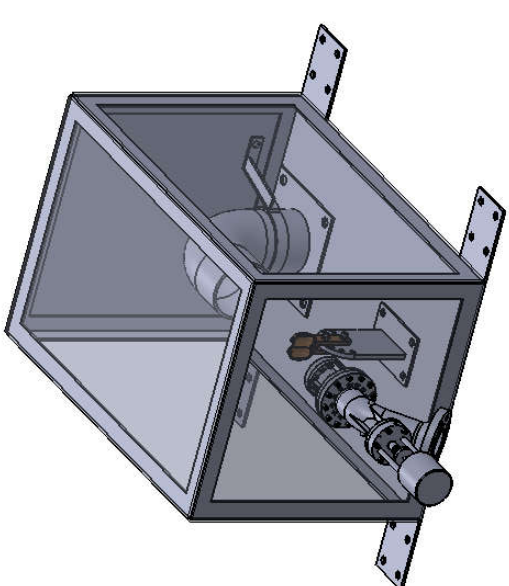
# B

## Technical drawings

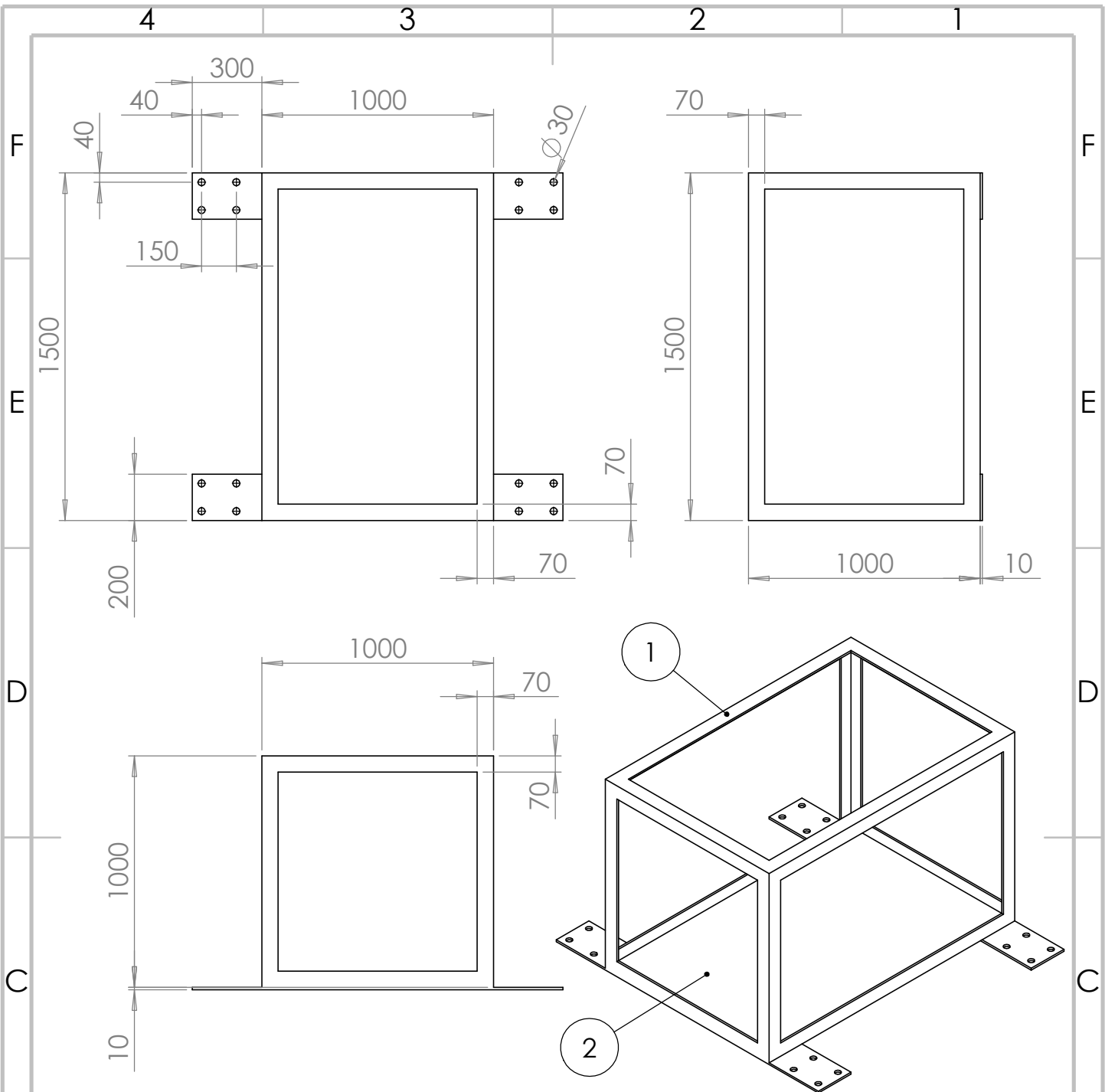


ITEM NO.	PART NAME	DESCRIPTION	MATERIAL	AMOUNT	DRAWING NO.
1	Test_rig_box	L or box profile plate	Steel	14 m	1.1
3	plate_0	plate	Steel	2.4 m <sup>2</sup>	
4	plate_2	plate	Steel	1.5 m <sup>2</sup>	
5	plate_1	plate	Plexiglas	1 m <sup>2</sup>	1
6	plate_4	plate	Steel	1.5 m <sup>2</sup>	
7	plate_3	plate	Plexiglas	1 m <sup>2</sup>	
8	Injector		Steel	1.5 m <sup>2</sup>	
9	Bucket stand	plate	Steel plate		1.2
10	Bucket	pipe	Steel	0.5 m	
11	Water extraction part	plate	Steel	0.2 m <sup>2</sup>	1
		90° pipe elbow	Steel		

Material	Total amount	Total amount +-10%
Steel plate	6.1 m <sup>2</sup>	7 m <sup>2</sup>
Plexiglas plate	3 m <sup>2</sup>	3.3 m <sup>2</sup>
Steel pipe	0.5 m	1 m
90° Elbow	1	2
L or box profile	14 m	16 m



DRAWING NO. 1  
 SCALE 1:5  
 SHEET 1 OF 1



ITEM NO.	PART NAME	DESCRIPTION	Amount
1	Test_rig_box	L or box profile	14 m
2	Bottom plate	Steel plate	2.4 m2

UNLESS OTHERWISE SPECIFIED:  
 DIMENSIONS ARE IN MILLIMETERS  
 SURFACE FINISH:  
 TOLERANCES:  
 LINEAR:  
 ANGULAR:

FINISH:

DEBURR AND  
 BREAK SHARP  
 EDGES

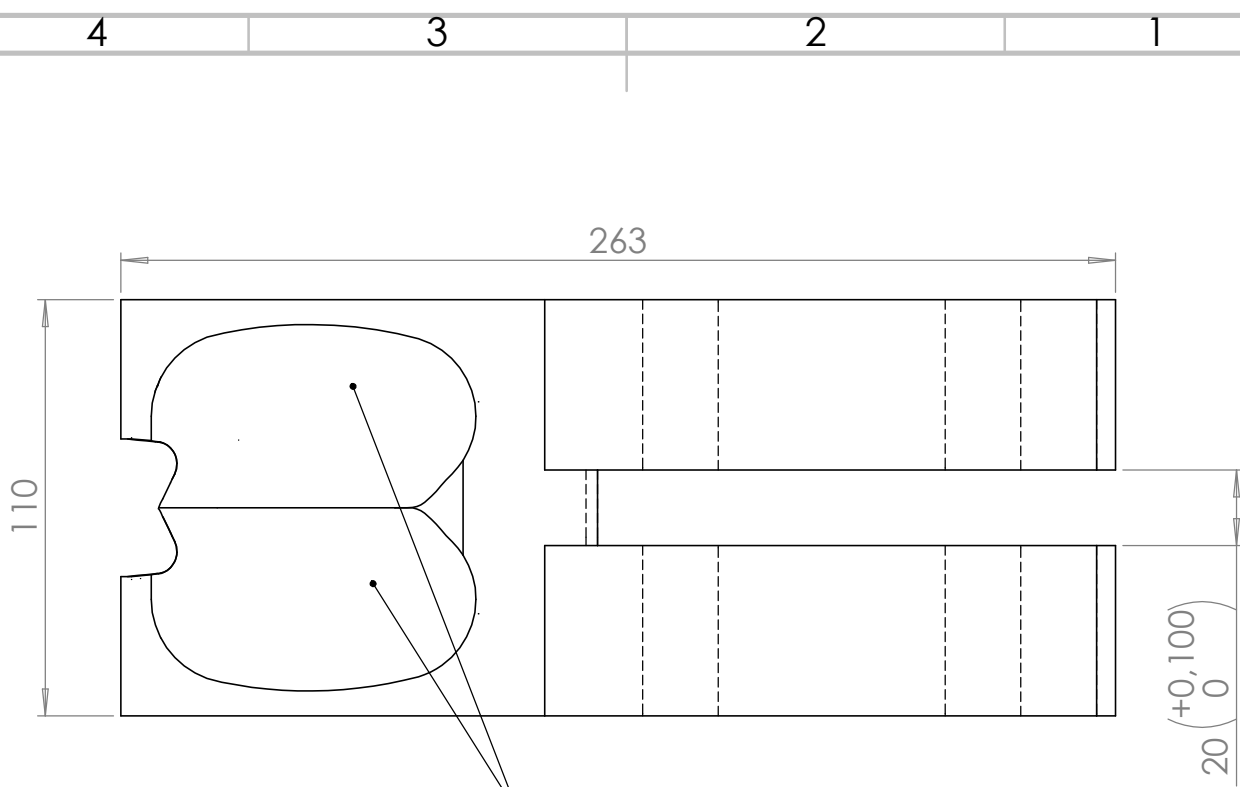
DO NOT SCALE DRAWING

REVISION

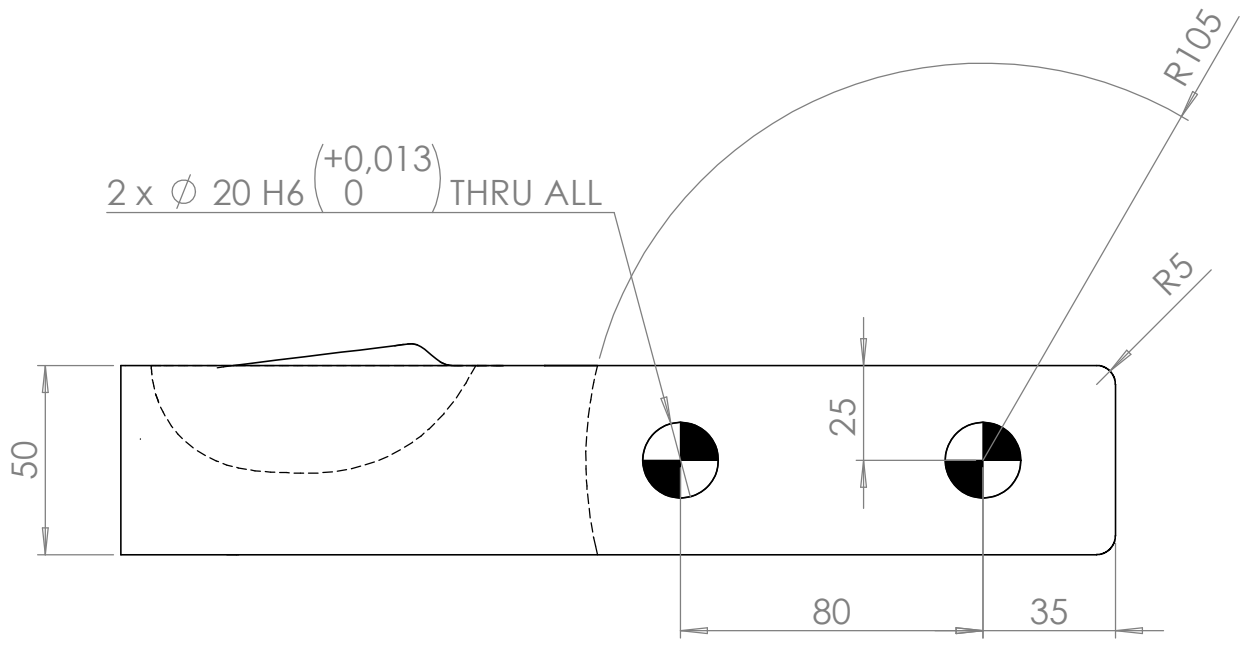
	NAME	SIGNATURE	DATE
DRAWN	Mladen Brajovic		
CHK'D			
APPV'D			
MFG			
Q.A			

TITLE: <b>Test_rig_box</b>	
DWG NO. <b>1.1</b>	A4
SCALE:1:25	SHEET 1 OF 1





Surface roughness:  
Ra=1.2



2 x  $\phi$  20 H6  $\left( \begin{smallmatrix} +0,013 \\ 0 \end{smallmatrix} \right)$  THRU ALL

UNLESS OTHERWISE SPECIFIED: DIMENSIONS ARE IN MILLIMETERS SURFACE FINISH: TOLERANCES: LINEAR: ANGULAR:				FINISH:	DEBURR AND BREAK SHARP EDGES	DO NOT SCALE DRAWING	REVISION
DRAWN				TITLE: <h1>Bucket</h1>			
CHK'D							
APPV'D							
MFG							
Q.A				MATERIAL:	DWG NO.	A4	
WEIGHT:				SCALE:1:5		SHEET 1 OF 1	



*Figure B.1: Manufactured bucket for phase II testing*